A Novel Concept For Hyperthermia Induced Local Chemotherapy

Inaugural-Dissertation

to obtain the academic degree
Doctor rerum naturalium (Dr. rer. nat.)
Submitted to the Department of Biology, Chemistry and Pharmacy
of Freie Universität Berlin

by

Jiang Gao

from Xi´an, China

March, 2011

The work for this PhD thesis was performed from August 2008 to March 2011 in the laboratory of Prof. Volker A. Erdmann in the Institute of Chemistry and Biochemistry at the Free University Berlin. Hereby I declare that I have written this thesis by myself, marked the sources of any quotations or content obtained otherwise.

Diese Arbeit wurde in der Zeit von August 2008 bis März 2011 unter der Aufsicht von Professor Dr. Volker A. Erdmann am Institut für Biochemie der Freie Universität Berlin angefertigt. Die Verfasserin versichert, die Arbeit eigenständig durchgeführt und alle Hilfsmittel angegeben zuhaben.

Gutachter: Prof. Dr. Volker A. Erdmann
Prof. Dr. Rudolf Tauber

Date of defence: 13.09.2011

Meinen Eltern

Index

1 Introduction

In the following chapter, some relevant information to understand this work will be provided, such as the basic features of nucleic acids and nanoparticles. Furthermore, the bioconjugate techniques applied in this work will be generally described and some facts about solid tumors will be explained.

1.1 Nucleic Acids

1.1.1 Basic Knowledge

Nucleic acids are one of the most important classes of biological macromolecules beside proteins, lipids and polysaccharides. The DNA (deoxyribonucleic acid) stores the genetic information and plays a key role in the central dogma of molecular biology (Fig. 1).

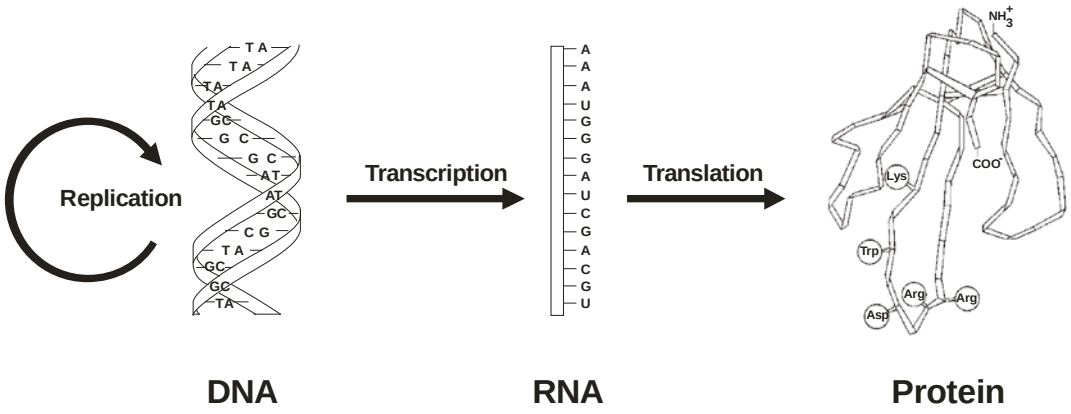

Figure 1: The central dogma of molecular biology. DNA is identically copied by replication. The genetic information of DNA is read out by transcription to mRNA. The information of the mRNA is expressed into a protein during translation (Kindly provided by J. P. Fürste).

The DNA is identically replicated and distributed into the new cells through cell division. To transfer the information from DNA into a functional protein, two processes are necessary: transcription and translation. Through transcription the genetic information from DNA is read out to mRNA. Subsequently, the mRNA is transported to the ribosome, where proteins are synthesized with the help of tRNAs. This latter process is called translation.

The building blocks of nucleic acids are nucleotides, which consist of three characteristic components: a nitrogenous base (purine or pyrimidine), a pentose and a phosphate (Fig. 2).

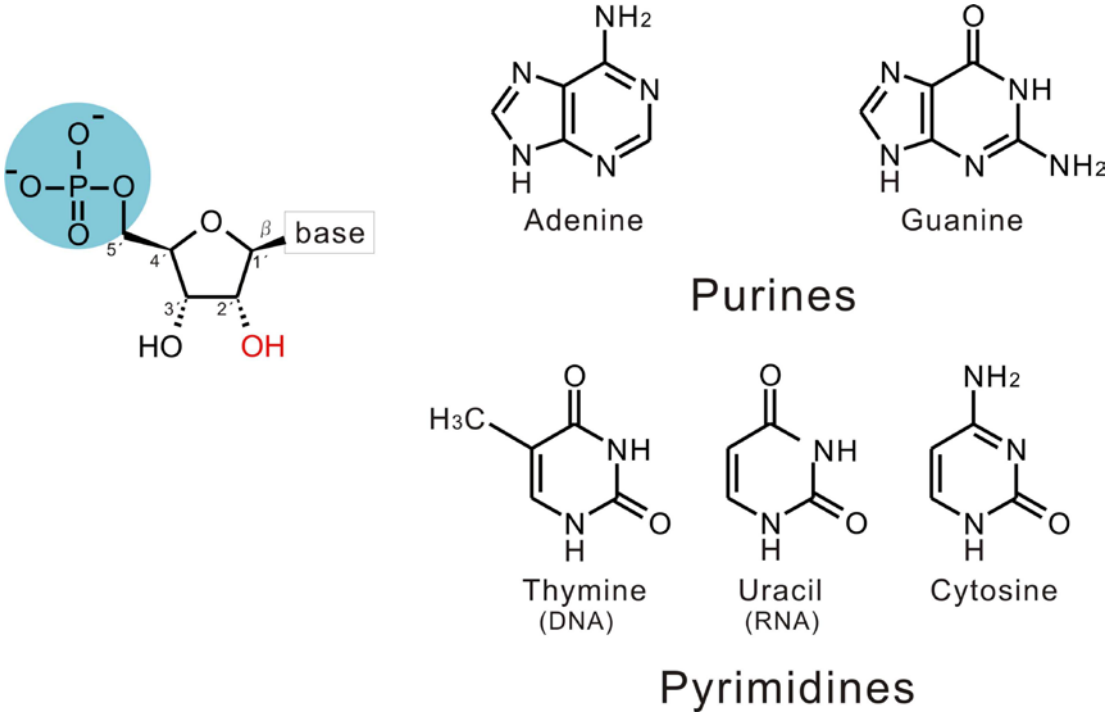

Figure 2: Structure of nucleotides. Left: The three components of a ribonucleotide: a nitrogenous base (purine or pyrimidine), a pentose and a phosphate (in blue shadow). The –OH group on the 2´carbon (in red) is in deoxyribonucleotides replaced with –H. **Right**: Major purine and pyrimidine bases of nucleic acids.

The two types of nucleic acids differ depending on the type of pentose: deoxyribonucleic acid (DNA) uses 2'-deoxy-ribose while ribonucleic acid (RNA) uses ribose. Nucleic acids are polymers of nucleotides covalently linked through phosphodiester bonds between the 5´-phosphate group of one nucleotide unit and the 3'-hydroxyl group of the next nucleotide (Fig. 3).

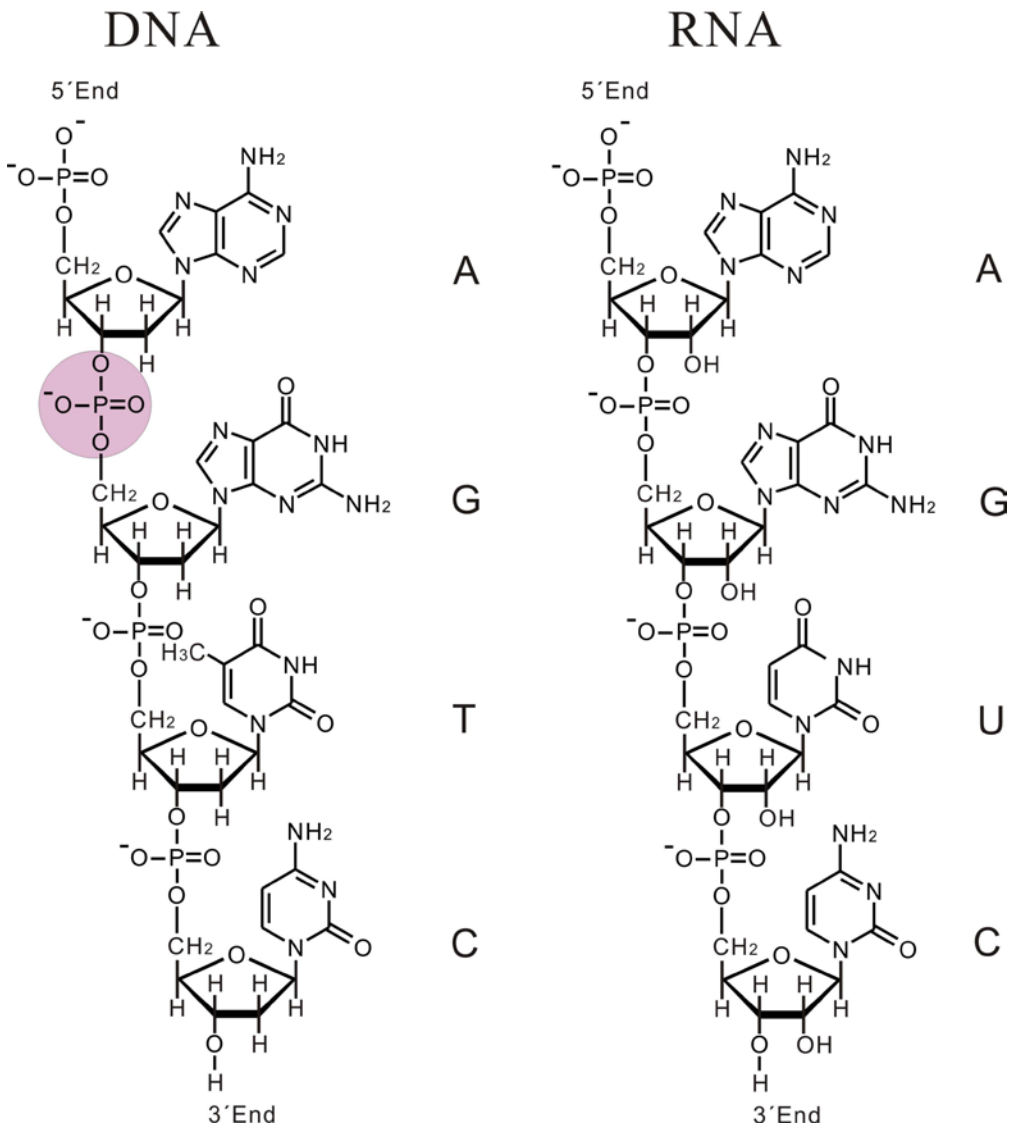

Figure 3: Chemical structure of DNA- and RNA-backbone. Phosphodiester linkages (one of which is shaded in the DNA) in the covalent backbone of DNA and RNA.

In 1953, the structure of DNA was discovered by Watson and Crick (Watson & Crick, 1953): DNA has a double-helical structure stabilized by base pairing via hydrogen bonds between adenine and thymine as well as between guanine and cytosine (Fig. 4).

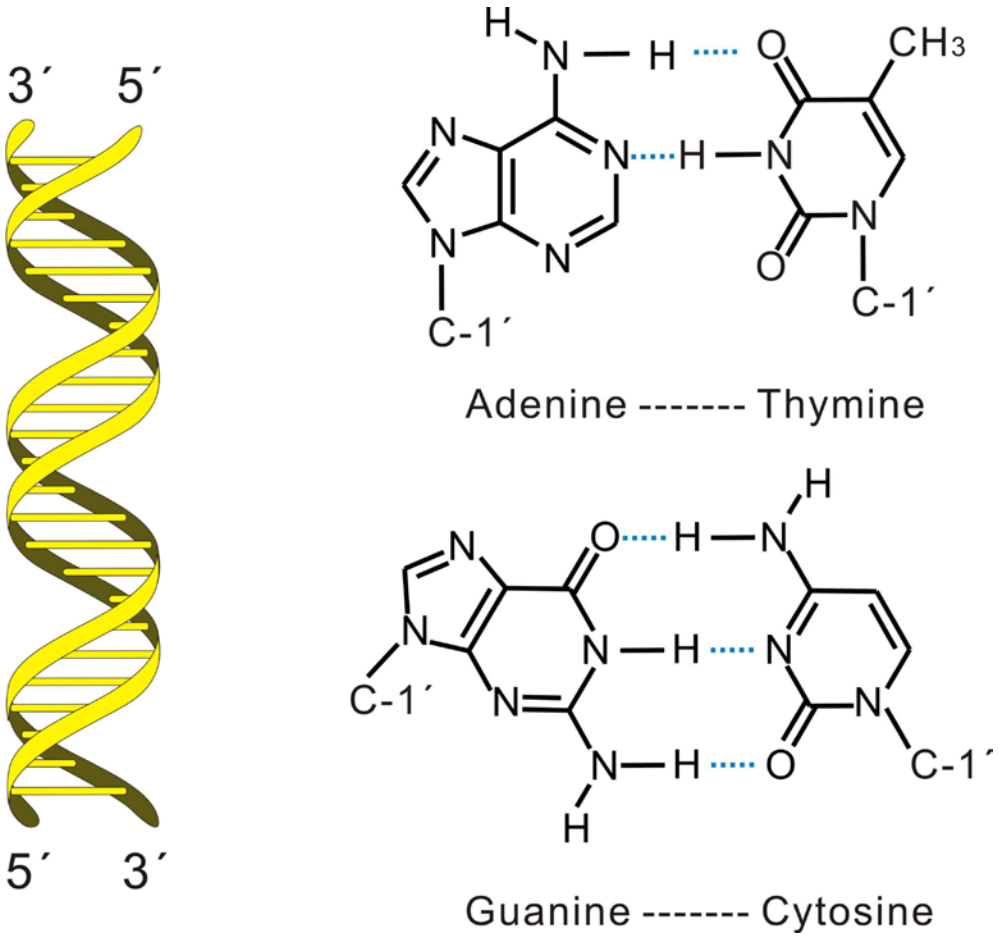

Figure 4: DNA double helix. Left: A two-dimensional model of the DNA double helix. **Right**: Watson-Crick base pairs. The base A pairs with T, and the base G pairs with C. The hydrogen bonds are represented in blue.

1.1.2 Melting Temperature of nucleic acids

Heat can cause the denaturation, or melting, of double-helical DNA. The hydrogen bonds between paired bases are disrupted and the double helix unwinds into two single strands. Noteworthily, during denaturing no covalent bonds of DNA are broken. The denaturation of double-stranded DNA is reversible and the reverse process is called renaturation or hybridization. The temperature at which half the helical structure is lost is defined as the melting temperature (T_m), which can be determined by measuring the absorption at a wavelength of 260 nm. Hypochromism describes the phenomenon that stacked bases in nucleic acids absorb less UV light than unstacked bases (Devoe & Tinoco, 1962). Vice versa, if the double-stranded nucleic acids melt into two single strands, more UV light is absorbed. This effect is called hyperchromism (Fig. 5).

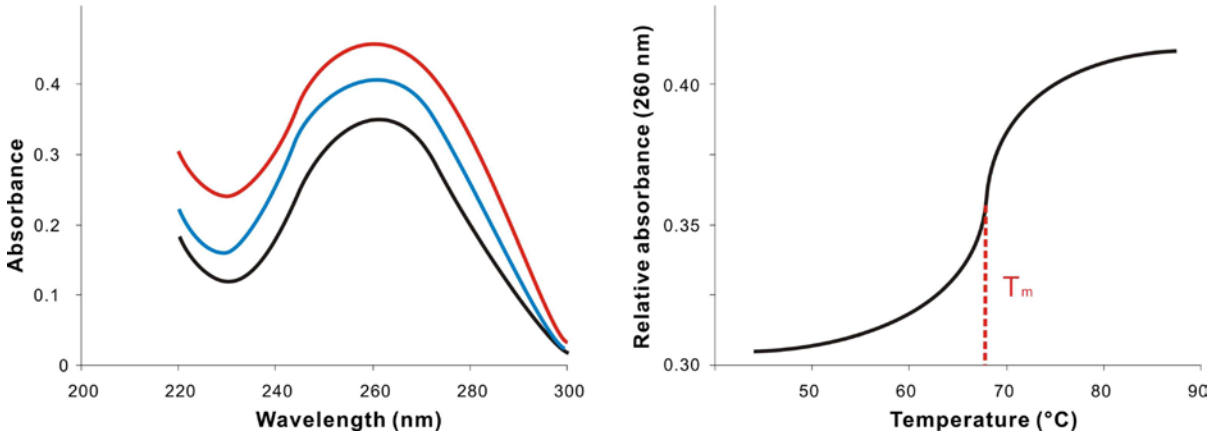

Figure 5. Hypochromism: Left: UV spectra of double-helix (in black), denatured DNA (in blue) and an equimolar mixture of nucleotides (in red). Right: The absorbance of a DNA solution at a wavelength of 260 nm increases with the rising temperature when the double helix is melted into single strands.

1.1.3 Nucleic Acids Synthesis and Nucleic Acids Analogues

Short fragments of nucleic acids can be artificially synthesized via a solid phase process (Letsinger *&* Mahadevan, 1965). In contrast to the biological synthesis, the chemical oligonucleotide synthesis is carried out in a 3' to 5' direction. Nucleoside phosphoramidites or 2'-deoxynucleoside phosphoramidites are used as building blocks.

With the development of the synthetic chemistry of oligonucleotides, several nucleic acids analogues such as peptide nucleic acid (PNA) (Egholm *et al.*, 1993; Wittung *et al.*, 1994), locked nucleic acid (LNA) (Satoshi *et al*., 1997; Koshkin *et al.*, 1998) as well as glycol nucleic acid (GNA) (Cook *et al.*, 1995; Zhang *et al.*, 2005) and threose nucleic acid (TNA) (Orgel, 2000; Schoning *et al.*, 2000) were introduced. In addition, mirror-image nucleic acid is a very important nucleic acids analogue. Mirror-image nucleic acids are the enantiomeric (L)-nucleic acids, containing nucleosides on 2´-deoxy-(L)-ribose or (L)-ribose (Fig. 6).

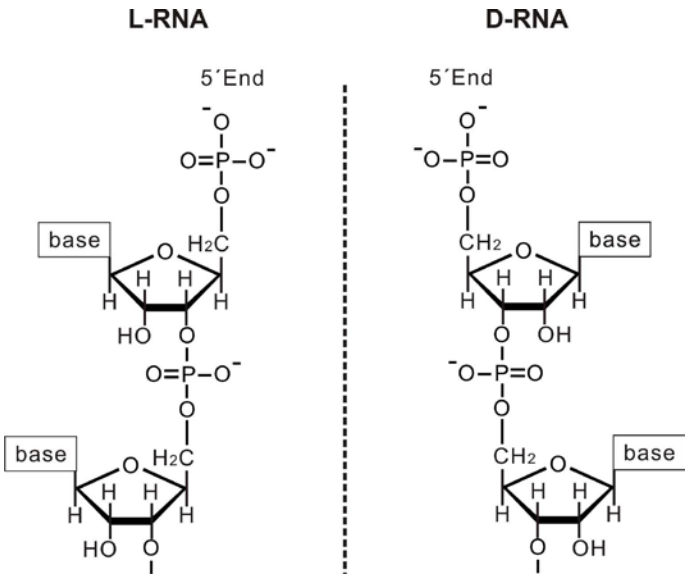

Figure 6. Structure of D-RNA and L-RNA.

The reciprocal chiral specificity of nucleic acids with their mirror-image aptamers, the so-called Spiegelmers, was shown in 1996 (Nolte *et al*. 1996; Klußmann *et al*. 1996) and an enantioselective ribozyme was developed in 2000 (Seelig *et al*., 2000). However, the mirror-image nucleic acids retain identical physical properties, for example melting temperature, as the normal D-form nucleic acids.

1.1.4 Hammerhead Ribozyme

It is known that the nucleic acids encode the genetic information for the enzymes that catalyze the replication of nucleic acids. The question arises what existed first, DNA, RNA or protein? At the end of the 1960s, a new theory was postulated by several scientists stating that the RNA acted not only as a carrier of information, but initially also as a catalyst (Woese, 1967; Crick, 1968; Orgel, 1968). With the discovery of the first catalytically active RNA in 1982 (Kruger *et al*, 1982; Guerrier-Takada *et al*, 1983) this idea was confirmed and the new term "RNA world" was chosen for a primordial state which existed before proteins were evolved as biocatalysts (Gilbert, 1986).

The catalytically active nucleic acids were called “ribozymes”. In 1986, the first hammerhead ribozyme was reported by Bruening (Prody *et al*, 1986) as a self-processing motif within RNA replicons associated with plant RNA viruses and virusoids. Later the hammerhead ribozymes were converted into trans-acting

ribozymes (Sampson *et al*, 1987). Biological and crystallographic analyses have shown that the hammerhead ribozyme, containing around 30 nucleotides, is one of the smallest catalytic RNAs active under physiological conditions (Symons, 1989; Uhlenbeck, 1987; Haseloff & Gerlach, 1988).

The essential structural elements of the hammerhead ribozyme can be two-dimensionally represented with three Watson-Crick base-paired helices I, II and III (Fig. 7).

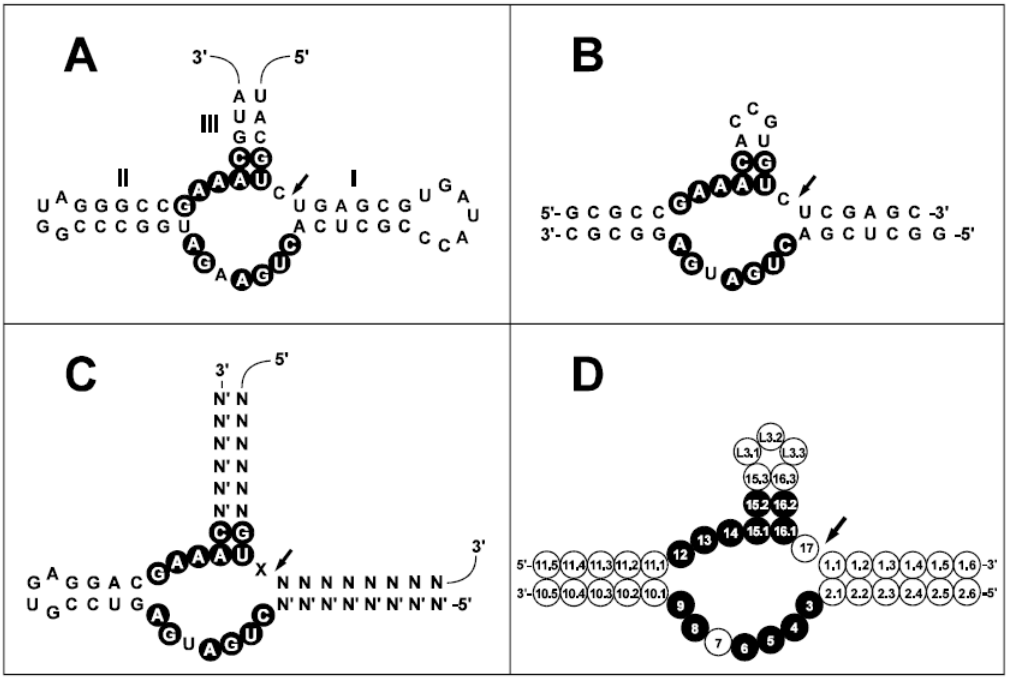

Figure 7: Secondary Structure of the hammerhead ribozyme. Conserved nucleotides are in black background, arrows indicate the cleavage site. N represents any nucleotide. (A) The hammerhead motif, which was proposed by Forster & Symons for the first time in 1987. I, II and III indicate the three helices. (B) The hammerhead structure by Uhlenbeck (1987), multiple turnover was shown for the first time. (C) The hammerhead motif by Haseloff & Gerlach (1988), which made a therapeutic application of the hammerhead ribozyme (cleavage of an mRNA) possible. (D) Since 1992, the nomenclature according to Hertel et al. has been adopted for the numbering of the nucleotide positions of the hammerhead ribozyme (Kindly provided by J. P. Fürste).

The cleavage mechanism of the hammerhead ribozyme is similar to general acid-base catalysis (Fig. 8). The proton of the 2´-hydroxyl group is removed and the 2´-oxygen attacks the adjacent 3´-phosphorus as a nucleophile. With the departure of the 5´-oxygen a cyclic 2´,3´-phosphate product and a 5´-hydroxyl product are created. The chirality of the phosphorus becomes inverted during this reaction (van Tol *et al*, 1990).

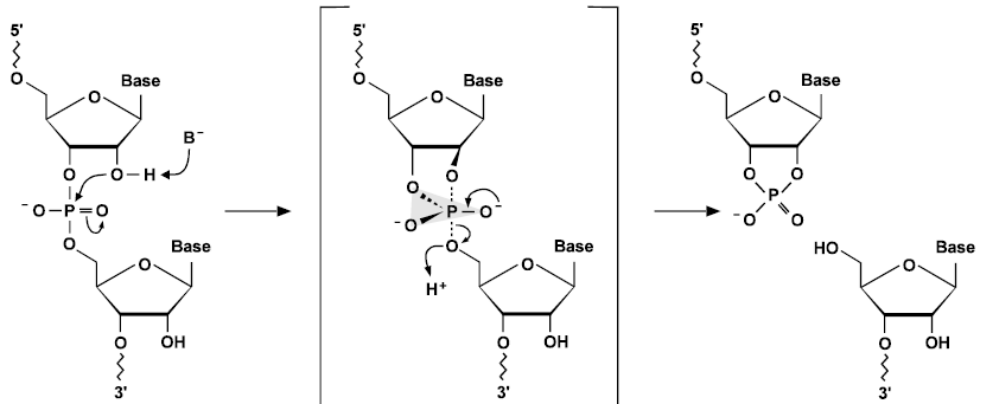

Figure 8. The catalytic mechanism of cleavage phosphodiester bond by small ribozymes. The 2´-OH group acts as the nucleophile in the reaction, a 2´, 3´- cyclic phosphate product and a 5´-hydroxyl product are generated (Kindly provided by J. P. Fürste).

Using in vitro selection techniques SELEX (*Systematic Evolution of Ligands by EXponential Enrichment*) (Ellington & Szostak 1990, Tuerk and Gold 1990), the first ribozyme able to cleave a DNA substrate and the first DNA ribozyme were developed in 1992 and 1994, respectively (Beaudry & Joyce, 1992; Breaker & Joyce, 1994).

1.2 Nanoparticles

1.2.1 Basic Properties of Nanoparticles

Nanoparticles are defined as solid aggregates smaller than 1000 nm (between 1 nm and 1000 nm) in size (Schmid, 1994). Under this definition the nanoparticles can be classified in two subgroups: clusters and colloids. The term “cluster” describes the smaller units with a defined and countable number of atoms. A cluster could consist of only a few, a dozen or a few hundred metal atoms. The term “colloids” refers to bigger aggregates with a few thousand metal atoms and they are in the 1 nm to 1000 nm size range. There is an overlap between the dimensions of the larger molecular clusters and the smallest metal colloids. Such large clusters like $[Ni_{34}Pt_6(CO)_{48}H]^{5-}$ are called “giant clusters”.

The size range of nanoparticles is situated between the molecular and the bulk phase. At this scale, quantum size effects (or “size quantization effects”) become dominant (Halperin, 1986; de Heer, 1993). The term “quantum size effects” describes the phenomena that a number of physical properties of solids (heat conductivity, electrical, optical and magnetic) are altered with great reductions in particle size. These effects can no longer be observed from macro to micro dimensions.

Variable synthetic procedures of different nanoparticles can be assigned to two basic approaches: top-down and bottom-up. In top-down approaches, macroscopic materials are dissipated into small particles with sizes in the nanometer range by e.g. milling or lithographic processes. In bottom-up approaches, smaller components like atoms or molecules are arranged into nanoparticles. The assembly is usually done via wet chemical routes.

In Figure 9, the nanoparticles with a “core/shell” structure are shown. Depending on the material composition, the core/shell nanoparticles can be classified into three groups: inorganic core/shell nanoparticles, organic-inorganic hybrid core/shell nanoparticles and polymeric core/shell nanoparticles (Sounderya & Zhang, 2008). In this work, iron oxide core/ silica shell nanoparticles are functionalized with different groups (such as amine, epoxyl and sulfhydryl) to realize further chemical modification.

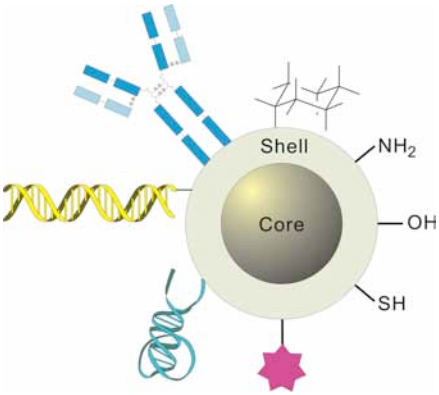

Figure 9. Core/shell structure of nanoparticles. The different ligands or active groups on the nanoparticle surface can offer various functions.

1.2.2 Magnetic Nanoparticles and Superparamagnetism

The term “magnetic nanoparticles” refers to nanoparticles, which can be manipulated using a magnetic field gradient and may display superparamagnetism. Their size is typically around 10–20 nm. The cores of superparamagnetic (SPM) nanoparticles are commonly made up of magnetic elements such as iron, nickel or cobalt. A coating layer can prevent magnetic nanoparticles from aggregation. Suspensions of SPM nanoparticles are called magnetic fluids.

Superparamagnetism occurs when the magnetic particles become so tiny that random thermal vibrations below Curie temperature cause them to lose their ability to hold their magnetic orientation, resulting in a spontaneous reversal of the magnetization (Kumar, 2006). The total magnetic moment of a fine particle system in the absence of an external field is zero. When an external magnetic field is applied, the system demonstrates a net average magnetization along the applied field (Andrä & Nowak,1998). Superparamagnetism can appear in ferromagnetic or ferrimagnetic nanoparticles. In ferromagnetic materials (ferromagnets) the magnetic moments of atoms are parallel and equal, while in ferrimagnetic materials (ferrites) the magnetic moments of atoms on different sublattices are opposed as in antiferromagnetism. The opposing moments are unequal and a net magnetization is generated by antiferromagnetic coupling. The size of superparamagnetic nanoparticles is much

smaller than a magnetic domain (1–100 nm), therefore each nanoparticle can be regarded as a single magnetic domain (Jordan et al. 1993). A single-domain particle is uniformly magnetized with all the spins aligned in the same direction. The energy which is responsible for holding the magnetic moments along a certain direction is called magnetic anisotropy energy. In an AC magnetic field, such particles will rotate to bring the magnetization to zero (Lu *et al*. 2007). During the rotation the superparamagnetic particles can generate heat due to the energy loss, which can be characterized by Brownian rotation and Néel relaxation processes. Brownian rotation refers to the physical rotation of the particles themselves within the fluid. This means: when the magnetic moment of single nanoparticle aligns with the magnetic field, the particle rotates as well. The Brownian process can be characterized by a relaxation time τ_B, which depends on the hydrodynamic properties and medium viscosity of the fluid. The Néel relaxation is known as the rotation of the magnetic moment within each particle core. The Néel process is characterized by a relaxation time τ_N, which is determined by the magnetic anisotropy energy of superparamagnetic nanoparticles relative to the thermal energy (Pankhurst et al, 2003; Rosensweig 2000).

Most magnetic nanoparticles currently applied *in vivo* are composed of the iron oxides magnetite (Fe_3O_4) or maghemite (γ-Fe_2O_3), because these exhibit a low toxicity compared to other magnetic materials (Thiesen & Jordan, 2007). Over the last several decades, superparamagnetic iron oxide nanoparticles have been widely used for biomedical applications, such as cell labeling and separation, tissue repair, drug delivery, magnetic resonance imaging (MRI) and hyperthermia (Arbab et al, 2003; Gupta & Gupta, 2005).

1.2.3 Hyperthermia and Magnetic Fluid Hyperthermia

Hyperthermia therapy is a type of medical treatment to fight cancer. In this therapy, body tissue is exposed to high temperatures and the cancer cells will be directly killed by heat damage or become more sensitive to the combined radio- and chemotherapy. The clinically relevant temperature range for hyperthermia is 39–45 °C (Kampinga, 2006). If the therapeutic temperature is higher than 46 °C, it is defined as thermoablation, a direct destruction due to high temperature. Hyperthermia can be

clinically classified in local hyperthermia (heating of the tumor itself), regional hyperthermia (heating of a part of body) and whole-body hyperthermia.

The temperature increase for hyperthermia can be achieved by many techniques, such as ultrasound, infrared radiation, microwave heating, induction heating, magnetic fluid hyperthermia, infusion of warmed liquids or direct exposure to the body in a hot room. As this work is relevant to magnetic fluid hyperthermia, this method will be described in more detail.

Magnetic fluid hyperthermia (MFH) is a heat treatment based on the fact that the superparamagnetic nanoparticles can be heated in an alternating magnetic field by Brownian and Néel relaxation processes. The heat production capability of superparamagnetic nanoparticles can be characterized by their specific absorption rate (SAR), which is dependent on the specific particle attributes (such as particle size, shape, composition and coating) and external parameters (such as H-field and frequency). The SAR can be determined as:

$$SAR = C\frac{\Delta T}{\Delta t}$$

In the equation, C is the specific heat capacity of the sample (MF) calculated as mass weighted mean value between magnetic component and water; $\Delta T/\Delta t$ is the initial slope of temperature increase versus the heating time. SAR is measured in units of W/g (Schmid, G. 2010).

MFH is a local thermotherapy and the target is precisely defined by the accumulation of magnetic nanoparticles. To protect healthy tissue, AC magnetic field strength, frequency, tissue conductivity and body cross-section should be considered during the therapy. The inductive normal tissue load at the surface of the body should not exceed 25 mW/g, which is a tolerable power absorption for human application (Jordan *et al*, 1993). In case of higher SAR, severe skin burns, erythema and other tissue damage as well as increasing pain will occur during AC magnetic field application. In terms of an undesirable electromagnetic stimulation of the peripheral and skeletal muscles, cardiac stimulation and arrhythmia should be avoided. The ranges of frequency and field strength considered to be safe for humans are 0.05-1.2 MHz and 0-15 kA/m (Schmid, G. 2010).

The history of the use of magnetic particles for hyperthermia dates back to half a century ago. In 1957 magnetic particles with a size of a few μm were used for inductive heating of lymph nodes in dogs (Gilchrist *et al.*, 1957). In 1979 a magnetic fluid was applied for hyperthermia (Gordon *et al*. 1979). Jordan et al. first reported a direct injection of dextran-coated magnetite nanoparticles with a core size of approximately 3 nm into a tumor in 1997 (Jordan, 1997). It was further reported that hyperthermia was applied successfully for the treatment of glioblastoma multiforme with iron oxide nanoparticles coated by an aminosilane-type shell (Thiesen & Jordan, 2008; Klaus Maier-Hauff *et al*, 2010).

The reason why hyperthermia can be applied for cancer treatment is that the activation energies for protein denaturation and heat-induced cell death are in the same range with hyperthermia: 39–45 °C (Kampinga, 2006, Jordan *et al.* 1997). Among all the proteins in the cells, nuclear proteins are most sensitive to heat-induced denaturation (Lepock *et al*. 1993; Lepock, 2004). In addition, the nuclear environment is the most favorable compartment for aggregation to occur (Michels *et al*, 1995; Michels *et al*, 1997). These two findings together explain why various nuclear processes are extremely heat-sensitive (Roti Roti *et al*. 1988) and why a correlation exists between nuclear protein aggregation and heat killing (Kampinga *et al.* 1989).

A few hours of chronic heating (T < 42.5°C) or a brief acute heating (priming heat shock) followed by a period of incubation at 37°C can cause thermotolerance, which is a transient state of thermal resistance following prior heat treatment (Jung & Dikomey, 1988). The thermotolerance is conferred by heat shock proteins (HSP), which are encoded by heat shock genes and belong to the superfamily of molecular chaperones.

Molecular chaperones are proteins that assist the folding of non-native or unfolded proteins in order to prevent their irreversible aggregation (Ellis & Van der Vies, 1991). HSP normally binds to the responsible transcription factor HSF-1 to inhibit the transcription of heat shock genes. Under thermal stress, as more proteins lose their native structure HSP is released from HSF-1 to bind to unfolded proteins with higher affinity. Free HSF-1 initiates the transcription of heat shock genes, and as a result

new HSP will be produced. Once the protein aggregation is reversed after heat shock by HSP, the HSP will rebind to HSF-1 (Morimoto, 1998). Therefore, when HSP levels in the cell are sufficiently high to cope with the aggregation, the heat-induced damage can be reversible (Kampinga, 2006).

It is well documented that additional heat treatment can enhance cellular radiosensitivity, so-called thermal radiosensitization. This phenomenon is caused mainly by aggregation of nuclear proteins (Kampinga, 2001; Lepock, 2004). The synergy between heat and radiation is expressed as thermal enhancement ratio (TER). The maximal TER appears during or immediately after heating before the HSP levels increase. When HSP levels reach maximum and the nuclear protein aggregation is reversed, cells have regained normal radiosensitivity (Kampinga, 2006).

Heat can also enhance the cellular sensitivity to some chemotherapeutic drugs like alkylating agents, nitrosureas, cisplatin and some antibiotics (Dahl, 1988). The major mechanisms of this relationship could be the increased uptake of chemotherapeutic drugs upon heating. However, the relation is not so clear and the combination of chemotherapy and hyperthermia needs to be investigated in detail for each drug applied with hyperthermia.

1.2.4 NanoTherm® Therapy

The NanoTherm® therapy, also termed magnetic fluid hyperthermia, combined with fractionated stereotactic radiotherapy, is a new local heat treatment of solid tumors (such as glioblastoma multiforme and prostate carcinoma). Jordan and his colleagues have started developing this method to fight solid tumors almost 20 years ago (Jordan *et al*. 1993). Three major components are required for NanoTherm® therapy: NanoTherm®, Nanoplan® and NanoActivator™ F100 (MagForce Nanotechnologies AG, Berlin, Germany).

NanoTherm is a magnetofluid consisting of superparamagnetic iron oxide nanoparticles which are colloidally dispersed in water with a high iron concentration, starting from 112 mg/ml. The iron oxide magnetite (Fe_3O_4) core is approximately

12 nm in diameter and coated with an aminosilane-type shell (Fig. 10), which causes the particles to aggregate as soon as they come in contact with physiological media. Thus, NanoTherm forms a stable deposit once it is injected into the tumor.

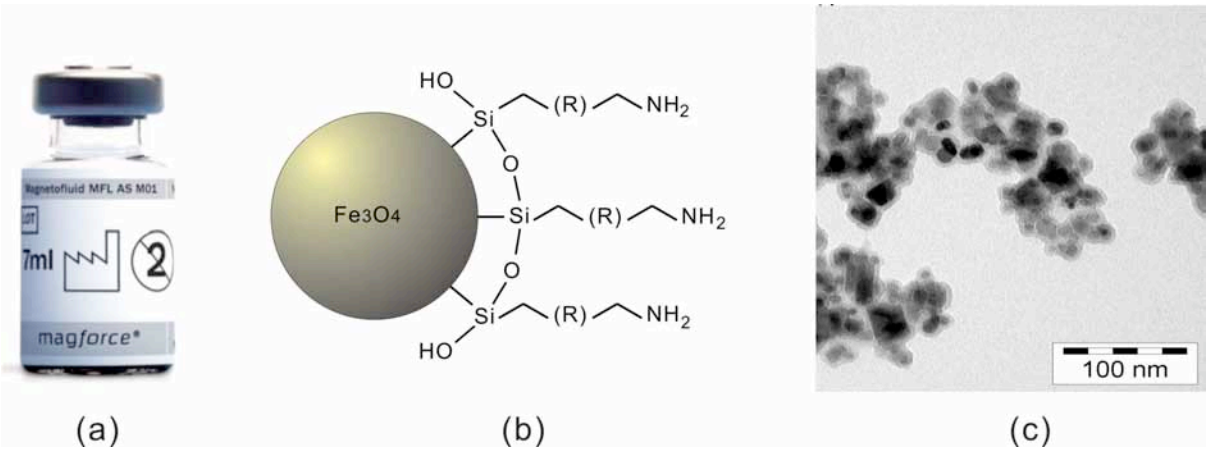

Figure 10: Nanotherm®. (a) Nanotherm® (MagForce Nanotechnologies AG, Berlin, Germany). (b) Structure of Nanotherm® nanoparticles. (c) TEM image of iron oxide nanoparticles. (a and c are reprinted with permission from MagForce Nanotechnologies AG, Berlin, Germany)

Nanoplan refers to a newly developed software platform, which is used for a precise treatment planning of NanoTherm® therapy. NanoActivator® F100 (Fig. 11) is a magnetic field applicator, which was developed specifically for NanoTherm® therapy. This applicator can generate the magnetic field of 100 kHz and variable field strength of 2−15 kA/m required for the therapy. Due to its universal design, the NanoActivator® F100 applicator can be used for the treatment of solid tumors at almost every location of the human body (Thiesen & Jordan, 2008).

Figure 11: NanoActivator® F100**.** The alternating magnetic filed applicator NanoActivator® F100 is developed by MagForce Nanotechnologies AG, Berlin, Germany. (Reprinted with permission from MagForce Nanotechnologies AG, Berlin, Germany)

NanoTherm® therapy has been used successfully to treat glioblastoma multiforme (Thiesen & Jordan, 2008; Maier-Hauff *et al.*, 2010). Glioblastoma multiforme (GBM) is the most prevalent malignant brain tumor in adults (Stupp *et al.*, 2005). Standard therapy consists of surgical resection, followed by radiotherapy and/or chemotherapy. A complete resection, however, is almost impossible due to the invasive nature of this malignant brain tumor. Median overall survival after first-line therapy is still not exceeding 12–15 months (Jordan *et al.*, 2006). NanoTherm® therapy provides an alternative therapeutic treatment against glioblastoma and median overall survival after primary tumor diagnosis was prolonged to 23.2 months (Maier-Hauff *et al.*, 2010).

In the phase II glioblastoma multiforme trial completed in 2009 (Maier-Hauff *et al.*, 2010), a combined treatment of fractionated stereotactic radiotherapy and NanoTherm® therapy was applied to 66 patients (59 with recurrent glioblastoma). The magnetic fluid MFL AS1 (NanoTherm AS1, c=112 mg/ml) was injected directly into the tumor with the help of a neuro-navigational guide by surgery. The nanoparticles remained in the tumor due to their special coating. A fiber-optic thermometry probe was installed into the tumor after injection of the nanoparticles for a temperature measurement during the hyperthermia sessions which were carried out in NanoActivator® F100. Patients received 6 semi-weekly sessions and each thermotherapy session lasted 1 h. The median temperature measured within the tumor area during the hyperthermia was 51.2°C (maximum 82.0°C). The combined fractionated stereotactic radiotherapy had a median dose of 30 Gy using a fractionation of 5 x 2 Gy/week. In 2010 MagForce Nanotechnologies AG received European regulatory approval for its NanoTherm® therapy.

1.2.5 Nanoparticles and Drug Delivery

Traditional chemotherapies are relatively non-specific and result in deleterious side effects as the drugs attack healthy cells, too. To overcome this disadvantage, magnetic nanoparticles have become an attractive candidate for drug delivery in the last several decades due to their unique physical properties and ability to function at

the cellular and molecular level of biological interactions (Pankhurst *et al.*, 2003; McNeil, 2005; Derfus *et al.,* 2007).

Magnetic nanoparticles have a suitable size as drug-delivery agents to get close to a biological target. Human cells have the size of 10,000 to 20,000 nm in diameter (McNeil, 2005), so they are almost 1,000 times larger than magnetic nanoparticles. A protein is normally 5–50 nm in diameter and a gene is 2 nm wide and 10–100 nm long (Pankhurst *et al.*, 2003). The magnetic nanoparticles are small enough to avoid rapid filtration (≥200 nm) by the spleen as well as small enough to pass through the fenestrae in liver (150-200 nm) (McNeil, 2005).

To target tumors either passive or active strategies can be used (Arruebo *et al.*, 2007). Passive delivery means that the nanoparticles transit through leaky tumor capillary fenestrations into the cell interstitium by passive diffusion or convection (Yuan, 1998). The blood vessels in the tumor are irregular in shape (e.g. dilated or leaky) and the endothelial cells are poorly aligned or disorganized with large fenestrations. In addition, the perivascular cells, the basement membrane or the smooth-muscle layer are often absent or abnormal in the vascular wall. This anatomical defectiveness results in an enhanced permeability of tumor vessels to allow macromolecules, such as nanoparticles, travel into tumor tissues. Furthermore, tumor tissues have poor lymphatic drainage and slow venous return, which lead to the retaining of macromolecules in the tumor tissues. This phenomenon is defined as enhanced permeability and retention (EPR) effect (Matsumura & Maeda, 1986; Lyer *et al.*, 2006) (Fig. 12) and a selective accumulation of nanoparticles in tumor could occur by this EPR effect.

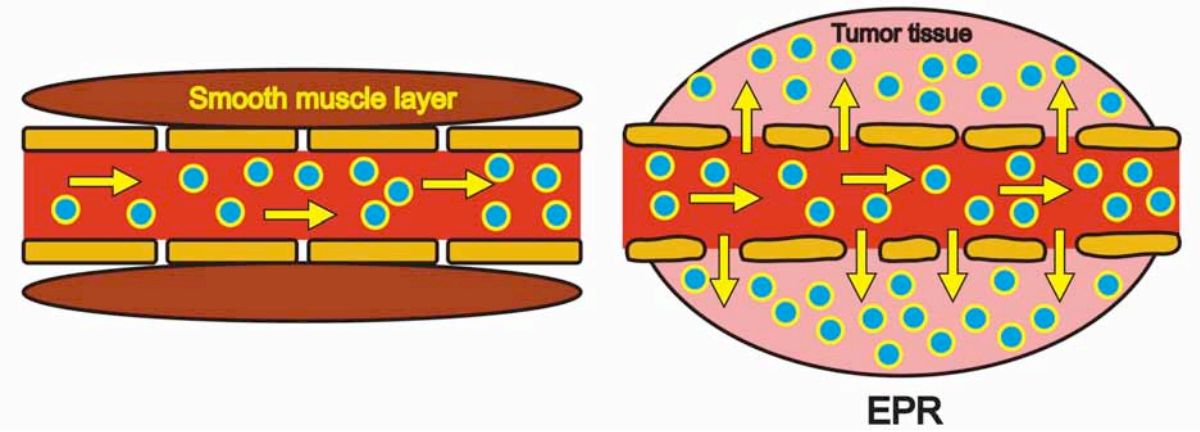

Figure 12: EPR effect. Left: normal blood vessels have regular endothelial cells and tighter endothelial gap junctions, which prevent that the macromolecules (blue spots with yellow circles) pass through the vessel wall into normal tissues. **Right:** Due to the irregular form of endothelial cells and the absence of a smooth-muscle layer, macromolecules can travel into the tumor tissue (in pink) by passive diffusion and accumulate in it. This phenomenon is called EPR effect (adopted from Lyer *et al.*, 2006).

Active targeting is based on specific recognition between molecules. A ligand able to specifically interact with a surface receptor of the target cell can be coupled on the nanoparticles (Haley & Frenkel, 2008). Antibody (Bhattacharyyaa *et al.*, 2010), aptamer (Nair *et al.,* 2010) and other ligands such as folate (Kukowska-Latallo *et al.,* 2005) have been conjugated on nanoparticles successfully for active targeting.

Once the conjugates of nanoparticle and drug accumulate at the target, the therapeutic drug can be released either via enzymatic activity or changes in physiological conditions such as pH value (Kohler *et al.,* 2005), temperature (Derfus *et al.,* 2007) or hydrolytic degradation (Gref *et al.,* 1994). This system theoretically can overcome the major disadvantage of the normal non-specific chemotherapy and realize a locally restricted cytotoxic drug therapy.

1.3 Crosslinker and Bioconjugation

In the following chapter, some crosslinkers will be introduced, which are relevant to this work. Depending on their chemical functionalities the crosslinkers can be classified as zero-length crosslinkers, homobifunctional crosslinkers and heterobifunctional crosslinkers. In this work, crosslinkers were used not only to conjugate iron oxide nanoparticles modified with differently active groups (such as amine, epoxyl and sulfhydryl) and oligonucleotides (Fig. 13), but also to couple cytostatic drugs to DNA.

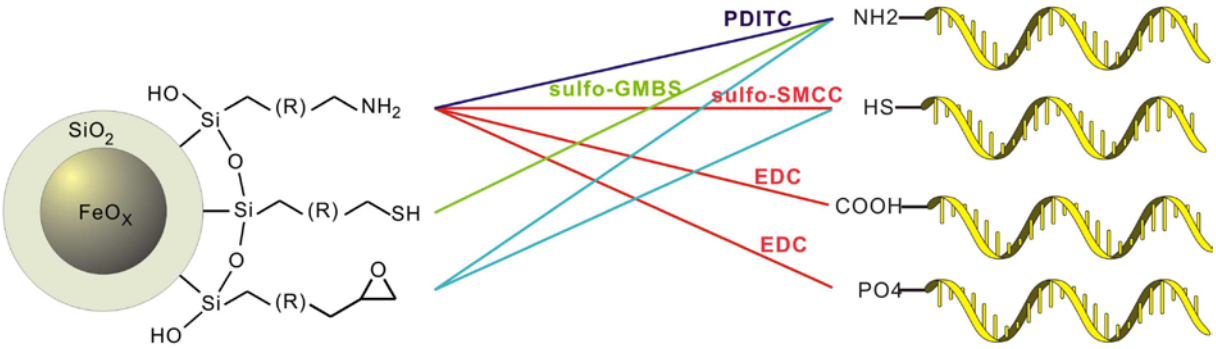

Figure 13: Nanoparticle–Oligonucleotides Conjugation via Crosslinkers.

1.3.1 Zero-Length Crosslinkers

Zero-length crosslinkers are the smallest reagent system for bioconjugation. They can mediate the conjugation of two molecules by forming a new bond without any additional atoms.

1.3.1.1 Carbodiimides

Carbodiimides are likely the most popular type of zero-length crosslinker and are used to form amide linkages or phosphoramidate linkages (Hoare & Koshland, 1966; Chu *et al.*, 1986; Ghosh *et al.*, 1990). According to their solubility carbodiimides can be divided into two classes: water-soluble (e.g. EDC) and water-insoluble (e.g. DCC).

EDC (1-ethyl-3-(3-dimethylaminopropyl)carbodiimide hydrochloride)

EDC is the most favored carbodiimide and also probably the most frequently used crosslinking agent of all for biochemical conjugation. EDC can mediate the coupling between substances containing carboxylates and amines as well as the substances containing phosphates and amines. EDC is water-soluble but labile in the presence of water. The bulk chemical should be stored at −20 °C. A concentrated stock solution should be dissolved rapidly in aqueous buffer and used immediately to avoid extensive loss of activity.

To conjugate substances containing carboxylates and amines, EDC reacts with a carboxyl group first to form a highly reactive O-acylisourea intermediate, which will react quickly with a nucleophile such as a primary amine to form an amide bond (Williams & Ibrahim, 1981). In this reaction, an isourea by-product is released (Fig. 14). The O-acylisourea intermediate could be hydrolyzed by water in aqueous solutions undesirably, forming an isourea and regenerating the carboxyl group (Gilles *et al*, 1990).

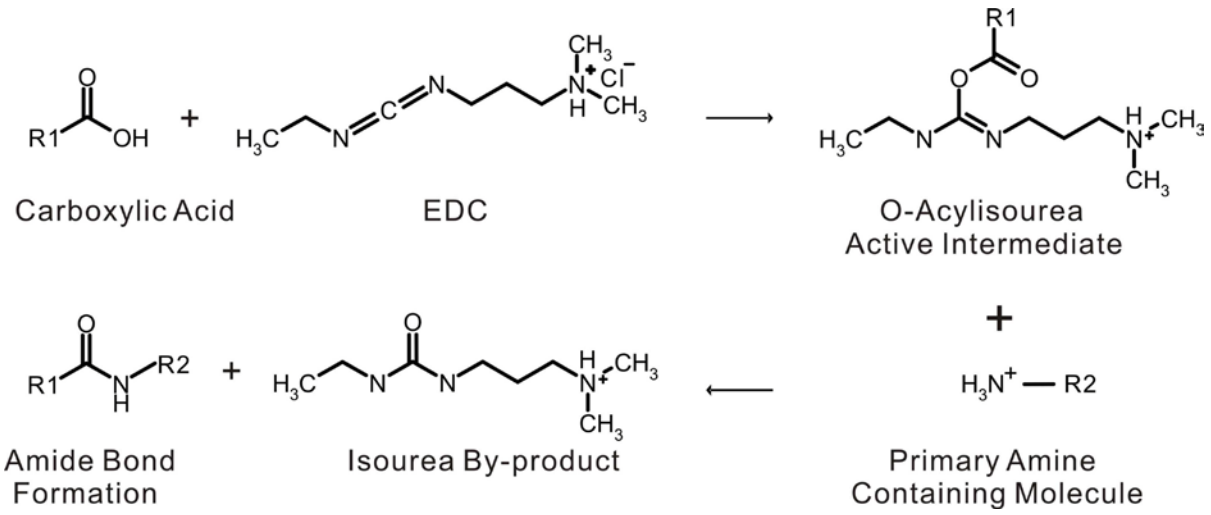

Figure 14: EDC mediates the conjugation between two molecules containing carboxyl and amine group. The unstable O-acylisourea intermediate is highly reactive and finally an amide bond is formed with release of an isourea by-product.

It was reported that carboxylate activation occurs most effectively with EDC at pH 3.5–4.5, while amide bond formation happens with highest yield at pH 4.0–6.0 (Nakajima & Ikyda, 1995). Most references use a reaction medium for EDC in the pH range 4.7-6.0. MES (2-(N-morpholino)ethane sulfonic acid) buffer at 0.1 M is usually recommended. Amine- or carboxylate-containing buffer systems should be avoided.

EDC can be used together with imidazole to conjugate molecules containing phosphate and amino group. EDC reacts with the phosphate group first to form an unstable active ester intermediate, which can react quickly with imidazole. Thus, an isourea by-product is released and reactive phosphorylimidazolide is formed. The reactive phosphorylimidazolide reacts further with the primary amine of the other molecule to form a phosphoramidate bond and an imidazole will be regenerated (Fig. 15). It is recommended to use PBS at pH 7.2 as reaction buffer and 0.1 M imidazole at pH 6.0.

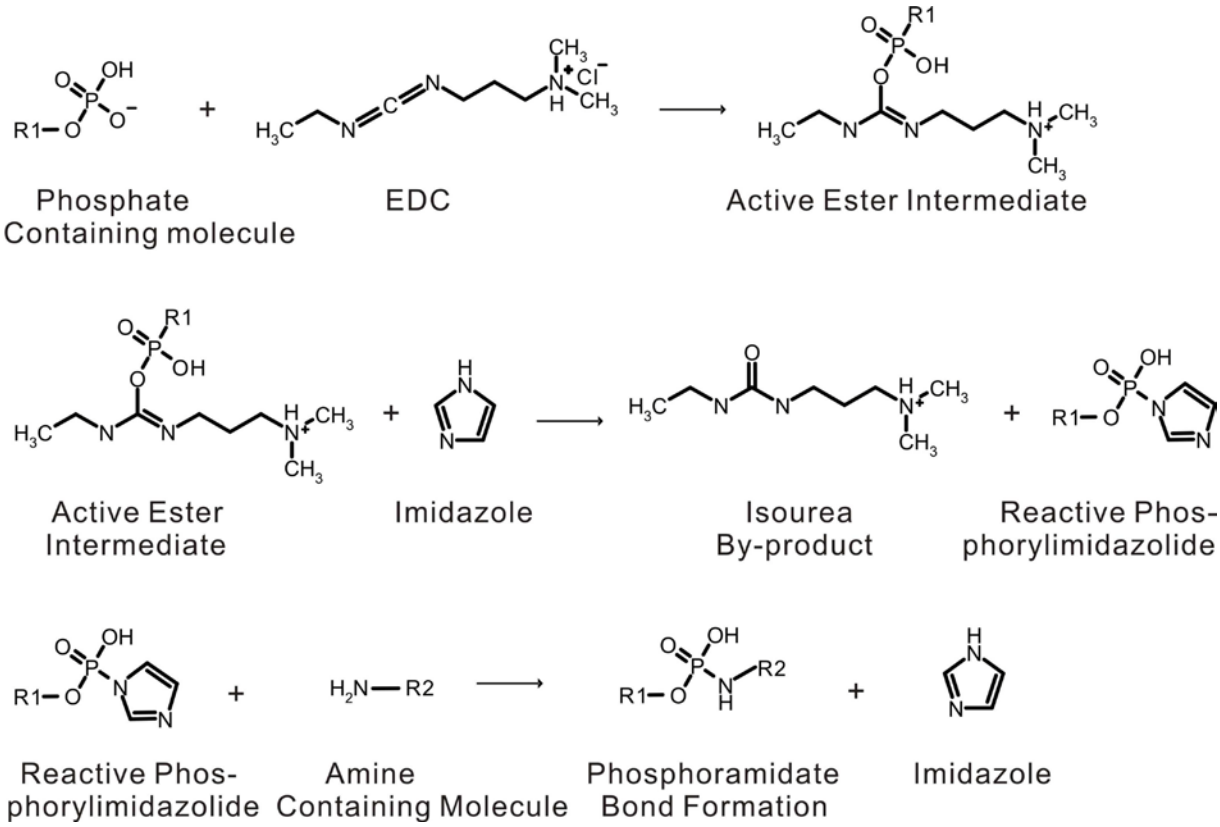

Figure 15: EDC and imidazole mediate the conjugation between two molecules containing a phosphate and an amine group.

DCC (dicyclohexyl carbodiimide)

DCC is a frequently used coupling agent in organic reaction environment for conjugating of molecules containing carboxyl and amino group. It was used for the first time for peptide synthesis in 1955 (Sheehan & Hess, 1955) and since has become a popular reagent for the formation of amide bonds (Barany & Merrifield, 1980). DCC is water-insoluble and the reaction is carried out in dimethylformamide

(DMF) normally. NHS (*N*-hydroxysuccinimide) or sulfo-NHS can be used with DCC to form amide linkages (Staros, 1982).

DCC reacts with a carboxyl group of one molecule first to form an unstable o-acylisourea intermediate, which can react quickly with NHS (or Sulfo-NHS) to form an NHS ester intermediate, while dicyclohexylisourea (solid) is released as by-product. The NHS ester intermediate reacts further with the primary amine of the other molecule to form an amide bond and NHS will be regenerated (Fig. 16). It is recommended to use dioxane or DMF as solvents.

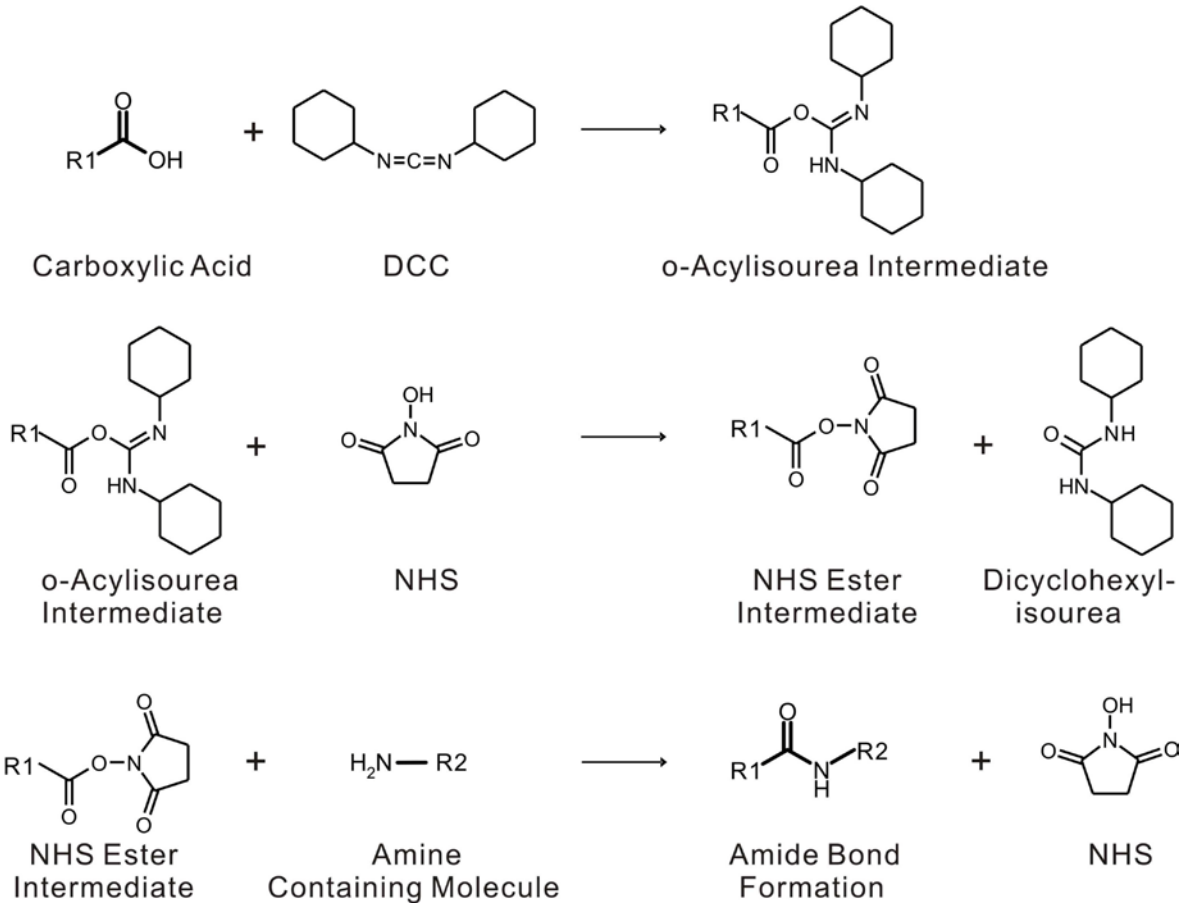

Figure 16: DCC and NHS mediate the conjugation between two molecules containing carboxyl and amine group forming amide bonds.

1.3.1.2 *N,N´*-Carbonyldiimidazole

CDI (*N,N´*-Carbonyldiimidazole) contains two acylimidazole leaving groups. It is a highly active carbonylating agent. CDI can activate carboxyl or hydroxyl groups for conjugation with other nucleophiles. The carboxylic acid group reacts with CDI first,

N-acylimidazole with high reactivity will be formed and an imidazole released. This reaction occurs with excellent yields (Anderson, 1958). The active intermediate reacts further with amine to create amide bonds (Fig. 17).

The activation of carboxyl or hydroxyl group must be carried out in non-aqueous environment, because CDI would be hydrolyzed into CO_2 and imidazole in aqueous solution. Solvents should contain less than 0.1% water to prevent extensive CDI breakdown. Bubble formation indicates either reagent hydrolysis or reaction with carboxylic acid. Dry organic solvents such as acetone, dioxane, DMF, THF (tetrahydrofuran) or DMSO (dimethylsulfoxid) can be used as solvents for the activation step.

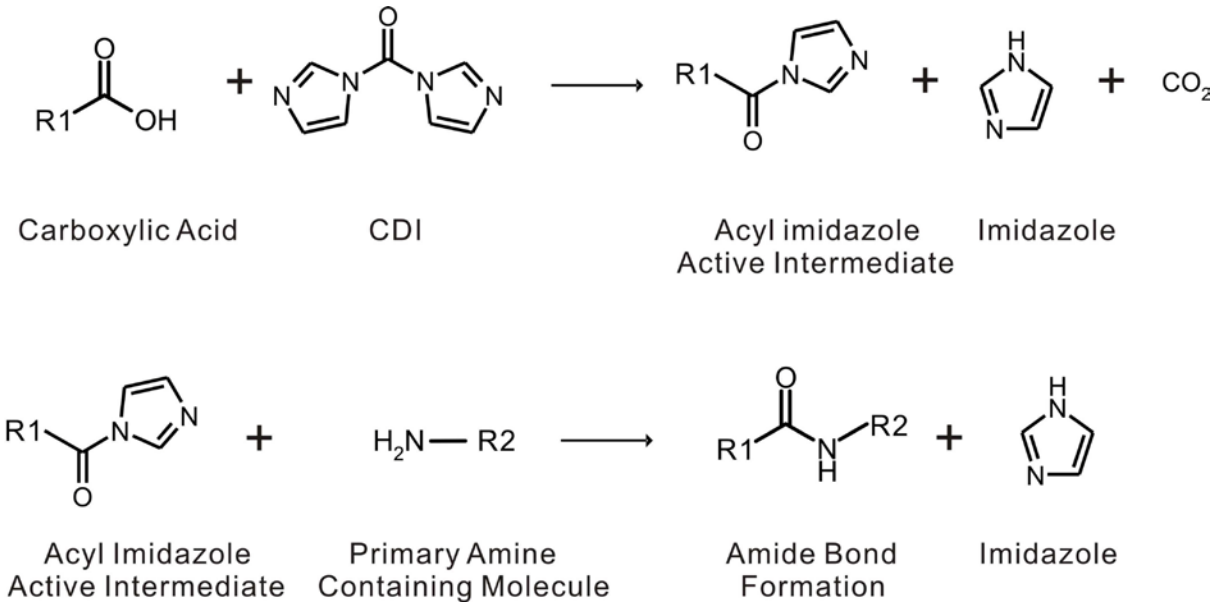

Figure 17: CDI mediates the conjugation between two molecules containing carboxyl and amine group to form an amide bond. CDI reacts first with the carboxylate group to form an active acylimidazole intermediate. CO_2 and imidazole are released. The intermediate reacts with a primary amino group and an amide bond will be created with the release of imidazole.

After the highly active N-acylimidazole intermediate is created, the conjugation with primary amine via amide bond formation takes place preferably in aqueous conditions to increase yields. The greatest yields are frequently obtained in alkaline buffers in the range of pH 8.0–10.0, for example 0.1 M sodium borate buffer at pH 9.3.

1.3.2 Homobifunctional Crosslinkers

Homobifunctional crosslinking reagents have normally a symmetrical structure, which contains a carbon chain spacer in the middle and two identical reactive groups at both ends. The first reagent used for conjugation of macromolecules was a homobifunctional crosslinker: dimethyladipimidate (Hartman & Wold, 1966). They are suitable for the formation of protein dimers or polymers, or for the immobilization of macromolecules. Their major disadvantage is that intramolecular crosslinks are difficult to avoid when two different substances are to be coupled in a one-step protocol.

PDITC

PDITC (1,4-phenylene diisothiocyanate) is a homobifunctional crosslinking reagent relevant to this work. It contains two amine-reactive isothiocyanate groups on a phenyl ring. PDITC can couple two molecules containing primary amino groups. An isothiourea linkage is formed between two molecules (Fig. 18).

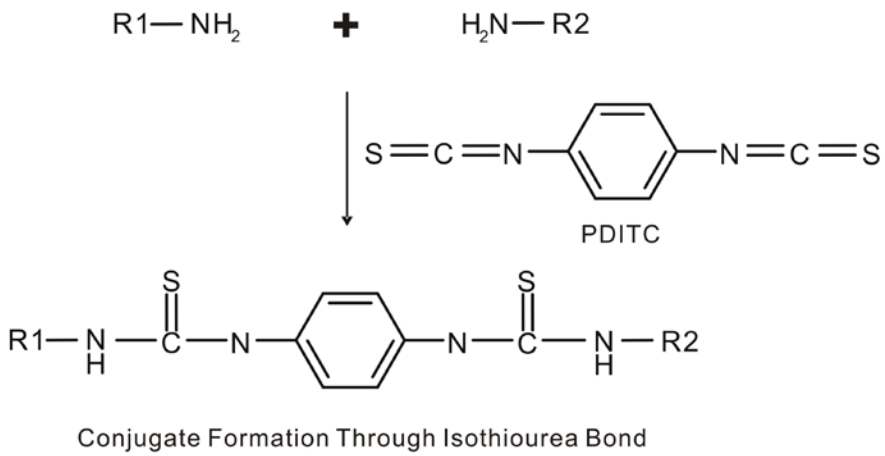

Figure 18: The homobifunctional crosslinker PDITC conjugates two molecules containing primary amino groups by creating an isothiourea linkage.

It is recommended to dissolve PDITC in DMF, while the reaction could be carried out in 0.1 M sodium borate buffer at pH 9.3 according to the protocol by Keller and Manak (Keller & Manak, 1989).

1.3.3 Heterobifunctional Crosslinkers

Heterobifunctional crosslinking reagents contain two different reactive groups, hence they can couple to two molecules with different functional groups. The coupling procedures usually imply two or more steps. Such multi-step protocols offer a possibility to control the reaction.

Two heterobifunctional crosslinking reagents relevant to this work will be introduced in this section: SMCC (and sulfo-SMCC) and GMBS (and sulfo-GMBS). Both of them belong to the group of amine-reactive and sulfhydryl-reactive crosslinkers.

SMCC and sulfo-SMCC

SMCC (succinimidyl-4-(*N*-maleimidomethy)cyclohexane-1-carboxylate) and its water-soluble analogue sulfo-SMCC (Fig. 19) contain NHS (N-hydroxysuccinimide) ester and maleimide groups. They allow covalent coupling between amine- and sulfhydryl-containing molecules. SMCC and sulfo-SMCC are likely the most popular crosslinkers for protein conjugations, particularly in the preparation of antibody-enzyme and hapten-carrier conjugates (Hashida & ishikawa, 1985; Dewey *et al.*, 1987).

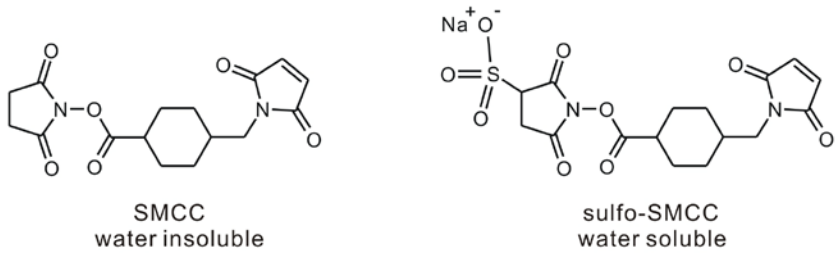

Figure 19: Structure of SMCC and sulfo-SMCC.

The NHS ester end of the reagents can react with primary amino groups to form stable amide bonds at pH 7.0–9.0. Their maleimide ends react with sulfhydryl groups in the range of pH 6.5–7.5. SMCC or sulfo-SMCC normally react first with the molecule containing the amine to create an SMCC-activated intermediate, the maleimide end of the intermediate then reacts further with the sulfhydrl group of the

other molecule. There is a spacer arm with a length of 8.3 Å between the two components in the newly created conjugate (Fig. 20).

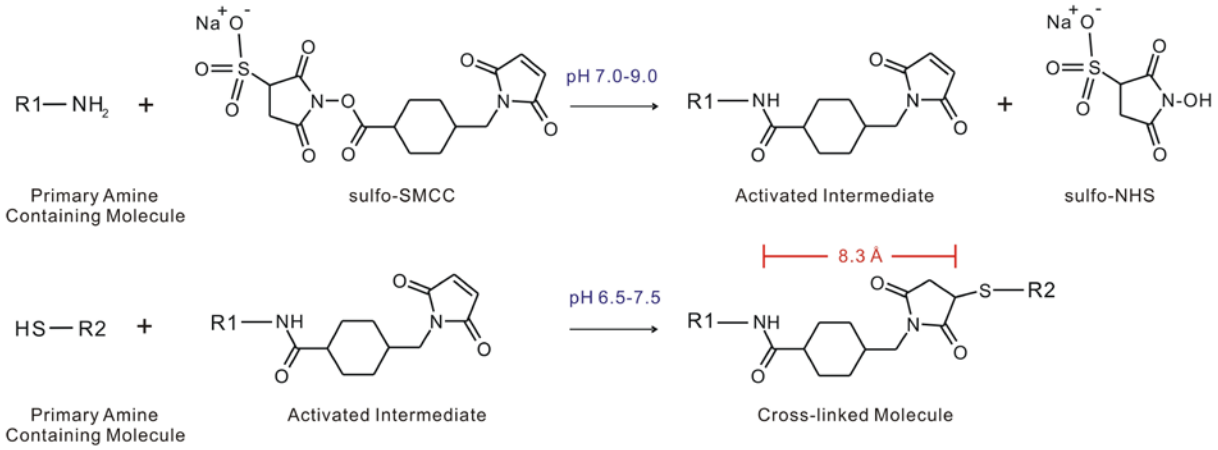

Figure 20: Sulfo-SMCC as crosslinker for the conjugation between two molecules containing primary amino group and sulfhydryl group. Sulfo-NHS ester of sulfo-SMCC reacts with amine to form a stable amide bond. Its maleimide end can be coupled to a sulfhydryl group upon forming of a thioether linkage. The spacer arm between two components in the conjugate is 8.3 Å.

At pH 7.0, the reaction of the maleimide group with sulfhydryls proceeds 1000 times faster than its reaction with amines. The maleimide end also can be hydrolyzed at higher pH values to an open maleamic acid form and become unreactive toward sulfhydryl groups. Hydrolysis may also occur after the coupling between maleimide and sulfhydryl. Thus, pH values higher than 7.5 should be avoided.

SMCC is water-insoluble and must first be dissolved in an organic solvent such as DMSO or DMF just before use, then it can be diluted with aqueous buffer or directly added into the reaction solution. Sulfo-SMCC is soluble in water due to the negatively charged sulfonate group on its NHS ring. A stock solution at a concentration of approximately 10 mM at room temperature in aqueous buffer can be prepared, but it should be dissolved rapidly and used immediately to prevent extensive loss of coupling capacity due to hydrolysis.

GMBS and sulfo-GMBS

GMBS (*N*-(γ-maleimidobutyryloxy)succinimide ester) and its water-soluble analogue sulfo-GMBS (Fig. 21) are heterobifunctional crosslinking agents that – like SMCC and sulfo-SMCC – contain an NHS (sulfo-NHS) ester on one end and a maleimide group on the other end (Fujiwara *et al*., 1988).

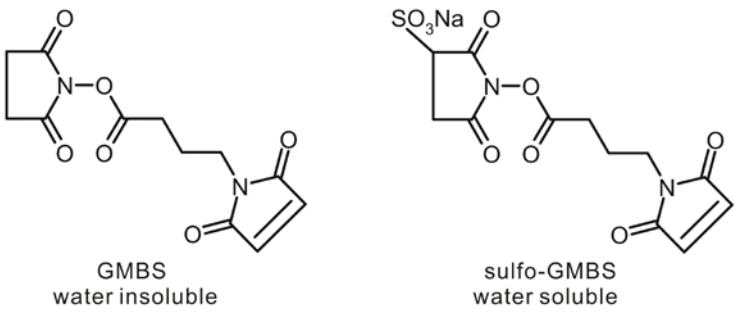

Figure 21. Structure of GMBS and sulfo-GMBS.

The conjugation mechanism and reaction conditions for using GMBS or sulfo-GMBS as crosslinker are similar to that of SMCC or sulfo-SMCC. The maleimide group of GMBS, however, is not as stable as of SMCC, because the cyclohexane ring of SMCC inhibits hydrolysis and ring opening.

2 Task

The aim of this work is to improve a novel approach in the clinical treatment of cancer. This approach concepts the thermally controlled release of cytotoxic drugs from nanoparticles, which can be heated by an externally applied alternating magnetic field. Since these particles can be administered directly into solid tumors, this strategy could lead to the development of a temperature controlled regional drug delivery system against cancer.

Nanoparticles have already proven to be successful agents in the treatment of solid tumors. MagForce Nanotechnologies AG (Berlin) has developed superparamagnetic nanoparticles, which already received a European approval as a medical device and are used in the clinic. After injection of these particles into tumors, patients are placed in a magnetic field applicator (Nano-Activator^{TM}), which produces an alternating magnetic field of a frequency that does not harm the patient. Through this field, the nanoparticles begin to oscillate and warmth is produced within the tumor tissue. Due to this temperature effect, tumor cells are either directly destroyed or sensitized for the accompanying chemotherapy.

This temperature control, however, could be used for the development of a conditional drug release and could eventually result in a local chemotherapy. Nucleic acids would be a suitable linker between nanoparticle and cytotoxic drug, since a dimeric DNA or RNA separates upon heat treatment into single strands. It is conceivable that one strand of the duplex is bound to the nanoparticle, while the complementary strand is bound to the cytotoxic drug. The particle and the drug will consequentially separate upon heat treatment. The nucleic acid would function as a conditional switch between the bound and the free status of the cytostatic drug. Thus, the objective of this work was to develop a proof of concept for this approach.

3 Methods

3.1 Analysis of Nucleic Acids

3.1.1 Gel Electrophoresis

Gel electrophoresis is the most widely used method for the analysis and purification of nucleic acids. A net charged molecule will move in an electric field. The velocity of migration of a molecule in an electric field is directly proportional to the electric field strength and the net charge on the molecule, and inversely proportional to the frictional coefficient, which depends on both the mass and shape of the migrating molecule as well as the viscosity of the medium. Electrophoretic separations are carried out in gels, and agarose and polyacrylamide are the most used gel matrices. With polyacrylamide gels, the separation of nucleic acids can be performed under either denaturing or native conditions, while normally the separation with agarose gel is possible only under native condition. The nucleic acids are negatively charged due to the phosphate groups of the sugar-phosphate backbone, so they migrate in an electric field from cathode to anode.

3.1.1.1 Agarose Gel Electrophoresis

Agarose gel electrophoresis is an easy and fast way of separating and analyzing large nucleic acids. Agarose is a linear polymer which consists of different galactose units and is extracted from red seaweeds. Diverse agarose concentration are applied for the analysis of different chain lengths of nucleic acids (Tab. 1).

Table 1: separating range of agarose gels.

Agarose-concentration (% w/v)	0,3	0,6	0,7	0,9	1,2	1,5	2	3
Separating range (bp)	500-60000	1000-20000	800-10000	500-7000	400 - 6000	200-3000	100-2000	< 100

In this work, 3% agarose gels were used for the analysis of nucleic acids fragments. Preparation was according to the instruction of the supplier (Roth, Germany). The

gels were prepared with 1xTBE buffer and were run in the same buffer at a current of 8 V/cm. Samples were mixed with a loading buffer that contained bromophenol blue and xylene cyanol. The gels were dyed with either ethidium bromide or SYBR Gold and visualized under ultraviolet (UV) light.

3.1.1.2 Polyacrylamide Gel Eletrophoresis (PAGE)

Polyacrylamide gels afford an accurate separation of nucleic acids due to their three-dimensional mesh form. The polymerization of the monomeric molecule acrylamide cross-linked by N,N'-methylene-bis-acrylamide forms polyacrylamide. Ammonium persulfate (APS) generates free radicals and N,N,N',N'-tetramethylethylene diamine (TEMED) acts as a catalyst to initiate the polymerization. Like agarose gels, diverse acrylamide concentrations are used for the analysis of different chain lengths of nucleic acids (Tab. 2).

Table 2: separation range of polyacrylamide gels

Acrylamide (%)	6-8	8-10	10-13,5	13,5-15	15-20	20-30
Separating range (bp)	70-300	45-70	35-45	25-35	8-25	2-8

3.1.1.2.1 Denaturing Polyacrylamide Gel Electrophoresis

Denaturing polyacrylamide gels are polymerized in the presence of urea to suppress the base pairing in nucleic acids. Denatured nucleic acids migrate through these gels at a rate that is independent of their base composition, secondary and tertiary structure. In this work, 10% to 20% polyacrylamide gels containing 7 M urea were prepared according to the instruction of the supplier (Roth, Germany) for the ssDNA and ssRNA analysis. The gels were run at 480–600 V (25–30 mA) in 1xTBE buffer.

Table 3: Protocol for denaturing polyacrylamide gel (7 M urea)

Acrylamide concentration	6 %	8 %	10 %	12 %	15 %	20 %
Acrylamide/Bisacrylamide(40%/2%) (ml)	7.5	10	12.5	15	18.75	25
5x TBE (ml)	10	10	10	10	10	10
Urea (g)	21	21	21	21	21	21
10%APS (w/v) (µl)	300	300	300	300	300	300
TEMED (µl)	30	30	30	30	30	30
With H_2O add to (ml)	50	50	50	50	50	50

3.1.1.2.2 Native Polyacrylamide Gel Electrophoresis

Native polyacrylamide gels were used to analyze either double-stranded nucleic acids or the secondary and tertiary structure of single-stranded nucleic acids. Due to the requirement of the native conditions, no urea was used for preparing polyacrylamide gels and a low electric field strength (4 V/cm) was applied to avoid the denaturation of nucleic acids at high temperature.

Table 4: Protocol for Native Polyacrylamide Gel

Acrylamide concentration	6 %	8 %	10 %	12 %	15 %	20 %
Acrylamide/Bisacrylamide(40%/2%) (ml)	7.5	10	12.5	15	18.75	25
5x TBE (ml)	10	10	10	10	10	10
10%APS (w/v) (µl)	300	300	300	300	300	300
TEMED (µl)	30	30	30	30	30	30
With H_2O add to (ml)	50	50	50	50	50	50

3.1.2 Detection of Nucleic Acids on Gel

3.1.2.1 Ethidium Bromide (EtBr) Staining

Ethidium Bromide (EtBr) is a heterocyclic cationic fluorescent dye, which can intercalate between the bases of nucleic acids. It was used in this work as a nucleic acids stain for agarose and polyacrylamide gels. The gels were stained by soaking in EtBr solution (1 µg/ml) for 10–20 min and visualized under an ultraviolet transilluminator at 302 nm (GelDoc 2000, Bio Rad).

3.1.2.2 SYBR® Gold Staining

Since 1993, SYBR® nucleic acid gel stains have rapidly become very popular due to their high sensitivity and ease of use. SYBR® Gold stain is a proprietary unsymmetrical cyanine dye which binds to double- or single-stranded DNA or to RNA. Presently it is the most sensitive fluorescent stain available for detecting double- or single-stranded DNA or RNA in electrophoretic gels. Excitation maxima for dye–nucleic acid complexes are at ~495 nm in the visible and ~300 nm in the ultraviolet

range. The emission maximum occurs at ~537 nm. SYBR® Gold stain is more than 10-fold more sensitive than ethidium bromide for detecting DNA and RNA in denaturing urea gels, even with 302 nm transillumination.

In this work, staining was performed according to the instruction of the supplier (Invitrogen, USA). The gels were stained by soaking in 1 : 10 000 diluted SYBR® Gold solution (in 1xTBE buffer) for 10–20 min and visualized on an ultraviolet transilluminator at 302 nm (GelDoc 2000, Bio Rad).

3.1.2.3 UV Shadowing

UV shadowing can be used for low-sensitivity detection of DNA/RNA in gels due to their UV absorbance. This technique uses shortwave UV light (254 nm) and a UV fluorescent (60 F_{254}) TLC plate (Merck). The gel is placed on a plastic wrap over a UV fluorescent TLC plate. The dye in the plate is excited by placing a UV source over the gel. The nucleic acids are shown as dark areas on the gels because they absorb the UV light. The sensitivity of this method is limited to 10–50 ng per band.

3.1.2.4 Phosphor Imaging

Phosphor imaging is a qualitative and quantitative method for the detection of radioactively labeled nucleic acids in gels. The advantages compared to the standard autoradiography are that the exposure times are considerably shorter (usually 5–10 times) and that is much more accurate in quantifying the amount of radioactivity in a sample.

The gels are clothed with plastic wrap, and put on an imaging plate and incubated in a film cassette for 30–60 min. An imaging plate consists of a thin layer of special crystals doped with lanthanides. Radioactive radiation excites the crystals and a latent image of the sample is formed on the plate. The image is read into the computer by scanning the plate with the phosphor-imager Storm 840 of Molecular Dynamics and analyzed with the software Image Quant NT.

3.1.2.5 Fluorescence Scanning

Fluorescence-labeled nucleic acids could be directly detected after gel electrophoresis by a fluorescence scanner. In this work a Fuji FLA-5100 multi-

purpose 2-dimensional scanner capable of scanning phosphor screens and fluorescence/chemifluorescence in gels/blots or microplates was used to record the image of the gels with fluorescence-labeled oligonucleotides.

3.1.3 Determination of Nucleic Acids Concentration

3.1.3.1 UV Spectrophotometry

The concentration of nucleic acids can be determined by the use of UV spectrophotometry. Both RNA and DNA absorb UV light due to the presence of purin and pyrimidine bases at about 260 nm efficiently. That makes it possible to detect and quantify nucleic acids at concentrations as low as 2.5 ng/µl. The Lambert-Beer Law describes the relation between the concentration and the absorbance:

$$OD = \varepsilon * c * d$$

The optical density (OD) is the product of the substance-specific molar extinction coefficient (ε), the concentration of the sample (c) and the optical pathlength in cm (d). If a 1-cm quartz cuvette is used for the UV spectrum, the concentration of nucleic acids can be estimated using the following values (Sambrock *et al*, 1989):

dsDNA: 1 OD_{260nm} = 50 µg / ml

ssDNA: 1 OD_{260nm} = 33 µg / ml

RNA: 1 OD_{260nm} = 40 µg / ml

Proteins have a UV absorption maximum at 280 nm due to the tryptophan residues. The absorbance of a nucleic acids sample at 280 nm gives an estimate of the protein contamination of the sample. The ratio of the absorbance at 260 nm / absorbance at 280 nm (A_{260}/A_{280}) of a pure nucleic acids sample should be between 1.65 and 1.85.

3.1.3.2 Fluorescence Labeling (Cy3 and Alexa Flour ®647)

Fluorescent labeling of nucleic acids offers another way for the concentration determination. Nucleic acids can be labeled with fluorescent dyes that have been modified with an amine-reactive N-hydroxysuccinimidyl ester (NHS ester) group. NHS esters react exclusively with aliphatic amine groups, so the nucleic acids have to be modified with aminoallyl groups. This is done by incorporating aminoallyl-

modified nucleotides during solid phase synthesis. In this work, the nucleic acids were labeled with fluorescent dyes (Cy3 or Alexa Fluor® 647) at either 5´- or 3´-end. A calibration curve for every oligonucleotide to be detected was measured. The commercially available oligonucleotides with Cy3 or Alexa Fluor® 647 (0.1 nmol / µl) were diluted with H_2O from 0 to 20,000 nM (Tab. 5). 2 µl of each sample was measured by a fluorospectrometer (NanoDrop 3300 Fluorospectrometer, for Cy3: excitation at 550 nm, emission at 570 nm; for Alexa Fluor® 647: excitation at 650 nm, emission at 670 nm), and a standard calibration curve was plotted. Then, the fluorescence signals of the oligonucleotide samples were measured, and their concentrations were calculated with the standard calibration curve.

Table 5: Dilution of oligonucleotide for a calibration curve

Dilution	Concentration (nM)	Oligonucleotides (µl)	H_2O (µl)
1:5	20000	4 of original sample	16
1:10	10000	10 of 1:5	10
1:20	5000	10 of 1:10	10
1:50	2000	10 of 1:20	15
1:100	1000	10 of 1:50	10
1:200	500	10 of 1:100	10
1:500	200	10 of 1:200	15
1:1000	100	10 of 1:500	10
1:2000	50	10 of 1:1000	10
1:5000	20	10 of 1:2000	15
1:10000	10	10 of 1:5000	10
1:20000	5	10 of 1:10000	10
zero	0	0	10

3.1.3.3 Quant-iT™ OliGreen® ssDNA Reagent

Quant-iT™ OliGreen® ssDNA reagent is an ultra-sensitive fluorescent nucleic acid stain for quantification of oligonucleotides and single-stranded DNA in solution. The OliGreen ssDNA reagent enables to routinely quantify as little as 100 pg/mL of ssDNA. Thus, quantitation with the OliGreen reagent is about 10,000 times more sensitive than quantitation with UV absorbance methods and at least 500 times more sensitive than detecting oligonucleotides on electrophoretic gels stained with ethidium bromide. The linear detection range of the Quant-iT™ OliGreen® assay in a standard fluorometer extends from 100 pg/ml to 1 µg/ml. In this work, a calibration curve for every oligonucleotide to be detected was measured before analysis. The

commercially available ssDNA (0.1 nmol / µl) was diluted with 1xTE buffer (10 mM Tris-HCl, 1 mM EDTA, pH 7.5) from 0 to 50,000 nM (Tab. 6). 5 µl sample of every concentration was mixed well with 5 µl 200-fold diluted OliGreen® ssDNA reagent and incubated for 5 min at room temperature. After incubation, 2 µl of the sample was measured by means of a fluorospectrometer (NanoDrop 3300 Fluorospectrometer, excitation at 485 nm, emission at 527 nm), and a standard calibration curve was plotted. In the same way, the fluorescence signals of the oligonucleotide samples were measured, and their concentrations were calculated with the standard calibration curve.

Table 6: Dilution of oligonucleotide for a calibration curve

Dilution	Concentration. (nM)	ssDNA (µl)	1x TE (µl)
1:2	50000	5	(2xTE) 5
1:20	5000	4 of 1:10	36
1:200	500	4 of 1:100	36
1:1 000	100	10 of 1:200	40
1:5 000	20	10 of 1:1000	40
1:10 000	10	20 of 1:5000	20
1:20 000	5	20 of 1:10000	20
1:50 000	2	20 of 1:20000	30
1:100 000	1	20 of 1:50000	20
1:200 000	0.5	20 of 1:100000	20
1:500 000	0.2	20 of 1:200000	30
zero	0	0	20

3.1.4 Purification of Nucleic Acids

3.1.4.1 Purification by Silica-Based Resins

StrataClean™ resin enables DNA purification without phenol. The solid-phase, silica-based resin, contains hydroxyl groups that react with proteins in a similar manner as the hydroxyl group of phenol. This is a rapid way to remove proteins from DNA samples.

In this work, this resin was used to separate T4 polynucleotide kinase from ssRNA after 5´-end labeling. For a 100 µl reaction, 10 µl resin was added according to the instruction of the supplier (Stratagene, USA). Before use, the slurry was very vortexed extensively.

After adding the resin, the sample was mixed by vortexing for 15 s and then incubated at room temperature for 1 min. The mix was spun in a microfuge at 2,000 g for 1 min. The supernatant containing the RNA was carefully transferred to a fresh tube.

3.1.4.2 Microcon Centrifugal Filter Devices

Microcon centrifugal filter devices offer a simple and efficient way to either concentrate or desalt nucleic acids solutions. Ultracel low-binding, anisotropic, hydrophilic regenerated cellulose membrane (YM Membrane) is used in the Microcon centrifugal filter devices. Molecules smaller than the cut-off length of the YM membrane pass through the filter, while molecules larger than the cut-off length are retained on the filter (Tab. 7). In this work, Microcon YM-3 and YM-30 were used to separate oligonucleotides with different lengths or to desalt the nucleic acids samples. The experiments were performed according to the instruction of the manufacturer (Millipore, USA).

Table 7. Centrifugation Guidelines for Microcon Devices

Ultracel YM Membrane	Color	Nucleotide cut-off for RNA/DNA		Maximum g-force	Spin Times (min) 25 °C
		SS	DS		
YM-3	Yellow	10	10	14,000	100
YM-10	Green	30	20	14,000	30
YM-30	Clear	60	50	14,000	12

3.1.4.3 Gel Filtration Chromatography

Gel filtration chromatography separates the oligonucleotides by size. The sample is applied to the top of a column consisting of porous beads; the molecules move through the column, diffusing into the beads. Smaller molecules diffuse further into the pores of the beads and therefore move through the column more slowly, while the larger molecules enter less or not at all and thus move through the column more quickly. Both molecular weight and three-dimensional shape contribute to the degree of retention.

In this work, illustra^{TM} NAP-10 column and illustra MicroSpin^{TM} G-25 Column (Colum matrix: Sephadex G-25 DNA grade) were used for separations of components in a mixture and for salt removal from a preparation of nucleic acids. The experiments

were performed according to the instruction of the manufacturer (GE Healthcare, England).

3.1.4.4 Ion-Exchange Chromatography

Ion exchange is one of the most frequently used chromatographic techniques for the separation and purification of nucleic acids. This technique is based on the different charge of molecules. An ion-exchange resin consists of an insoluble matrix with charged groups covalently attached. Ion-exchange chromatography can be subdivided into cation-exchange chromatography, in which positively charged ions bind to a negatively charged resin; and anion-exchange chromatography, in which the binding ions are negative, and the immobilized functional group is positive.

The experiments were performed according to the instruction of the manufacturer (Dow, USA). DOWEX^{TM} 50WX8 Fine Mesh Resin (a strong acid cation resin containing 8% divinylbenzene in the resin copolymer with 50–100 mesh size) was used for salt removal from a preparation of nucleic acids. For a 100 µl reaction, 10 µl resin was added. After adding the resin, the sample was mixed by vortexing for 15 s and then incubated at room temperature for 5 min. The mix was spun in a microfuge at 2,000 g for 1 min. The supernatant containing the oligonucleotides was carefully transferred to a fresh tube.

3.1.5 Nucleic Acids 5´-End Labeling

Nucleic acids can be phosphorylated by T4 polynucleotide kinase at the 5'-hydroxyl terminus. The kinase catalyzes the transfer and exchange of γ-phosphate of ATP to the 5'-hydroxyl-group of oligonuleotides.

The experiments were performed according to the instruction of the manufacturer (NEB, England). The oligonucleotides were radioactively labeled with γ-^{32}P-ATP by T4 polynucleotide kinase. The reaction mixture (Tab. 8) was incubated for 30 min at 37°C and stopped by heating for 10 min at 80°C.

Table 8: The reaction mixture for the radioactive labeling of oligonucleotides

Oligonucleotide	10 µl (1 nmol)
10x reaction buffer for T4 Polynucleotide Kinase	2 µl
γ-^{32}P-ATP	1 µl (0.1 nmol)
T4 Polynucleotide Kinase	1 µl (1 unit)
H_2O	6 µl

3.2. Bioconjugate Chemistry

3.2.1 Coupling of Nanoparticles to Nuleic Acids with Sulfo-SMCC

Sulfo-SMCC was used as cross-linker for the coupling between thiol-group-modified oligonucleotides and amino-group-modified iron oxide nanoparticles and vice versa. The experiments were essentially performed as described (Derfus *et al.* 2007). The thiol-group-modified oligonucleotides were purchased from IBA GmbH (Göttingen, Germany). The oligonucleotide sequences (5´ to 3´) used in this work are shown in Table 9. The 15 nm iron oxide nanoparticles carrying amino groups were synthesized by MagForce AG (Berlin, Germany) and have been shown to contain ~550 amine groups by nitrobenzaldehyde assay. At first the oligonuleotides were reduced with 1 mM TCEP (Sigma). Iron oxide nanoparticles were first reacted with 2.2 mM Sulfo-SMCC (Sigma) in PBS (pH 7.4) for 1 h at room temperature in a thermomixer at 1000 rpm, centrifuged to remove excess cross-linker, washed two times with distilled water, added to the reduced oligonuleotides (oligonucleotide:nanoparticle = 65:1; molar concentration of nanoparticles was calculated from iron concentration assuming that one nanoparticle contains 70,000 iron atoms), and reacted in PBS (pH 6.7) at 4 °C overnight with rotation (for the Ribozyme-Nanoparticle-Drug-Delivery System, the L-inhibitor and the L-ribozyme were hybridized with the molar ratio 1.1:1 in PBS (pH 6.7) before the coupling step. Unconjugated oligonucleotides were removed by centrifugation.

Tab. 9: The oligonucleotide sequences (5´ to 3´) used for the coupling with Sulfo-SMCC

Name of Oligo-nucleotide	Sequence (5´ to 3´)	Type of Oligo-nucleotide	*Type of Project
Si-SH	SH-ATG CTT CCA CGA GCC TTT CGA ATA GAC TAC CGC CTC GCA G	DNA	1
Yi-SH	SH- TTT TTT TTT GGG TTT TTT TTT CGC	DNA	1
Er-SH	SH- TTT TTT TTT TTT TTT TTT TTT GCC	DNA	1
San-SH	SH-TTT TTA GGT GTA GTG CGT GTC	DNA	1
SH-TG	SH -TTT TTT TTT TTG GGT TTT T	DNA	1
NH_2-TG	NH_2 -TTT TTT TTT TTG GGT TTT T	DNA	1
Sub1	SH -GCG CCG AAA CAC CGU GUC UCG AGC – Alexa 647	RNA	2
Inh1-2bp	SH –GCC TCA TCA GTC GAG CC	DNA	2
L-Sub1	SH -GCG CCG AAA CAC CGU GUC UCG AGC – Alexa 647	L-RNA	2
L-Inh1-2bp	SH –GCC TCA TCA GTC GAG CC	L-DNA	2
***Type of Project: 1:** dsDNA-Nanoparticle-Drug-Delivery System **2:** Ribozyme-Nanoparticle-Drug-Delivery System			

3.2.2 Coupling of Nanoparticles to Nuleic Acids with Sulfo-GMBS

Sulfo-GMBS was used as cross-linker for the coupling between thiol-group-modified iron oxide nanoparticle and amino-group-modified oligonucleotides and vice versa. The experiments were performed according to the protocol supplied by the manufacturer (ThermoScientific, USA). The amino-group-modified oligonucleotides were purchased from IBA GmbH (Göttingen, Germany). The oligonucleotide sequences (5´ to 3´) used in this work are shown in Table 10. The 15 nm iron oxide nanoparticles with thiol groups on the surfaces were synthesized by MagForce AG (Berlin, Germany). The amino-group-modified oligonucleotides (as DNA pellet) were first reacted with Sulfo-GMBS (at the concentration of 10 mg/ml) in PBS (pH 7.2) for 2 h at room temperature in a thermomixer at 1000 rpm, purified with YM-3 Microcon centrifugal filter devices to remove excess cross-linker, washed two times with

distilled water, eluted into a new tube and lyophilized. Nanoparticles were resuspended freshly in 20 mM phosphate buffer (pH 6.8) at the concentration of 5 µM (molar concentration of nanoparticles was calculated from iron concentration assuming an iron content of 70,000 iron atoms per nanoparticle); they were then reacted with 0.5 mM TCEP for 30 min. The reduced nanoparticles were mixed with oligonuleotide pellet activated by Sulfo-GMBS (oligonucleotide:nanoparticle = 8:1), and reacted at room temperature overnight with rotation. Unconjugated oligonucleotides were removed by centrifugation.

Tab. 10: The oligonucleotide sequences (5´ to 3´) used for the coupling with Sulfo-SMCC

Name of Oligo-nucleotide	Sequence (5´ to 3´)	Type of Oligo-nucleotide	*Type of Project
PolyT-CC NH_2	NH_2- TTT TTT CGT TTT TTT TCC	DNA	1
PolyT-CC SH	SH - TTT TTT CGT TTT TTT TCC	DNA	1
NH_2-TG	NH_2 -TTT TTT TTT TTG GGT TTT T	DNA	1
***Type of Project: 1:** dsDNA-Nanoparticle-Drug-Delivery System **2:** Ribozym-Nanoparticle-Drug-Delivery System			

3.2.3 Coupling of Nanoparticles to Nuleic Acids with EDC

EDC was used as cross-linker for the coupling between amino-group-modified iron oxide nanoparticles and either carboxyl-group-modified or phosphate-group-modified oligonucleotides. The experiments were performed according to the protocol provided by the manufacturer (ThermoScientific, USA). The carboxyl-group-modified and phosphate-group-modified oligonucleotides were purchased from IBA GmbH (Göttingen, Germany). The 15 nm iron oxide nanoparticles with PEG-Silane and DIAMO (N-(2-aminoethyl)-3-aminopropyltrimethoxysilane) on the surface were synthesized by MagForce AG (Berlin, Germany).

(A) Carboxyl-group-modified DNA

1 nmol iron oxide nanoparticles (molar concentration of nanoparticles was calculated from iron concentration upon the assuming an iron content of 70,000 iron atoms per nanoparticle) with PEG-Silane and DIAMO modification was resuspended in 500 µl

0.1 M MES buffer (pH 4.6). 10 mg of EDC was dissolved in 1 ml of water and immediately 100 µl of this solution was added into the nanoparticle solution. After mixing well, the sample was added into the new tube with 10 nmol carboxyl-group-modified DNA pellet (Poly T-CC COOH: 5´- COO-TTT TTT CGT TTT TTT TCC- 3´), and reacted at room temperature overnight with rotation. Unconjugated oligonucleotides and cross-linker were removed by centrifugation.

(B) Phosphate-group-modified DNA

7.5 nmol phosphate-group-modified DNA (Poly T-CC PO_4: 5´- PO_4-TTT TTT CGT TTT TTT TCC- 3´) was lyophilized and dissolved in 75 µl reaction buffer (PBS buffer with 10mM EDTA, pH 7.2). Iron oxide nanoparticles with PEG-Silane and DIAMO modification were dissolved to a final concentration of 0.25 M in 10 µl of 0.1 M imidazole (pH 6.0). 1.25 mg (6.25 µmol) EDC was weighed into a microcentrifuge tube. The DNA and nanoparticle solution were added in this tube and mixed well. 20 µl 0.1 M imidazole (pH 6.0) was added into the tube. The reaction was incubated at room temperature overnight.

3.2.4 Coupling of Nanoparticles to Nuleic Acids with EDC/Sulfo-NHS

EDC/Sulfo-NHS was used as cross-linker for the coupling between amino-group-modified iron oxide nanoparticles and carboxyl-group-modified DNA. The experiments were performed according to the protocol provided by the manufacturer (ThermoScientific, USA). 10 nmol carboxyl-group-modified DNA (Poly T-CC COOH: 5´- COO-TTT TTT CGT TTT TTT TCC- 3´) was lyophilized in a microcentrifuge tube. 100 mM EDC solution and 50 mM Sulfo-NHS solution were freshly prepared (in 0.1 M MES, 0.5 M NaCl buffer, pH 6.0). 2 µl 100 mM EDC, 10 µl 50 mM Sulfo-NHS and 88 µl 0.1 M MES, 0.5 M NaCl buffer, pH 6.0 were added together into the microcentrifuge tube with DNA pellet. The tube was vortexed well and incubated at room temperature for 15 min. 1.4 µl 2-mercaptoethanol, which was 10-fold diluted in H_2O, was added into the reaction to quench the EDC. The sample was purified with YM-3 Microcon centrifugal filter devices to remove excess cross-linker, washed two times with PBS buffer pH 7.4, eluted with 100 µl of the same buffer into a new tube. 0.6 nmol nanoparticles (in 100 µl PBS buffer, pH 7.4) was added to the DNA solution.

The sample was incubated at room temperature for 2 h with shaking. Unconjugated DNA was removed by centrifugation.

3.2.5 Coupling of Nanoparticles to Nuleic Acids with PDITC

PDITC was used as cross-linker for the coupling between amino-group-modified iron oxide nanoparticles and amino-group-modified DNA. 70 µg (13 nmol) amino-group-modified DNA (Poly T-CC NH_2: 5´- NH_2-TTT TTT CGT TTT TTT TCC- 3´) was lyophilized and dissolved in 25 µl 0.1 M sodium borate, pH 9.3. 10 mg of PDITC was dissolved in 500 µl DMF and this solution was added to the prepared DNA. The reaction was incubated at room temperature for 2 h in the dark. 3 ml of n-butanol and 3 ml of water were added to the reaction medium to extract the excess reactant. The reaction mixture was mixed well and centrifuged at 4000 x g for 10 min. The upper yellow layer was discarded. The extraction process was repeated three times, and then the remaining solution containing activated DNA was lyophilized. 260 pmol amino-group-modified iron oxide nanoparticles were dissolved in 100 µl 0.1 M sodium borate, pH 9.3 and added to the activated DNA. The reaction was incubated at room temperature overnight in the dark. Unconjugated DNA was removed by centrifugation.

3.2.6 Coupling of Nanoparticles to Nuleic Acids with Epoxide Particles

Iron oxide nanoparticles containing epoxide groups were used to couple thiol-group- and amino-group-modified DNA. The thiol-group- and amino-group-modified oligo-nucleotides were purchased from IBA GmbH (Göttingen, Germany). The iron oxide nanoparticles containing epoxide groups were synthesized by MagForce AG (Berlin, Germany).

(A) Thiol-group-modified DNA

Iron oxide nanoparticles containing epoxide groups were dissolved in 20 mM sodium phosphate buffer (pH 7.5) at a concentration of 5 µM. 10 nmol thiol-group-modified DNA (SH-TG: 5´- SH -TTT TTT TTT TTG GGT TTT T -3´) was lyophilized and dissolved in 100 µl of the same buffer. 40 µl nanoparticle solution was added to the

DNA solution and reacted at room temperature for 24 h. Unconjugated DNA was removed by centrifugation.

(B) Amino-group-modified DNA
Iron oxide nanoparticles containing epoxide groups were dissolved in 0.1 M sodium borate (pH 9.3) at a concentration of 5 µM. 10 nmol amino-group-modified DNA (NH_2-TG: 5´- NH_2 -TTT TTT TTT TTG GGT TTT T -3´) was lyophilized and dissolved in 100 µl of the same buffer. 40 µl nanoparticle solution was added to the DNA solution and reacted at room temperature for 24 h. Unconjugated DNA was removed by centrifugation.

3.2.7 Coupling of Nanoparticles to Nuleic Acids with gold-coated Nanoparticles

The iron oxide nanoparticles coated with gold were synthesized by MagForce AG (Berlin, Germany). The thiol-group-modified oligonucleotides were purchased from IBA GmbH (Göttingen, Germany).
Samples of dsDNA (one strand with thiol modification, the other strand with Cy3-modification) were treated with TCEP and incubated with iron oxide nanoparticles coated with gold at 4 °C overnight. Unconjugated DNA was removed by centrifugation.

3.2.8 Coupling of Cytostatic Drug to Nucleic Acids

3.2.8.1 Coupling of Chlorambucil to DNA via EDC

The experiments were performed mainly according to the protocol provided by the manufacturer (ThermoScientific, USA). Chlorambucil was dissolved in DMSO at the concentration of 20 mM. EDC was dissolved in different coupling buffers (i.e. D-PBS, pH 6.7; 0.1 M MES, pH 4.8) at the concentration of 0.12 M. 2.5 µl Chlorambucil solution, 5 µl EDC solution, 20 µl DMSO and 10 µl coupling buffer were added to 5 nmol DNA pellet (Yi-NH_2: 5´-NH_2-GCG AAA AAA AAA CCC AAA AAA-3´). The

reaction was incubated at 25 °C for 4 h with 1200 rpm mixing. Excess EDC was quenched by the addition of 2-mercaptoethanol to a final concentration of 20 mM. 60 µl H_2O was added to dilute the DNA solution. The sample was purified at first with illustra MicroSpin^{TM} G-25 Column; then with YM-30 Microcon centrifugal filter devices. The product was analyzed by gel electrophoresis and MALDI-TOF-MS.

3.2.8.2 Coupling of Chlorambucil to DNA via CDI

The experiments were performed mainly according to the protocol provided by the manufacturer (ThermoScientific, USA). Chlorambucil was dissolved in DMSO at the concentration of 0.2 M. CDI was dissolved in DMSO at the concentration of 0.4 M. Both solutions were mixed 1/1 (v/v). The mixture was incubated at 40 °C for 48 h with 1000 rpm shaking. Intermediate product (1:10 diluted with DMSO) was detected by TLC. The experiments were carried out according to Table 11 in different buffer system at 25 °C for 48 h with 1000 rpm shaking.

Table 11: CDI coupling

	DNA pellet	**Inter-mediate 1:10**	**DMSO**	**coupling buffer**				**Vol.**
				PBS pH 7,4	**$Na_3B_4O_7$ 0.1 M pH 9.3**	**MES 0.1 M pH 4.8**	**DMSO**	
1	20 nmol	2 µl	10 µl	18 µl	-	-	-	30 µl
2	20 nmol	2 µl	10 µl	-	18 µl	-	-	30 µl
3	20 nmol	2 µl	10 µl	-	-	18 µl	-	30 µl
4	20 nmol	2 µl	10 µl	-	-	-	18 µl	30 µl

The used DNA named Poly T-NH_2 has the following sequence: 5´-NH_2-TTT TTT TTT TTT TTT TTT-3´.The sample was purified at first with illustra MicroSpin^{TM} G-25 Column; then with YM-30 Microcon centrifugal filter devices. The product was analyzed by gel electrophoresis and MALDI-TOF-MS.

3.2.8.3 Coupling of Chlorambucil to DNA via DCC/NHS

The experiments were performed mainly according to the protocol provided by the manufacturer (ThermoScientific, USA). NHS and DCC were dissolved in DMF at the concentration of 0.72 M and mixed 1/1 (v/v). Chlorambucil was dissolved in DMF at

the concentration of 0.36 M. Both solutions were cooled to 12 °C. 50 µl NHS/DCC mixture was slowly added to 50 µl chlorambucil solution over 15 minutes at 12 °C. The reaction was incubated at 25 °C for 24 h with 1000 rpm mixing. Then the sample was centrifuged at room temperature at 2000 x g for 5 min. The supernatants were carefully removed and transferred into a fresh microfuge tube. The supernatant (contains reaction intermediate) was diluted 1:10 with DMF and detected by TLC. 20 µl of 1:10 intermediate product and 80 µl coupling buffer (A: 0.1 M sodium borate, pH 9.3; B: 50 mM sodium phosphate, pH 7.4) were added to 100 nmol DNA pellet (Poly T-NH_2: 5´-NH_2-TTT TTT TTT TTT TTT TTT TTT-3´). The reaction was incubated at 25 °C for 48 h with 1000 rpm mixing. The sample was purified at first with illustra^{TM} NAP-10 column; then with YM-30 Microcon centrifugal filter devices; at last with DOWEX^{TM} 50WX8 Fine Mesh Resin. The product was analyzed by gel electrophoresis and MALDI-TOF-MS.

3.2.8.4 Coupling of Methotrexate to DNA via DCC/NHS

The experiments were performed mainly according to the protocol provided by the manufacturer (ThermoScientific, USA). NHS and DCC were dissolved in DMF at the concentration of 0.72 M and mixed 1/1 (v/v). Methotrexate (MTX) was dissolved in DMF at the concentration of 0.36 M. Both solutions were cooled to 12 °C. 50 µl NHS/DCC mixture was slowly added to 50 µl MTX solution over 15 minutes at 12 °C. The reaction was incubated at 25 °C for 24 h with 1000 rpm mixing. Then the sample was centrifuged at room temperature at 2000 x g for 5 min. The supernatants were carefully removed and transferred into a fresh microfuge tube. The supernatant (contains reaction intermediate) was diluted 1:10 with DMF. 20 µl of 1:10 intermediate product and 80 µl coupling buffer (0.1 M sodium borate, pH 9.3) were added to 100 nmol DNA pellet (DNA sub1: 5´- NH_2 - GCG CCG AAA CAC CGU GUC UCG AGC -3´, MW: 7538 g/mol). The reaction was incubated at 25 °C for 48 h with 1000 rpm mixing. The sample was purified at first with illustra^{TM} NAP-10 column; then with YM-30 Microcon centrifugal filter devices; at last with DOWEX^{TM} 50WX8 Fine Mesh Resin. The product was analyzed by MALDI-TOF-MS.

3.3. Biochemical and Biophysical Methods

3.3.1 Serum stability assays

The stability assays were performed essentially as decribed by Klussmann et al (1996). Human serum S7023 was purchased from Sigma (USA). The R-ribozyme and L-ribozyme were incubated at a concentration of 10 µM with 90% human serum in an incubator at 37 °C, 94.5% humidity and 5% carbon dioxide. Aliquots were mixed 1:1 with stop solution (8 M Urea, 50 mM EDTA, 2% SDS) and immediately frozen in liquid nitrogen. The samples were filtered with Microcon YM-30 (Millipore) and 30 pmol of each RNA was loaded onto the denaturing 15% polyacrylamide gel (7M urea). The gel was stained by soaking in EtBr solution (1 µg/ml) solution for 15 min and visualized on an ultraviolet transilluminator at 302 nm.

3.3.2 MALDI-TOF-MS

Matrix-assisted laser desorption ionization-time of flight -mass spectrometry (MALDI-TOF-MS) was applied to analyze DNA–chlorambucil conjugates. 3-hydroxypicolinic acid (3-HPA) was used as matrix. The DNA samples were prepared as 1 / 1 / 1 mixture of 3-HPA (50mg/ml in water) / 25mM ammonium citrate / DNA sample. Samples (undiluted and 1:10 in water) were spotted and analyzed by MALDI-TOF-MS. The MALDI-TOFMS was carried out by Christoph Weise.

3.3.3 DNA Melting Curve

In this work an HP 8452A Diode-Array Spectrophotometer was used to measure the melting curve of nucleic acids. 1.2 ml oligonucleotide sample (OD: 0.2 – 1.0) was prepared in different buffers (Tab. 12). After denaturing (5 min at 95 °C) and renaturing (cool down from 95 °C to 20 °C slowly) the samples were measured according the following program:

Step	Start	Stop	Increment	Hold time
1	20 °C	90 °C	1 °C	1 min
2	90 °C	20 °C	-1 °C	1 min

Table 12: buffers for the melting curve

Sequence of Oligonucleotides	Buffer
5'- SH-ATG CTT CCA CGA GCC TTT CGA ATA GAC TAC CGC CTC GCA G -3' COMPLEMENT: 5'- CTG CGA GGC GGT AGT CTA TTC GAA AGG CTC GTG GA -3'	PBS pH 7.2
5'- SH-ATG CTT CCA CGA GCC TTT CGA ATA GAC TAC CGC CTC GCA G -3' COMPLEMENT: 5´- Cy3- CTG CGA GGC GGT AGT CTA TT –3´	PBS pH 7.2
5´- SH- TTT TTT TTT GGG TTT TTT TTT CGC-3´ COMPLEMENT: 5´-Cy3- GCG AAA AAA AAA CCC AAA AAA-3´	PBS pH 7.2
5´- SH- TTT TTT TTT TTT TTT TTT TTT GCC-3´ COMPLEMENT: 5´-Cy3- GGC AAA AAA AAA AAA AAA AAA-3´	PBS pH 7.2
5´-SH-TTT TTA GGT GTA GTG CGT GTC- 3´ COMPLEMENT: 5'- Cy3-GAC ACG CAC TAC ACC TAA -3'	PBS pH 7.2
5´-PO_4-TTT TTT CGT TTT TTT TCC -3´ COMPLEMENT: 5´- Cy3-GGA AAA AAA ACG AAA AAA-3´	PBS pH 7.2
5´- COO-TTT TTT CGT TTT TTT TCC- 3´ COMPLEMENT: 5´- Cy3-GGA AAA AAA ACG AAA AAA-3´	PBS pH 7.2
5´- SH -TTT TTT CGT TTT TTT TCC -3´ COMPLEMENT: 5´- Cy3-GGA AAA AAA ACG AAA AAA-3´	PBS pH 7.2
5´- NH_2 -TTT TTT CGT TTT TTT TCC -3´ COMPLEMENT: 5´- Cy3-GGA AAA AAA ACG AAA AAA-3´	PBS pH 7.2
5´- SH -TTT TTT CGT TTT TTT TCC -3´ COMPLEMENT: 5´- Cy3-GGA AAA AAA ACG AAA AAA-3´	PBS pH 7.2
5´- NH_2 -TTT TTT TTT TTG GGT TTT T -3´ COMPLEMENT: 5´- Cy3-CGA AAA ACC CAA AAA AAA-3´	PBS pH 7.2
5´- SH -TTT TTT TTT TTG GGT TTT T -3´ COMPLEMENT: 5´- Cy3-CGA AAA ACC CAA AAA AAA-3´	PBS pH 7.2
5´- GCG CCG AAA CAC CGU GUC UCG AGC-3´ COMPLEMENT: 5´-GCG CCT CAT CAG TCG AGC C-3´	50 mM Tris HCL pH 7.5
5´- GCG CCG AAA CAC CGU GUC UCG AGC-3´ COMPLEMENT: 5´-GCC TCA TCA GTC GAG CC-3´	50 mM Tris HCL pH 7.5
5´-ACG GUC GGU CGC C-3´ COMPLEMENT: 5´- ACG GTT TCG GCC TTT CGG CCT CAT CAG GGT CGC C-3´	50 mM Tris HCL pH 7.5
5´-ACG GUC GGU CGC C-3´ COMPLEMENT: 5´- CG GTT TCG GCC TTT CGG CCT CAT CAG GGT CGC -3´	50 mM Tris HCL pH 7.5

5´-ACG GUC GGU CGC C-3´ COMPLEMENT: 5´- ACG GTC GGT CGC C -3'	50 mM Tris HCL pH 7.5

3.3.4 Determination of the 50% Release Temperature (T_r) with Release Curve

A new method to measure the temperature of 50% melting of dsDNA with the help of fluorescently labeled nucleic acids was established in this work. The solutions of dsDNA–nanoparticle conjugates were incubated in a thermomixer running the following temperature program:

Step	Start	Stop	Increment	Hold time
1	20 °C	25°C	5 °C	5 min
2	25 °C	30 °C	5 °C	5 min
3	30 °C	35 °C	5 °C	5 min
4	35 °C	40 °C	5 °C	5 min
5	40 °C	45 °C	5 °C	5 min
6	45 °C	50 °C	5 °C	5 min
7	50 °C	55 °C	5 °C	5 min
8	55 °C	60 °C	5 °C	5 min
9	60 °C	65 °C	5 °C	5 min
10	65 °C	70 °C	5 °C	5 min
11	70 °C	75°C	5 °C	5 min
12	75°C	80 °C	5 °C	5 min
13	80 °C	85 °C	5 °C	5 min
14	85 °C	90 °C	5 °C	5 min
15	90 °C	95 °C	5 °C	5 min

Aliquots were taken from each sample at each step and immediately centrifuged. The supernatants were carefully removed and transferred into a fresh microfuge tube. RFU (relative fluorescence unit) signals of the supernatants were measured by NanoDrop 3300 Fluorospectrometer (Thermo Scientific), and the release curve was plotted.

3.3.5 Release Experiment in the Applicator MFH®-12-TS A

Magnetic field applicator MFH ®-12-TS A is produced by MedTech Engineering GmbH (Berlin). This device can be applied for experiments in the laboratory scale and with small animals. MFH ®-12-TS A consists basically of a resonant circuit at a ferrite yoke that generates a homogeneous 100 kHz alternating magnetic field. The coil current can be continuously adjusted to regulate the magnetic field strength from 0 to 15 kA/m (Jordan *et al.* 1993, Gneveckow *at al.* 2004).

The solutions of dsDNA–nanoparticle conjugates were mixed 1:1 with the iron oxide nanoparticles. The samples were put into the applicator MFH®-12-TS A, where in the AC magnetic field the particles generated heat which was monitored by fiberoptic probe. Aliquots were taken from each sample at 40°C, 45°C, 50°C, and 60°C respectively and immediately centrifuged. The supernatants were carefully removed and transferred into a fresh microfuge tube. RFU (relative fluorescence unit) signals of the supernatants were measured by NanoDrop 3300 Fluorospectrometer (Thermo Scientific), and the result was plotted with Excel.

3.3.6 Atomic Absorption Spectroscopy (AAS)

Atomic absorption spectroscopy is a technique, which can be used to determine the concentration of over 70 different metals in a solution. The analyte atoms or ions must be vaporized in a flame or graphite furnace at first. In their elemental form metals absorb ultraviolet light and undergo transitions to higher electronic energy levels. Each metal has a characteristic wavelength at which absorption will occur. If that analyte metal is present in the sample, it will absorb some of the light, and the amount of absorption will be determined. With a standard calibration curve of known concentration, the concentration of analyte atom in the sample can be calculated.

In this work, quantification of iron up-take into the cells was obtained via AAS analysis and performed at MagForce (Berlin). The atomic absorption spectrometer (Varian SpectrAA Teeman 220) was calibrated using the commercial iron standard solution (Fluka, Switzerland) at the concentrations of 2.0, 4.0, 6.0, 8.0 and 10.0 µg/L, the iron concentrations in C3H RS1 cells were then determined.

3.3.7 TEM Imaging of Cells

TEM (transmission electron microscopy) analysis was performed at MagForce (Berlin) to evaluate the distribution of the FeO_xNP–nucleic acids conjugates into cells. The C3H RS1 cells (this cell line was derived from a spontaneous murine mamma carcinoma) were seeded in a 6-well cell culture plate at a density of $2.5x10^5$ cells/well and grown at 37°C for 24 h. Afterwards, the medium was completely replaced with 2 ml / well fresh medium containing FeO_xNP/L-Sub1 conjugates or FeO_xNP/L-Inh1-2bp/Rib1 conjugates with Fe concentration of 50 µg/ml. The cells were incubated at 37°C, after 4h and 24 h the C3H RS1 cells were washed two times with 2.5 ml fresh medium, detached by trypsin treatment, and centrifuged at 800 rpm for 5 min. The cell pellets were resuspended in 5 ml fixative, incubated for 10 min at 37°C and stored at 4°C. The cells were observed in an EM 906 transmission electron microscope.

3.3.8 Thin Layer Chromatography (TLC)

TLC is a chromatography technique used to separate mixtures. It is performed on a sheet of glass, plastic, or aluminum foil, which is coated with a thin layer of adsorbent material, such as silica gel. This layer of adsorbent is the stationary phase. After the sample has been applied on the plate, a solvent or solvent mixture (the mobile phase) is drawn up the plate via capillary action. Different compounds in the sample mixture travel at different rates due to the differences in their extent of attraction to the stationary phase and the differences in solubility in the solvent.
In this work, HPTLC Silica gel $60F_{254}$ was used to examine the reaction intermediate of chlorambucil. The experiments were performed mainly according to the protocol given by Reuben *et al.* (1981). The plates were developed in MeOH/H_2O (7/3).

3.3.9 MTT Assay

The MTT assay is a colorimetric assay for measuring the activity of enzymes that reduce MTT (3-(4,5-Dimethylthiazol-2-yl)-2,5-diphenyltetrazolium bromide) (yellow

color) to formazan dyes (purple color) in living cells (Mosmann, 1983). This assay is mainly performed to assess the viability (cell counting) and the proliferation of cells (cell culture assays), parameters that are very useful to determine the cytotoxicity of potential medicinal agents.

In this work, MTT assay was used to test the cytotoxicity of chlorambucil–DNA polyT NH_2 conjugates and methotrexat–DNA sub1 conjugates. The cell line RuSi-RS1 which was derived from a 67-yr-old glioblastoma multiformae patient (Jordan et al., 1999) was used to determine the activity of chlorambucil–DNA conjugates. The colonic adenocarcinoma line WiDr (ATCC CCL 218) (Jordan et al., 1999) was applied to check the cytotoxicity of methotrexat–DNA conjugates. After the incubation with cytostatic drug–DNA conjugates, the medium was completely replaced with 200 µl MTT solution. The cells were incubated at 37°C in an incubator for 3 h. After 3 h incubation the MTT solution was discarded and the resulting violet dye can be extracted from the cells by adding 100 µl DMSO per well. The absorbance of the violet solutions at 540 nm and 690 nm were measured by a Tecan-plate reader.

The results were evaluated by taking the difference of absorption at 540 nm and 690 nm (A_{540nm}-A_{690nm}). Comparing the dye concentration of untreated cells (control, equal to 100% survival) with treated cells allows to calculate the survival rate.

3.4. Nucleic Acids-Dependent-Drug Delivery System

3.4.1. dsDNA-Nanoparticel-Drug Delivery System

ssDNA–nanoparticle conjugates were prepared as described and resuspended in 100 µl PBS buffer pH 7.2. Subsequently, complement DNA was added to the sample, the hybridization was performed at room temperature for 6 h (or overnight). Not hybridized ssDNA was removed by centrifugation. Then, the nanoparticle–dsDNA conjugates were incubated in a thermomixer as described before, and the release curve was drawn as described above for the drug (fluorescent) release.

3.4.2. Ribozyme-Nanoparticel-Drug Delivery System

Nanoparticle/(L)-substrate* conjugates and nanoparticle/(L)-inhibitor/ribozyme conjugates were prepared as described. The release experiments were performed in different buffer systems (buffer A with normal nucleic acids and L-nucleic acids and B with L-nucleic acids only).

*** (L) = normal nuclei acids and L-nucleic acids**

(A) in reaction buffer (Tris-HCl 50 mM, pH 7.5, with 10 mM $MgCl_2$)
positive solution: reaction buffer with 0.625 µM L-ribozyme
Nanoparticle/(L)-substrate conjugates and nanoparticle/L)-inhibitor/ribozyme conjugates previously separated were resuspended in the reaction buffer and then mixed in the ratio of 1:1 in 1.5 ml reaction tubes. For the positive control, the nanoparticle/(L)-substrate conjugates were added to the positive solution, and accordingly for the negative control, the reaction buffer was mixed with nanoparticle/L-substrate conjugates. The end concentration of nanoparticle/(L)-substrate conjugates was identical in all four reaction samples. One of the conjugated nanoparticle-mix was incubated at 37°C, while the other one was incubated at 49°C in a thermomixer. The controls were incubated at either 37°C or 49°C; no significant difference was observed between the two temperatures. Aliquots were taken from each sample after 1, 2, 3, and 4 h and immediately centrifuged. The supernatants were carefully removed and transferred into a fresh microfuge tube. RFU (relative fluorescence unit) signals of the supernatants were measured by NanoDrop 3300 Fluorospectrometer (Thermo Scientific).

(B) in human serum
The whole set of experiments with L-nucleic acids was also performed in human serum (Sigma) instead of the reaction buffer, in an incubator at 37°C or 49°C, 94.5% humidity and 5% carbon dioxide.

4. Results

The initial strategy of this work comprised the melting of double-stranded nucleic acids to trigger a temperature-controlled release of drugs from the surface of nanoparticles (Chapter 4.1). Due to unsatisfactory performance of this concept, a novel strategy was developed that employed ribozymes (Chapter 4.2). After the initial proof of concept with fluorescent dyes as model substrate, a cytostatic drug was attached to the ribozymal release system (Chapter 4.3).

4.1. dsDNA-Nanoparticle-Drug Delivery System

The concept of controlled drug release from nanoparticles employed the melting ability of double-stranded DNA (dsDNA). This scheme of a thermolabile DNA linker is outlined in Figure 22. One strand, the immobile strand, is covalently linked to a magnetic nanoparticle. The complementary strand, the mobilizable strand, which is covalently linked to a drug, is then released by double strand dehybridazition upon temperature enhancement. This enhancement is generated by heat production of superparamagnetic nanoparticles in an alternating magnetic field.

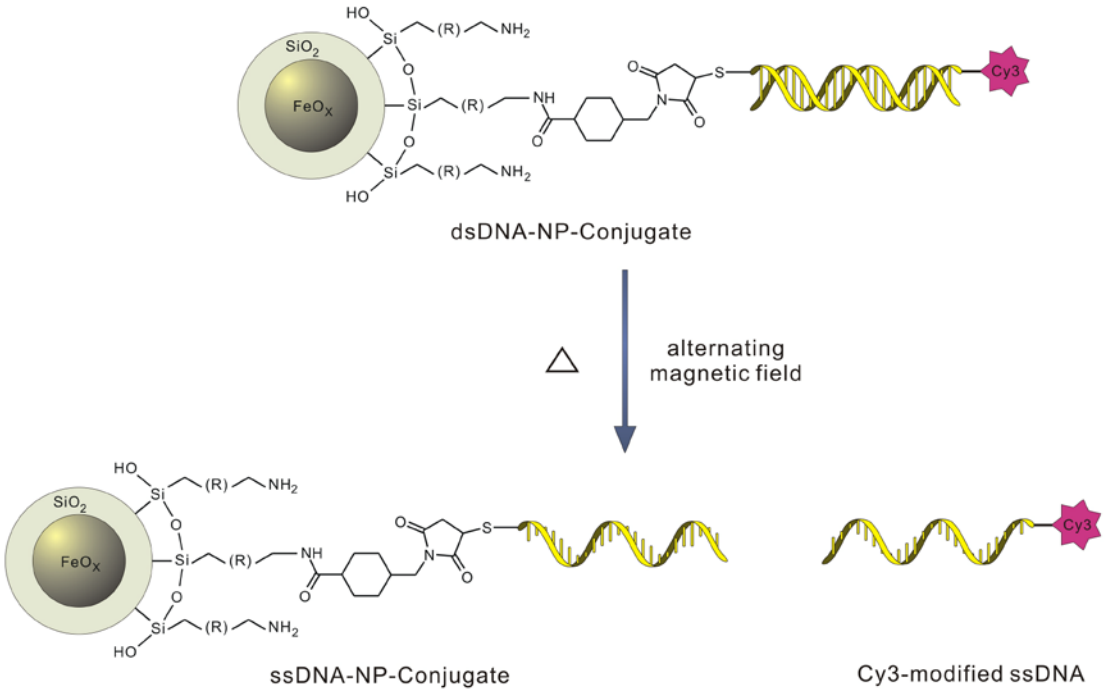

Figure 22: dsDNA-nanoparticle-drug delivery system. The dsDNA-NP-conjugates could be heated in a thermomixer or in an AC magnetic field. The dye Cy3, which can be monitored by its

fluorescence, serves as a substitute for the cytostatic drug. Upon local temperature increase, single-stranded DNA is released via dehybridization.

There are two essential requirements to realize a proof of concept for this strategy. First, the oligonucleotide needs to be modified at the 3'- or 5'- ends with functional groups that allow covalent coupling to the particles and to the drugs. Second, the melting of the DNA duplex needs to be optimized, since any drug release should be avoided at body temperature, while the DNA strands should be fully separated at the temperature that can be reached in the tumor during thermotherapy sessions. Even though the maximal temperature reached 82°C in tumor tissue, the median peak temperature was measured at 51.2°C (Maier-Hauff *et al.*, 2010). The melting of the DNA duplex should thus be limited to a temperature interval between 40 °C and 50 °C. The drugs released via hyperthermia can subsequently diffuse even into the tumor periphery, where few nanoparticles accumulate and no significant temperature increase occurs.

To achieve the first aim, different crosslinkers were used to conjugate nucleic acids and nanoparticles. Nanoparticles with different modifications on the surface were tested to get the optimal coupling efficiency and the best dispersion after the conjugation.

To achieve the second aim, different DNA sequences were tested to compare the melting properties of the DNA duplex for the drug delivery system. The temperature-controlled drug release experiments were performed either in a thermomixer (direct heating) or in a magnetic field applicator (indirect heating).

4.1.1 Immobilization of Oligonucleotides to Nanoparticles

Different strategies were tested to link the immobile strand to the nanoparticles in a covalent manner. Superparamagnetic iron oxide nanoparticles with three different active groups on the surface were provided by the cooperation partner (MagForce Nanotechnologies AG, Berlin) as outlined in Table 13. Accordingly, oligonucleotides were synthesized by solid phase synthesis by IBA (Göttingen) with different functionalities at their 5'-ends. Coupling reactions were then performed either directly

or in the presence of crosslinkers, such as the zero-length crosslinker EDC, the homobifunctional crosslinker PDITC and the heterobifunctional crosslinkers Sulfo-SMCC or Sulfo-GMBS (Tab. 13).

To evaluate the efficiency of immobilization, the number of bound oligonucleotides per nanoparticle needs to be determined. A direct quantification of the immobile strands by radioactive labeling of the DNA is not feasible due to the chemical composition of the nanoparticles. Since these particles contain iron oxide, this would lead to significant “Bremsstrahlung” upon ß-emission. Therefore, the number of bound oligonucleotides was measured indirectly by annealing Cy3-labelled complementary strands to the immobile strands. Upon dehybridization by heating, the number of complementary strands was determined by measuring their fluorescence. The number thus obtained was defined as the apparent number of bound oligonucleotides.

The fluorescence was determined in a NanoDrop 3300 fluorescence spectrometer (Thermo Scientific, USA), since this device allows the measurement of very small sample volumes (1–2 µl). It was essential to first evaluate whether the RFU (**R**elative **F**luorescence **U**nit) values correlate with the actual concentrations in a linear fashion. Standard calibration curves confirmed that Cy3-labelled oligonucleotides displayed a linear relationship within a range of 10 uM to 20 nM. The standard calibration curve of DNA Si-Cy3 (5´- Cy3- CTG CGA GGC GGT AGT CTA TT –3´) is shown in Figure 23 as an example. The comparison with UV-absorption, however, revealed that different Cy3-labelled oligonucleotides had different fluorescence coefficients. Therefore, an individual standard calibration curve was recorded for all oligonucleotides investigated in this work.

The number of nanoparticles was calculated from the measurement of iron concentrations, which were determined by AAS (**A**tomic **A**bsorption **S**pectroscopy). As estimated from the particle size seen on TEM micrographs, one nanoparticle consists of about 70,000 iron atoms. The number of bound oligonucleotides per nanoparticle was calculated from the amount of oligonucleotides released and the number of nanoparticles.

To evaluate the number of specifically bound oligonucleotides per nanopaticle, the unspecific binding of DNA was determined in control experiments. Here, the

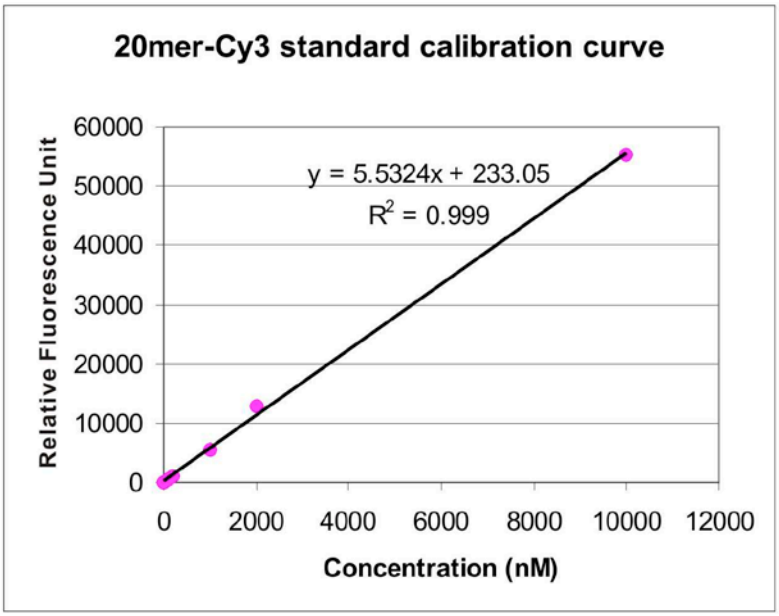

Figure 23: Standard calibration curve for DNA Si-Cy3. The RFU was plotted against the concentration (nM) of Si-Cy3.

functionalized oligonucleotides were omitted in the coupling reactions and the nanoparticles were only exposed to complementary strands. Again, the complementary strands were released at high temperature and their amount was determined by measuring their fluorescence. The total number of bound oligonucleotides per nanoparticles, the number of unspecifically bound oligonucleotides per particle, and the number of specifically bound oligonucleotides per particle using different crosslinkers are shown in Table 13.

Table 13. Efficiency for the coupling of crosslinker

Crosslinker	Active Group on NP surface	Modifica-tion of Nucleic Acids	Total number of bound oligonucleotides per nanoparticles	Number of unspecifically bound oligonucleotides per particle	Number of specifically bound oligonucleotides per particle
Sulfo-SMCC	$-NH_2$	-SH	18.5±2.5	2.75±0.77	15.85
Sulfo-GMBS	$-NH_2$	-SH	0.36±0.5	0	0.36
EDC	$-NH_2$	-COO	10.3±0.4	8.85±0.77	1.45
EDC	$-NH_2$	$-PO_4$	17.3±2.5	16.5±0.7	0.8
PDITC	$-NH_2$	$-NH_2$	0.11±0.15	0.18±0.25	0

---	epoxide	-NH_2	0.45±0.48	0.32±0.29	0.13
---	epoxide	-SH	0.085±0.03	0.05±0.07	0.03
---	Au-coated	-SH	0.75±1.06	0	0.75

The attempts to covalently bind amino- or thio-functionalized oligonucleotides to a reactive nanoparticles surface in the absence of crosslinkers were unsuccessful (Tab. 13). The coupling of amino- and phosphate-functionalized oligonucleotides with EDC showed promising results. The control reactions, however, revealed that the apparent binding efficiency was due to unspecific interactions. In contrast, coupling reactions of amino-functionalized oligonucleotides with sulfo-GMBS showed specific binding, but the efficiency was lower than one immobilized strand per nanoparticle. Sulfo-SMCC displayed the best coupling efficiency and specificity. On average, 15 oligonuleotides with thiol group modification could be coupled specifically to one iron oxide nanoparticle. The Sulfo-SMCC coupling scheme is depicted in Figure 24.

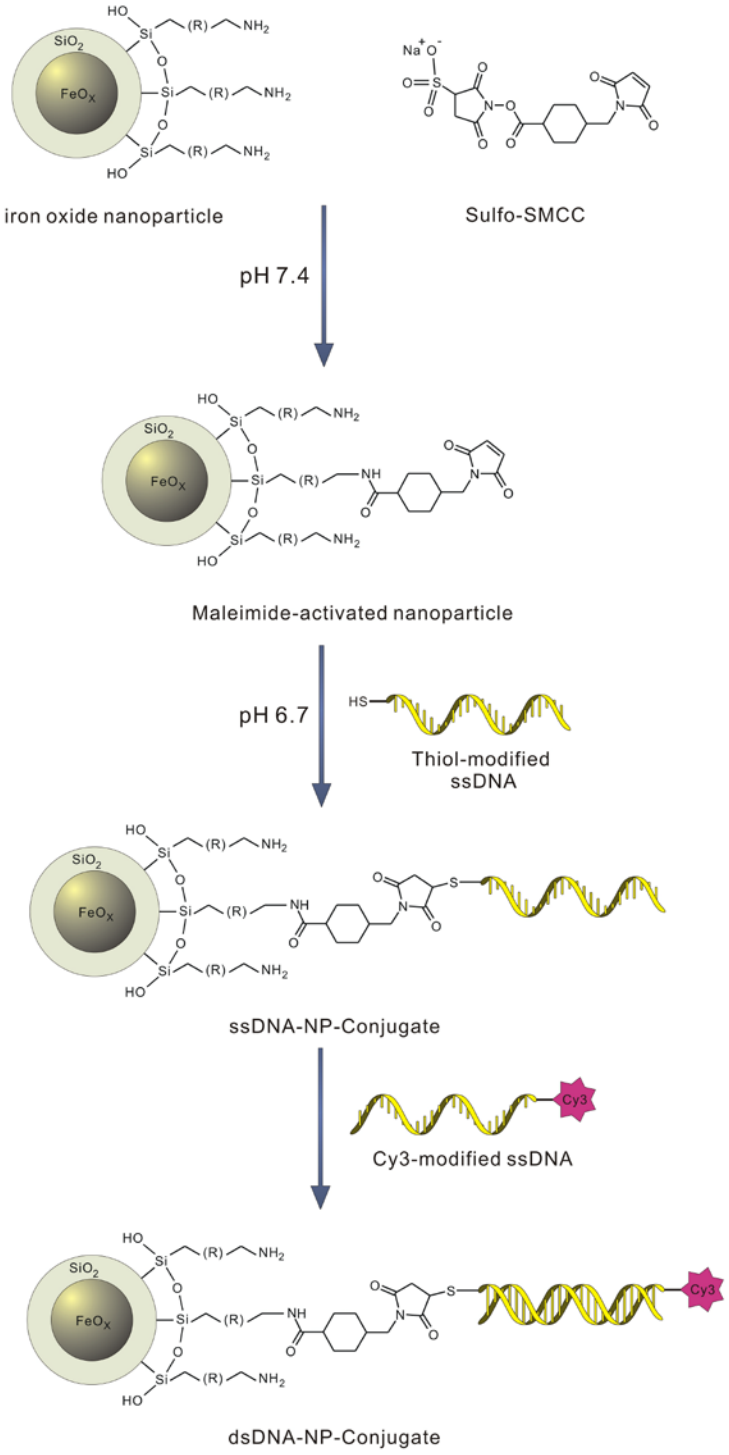

Figure 24: Sulfo-SMCC as crosslinker for the coupling of dsDNA-NP-conjugates. The reaction is a pH-dependent two-step coupling.

The coupling protocol with Sulfo-SMCC of Derfus *et al.* (2007) was optimized to assemble dsDNA-NP-conjugates (see chapter 3.2.1). Sulfo-SMCC is a water-soluble, non-cleavable heterobifunctional crosslinker. It works in a two-step reaction under different pH conditions to conjugate thiol group-containing and amino group-

containing molecules. In the first step, the NHS esters of Sulfo-SMCC were reacted with primary amines of nanoparticle at pH 7.4 to form stable amide bonds. In the second step, maleimides were reacted with sulfhydryl groups of the modified DNA at pH 6.7 to form stable thioether bonds. To finally assemble the dsDNA-nanoparticle-conjugates, the ssDNA-NP-conjugates were hybridized with Cy3-labeled complementary ssDNA. Extensive washing with distilled water and rigorous mixing after every reaction step were essential to enhance the dispersion of DNA-nanoparticle-conjugates.

4.1.2 Comparison of Melting and Release Curves of dsDNA

To optimize the release of mobilizable strands, the melting properties of the DNA duplexes involved need to be evaluated. The measurement of a UV melting curve of a dsDNA bound to nanoparticles, however, is prohibited by the strong absorption of these particles. Therefore, a new method was established to measure the amount of released ssDNA, which is outlined in Figure 25. The mobilizable strand was labelled by a fluorescent dye and the amount of released label was measured at different temperatures as a release curve.

This approach was established with the dsDNA Si-SH/Si-Cy3 (**Si-SH:** 5'- SH-ATG CTT CCA CGA GCC TTT CGA ATA GAC TAC CGC CTC GCA G -3', **Si-Cy3**: 5´-Cy3- CTG CGA GGC GGT AGT CTA TT –3´). The Si-SH-NP conjugates with hybridized Si-Cy3 were prepared as described above (section 4.1.1). A solution of these dsDNA-NP-conjugates (50 pmol conjugate in 200 µl) was incubated for 5 min in a thermomixer at a start temperature of 30 °C. After mixing, a first aliquot of 5 µl solution was taken and transferred into a new tube. This sample was immediately centrifuged for 5 min at 13,000 g. The supernatant was carefully removed and transferred into a fresh tube (Fig. 25). This removal of aliquots was repeated at increasing temperature intervals of 10°C until reaching the final temperature of 90°C. The RFU (relative fluorescence unit) values of Cy3-modified ssDNA in the supernatants were measured by a NanoDrop 3300 Fluorospectrometer (Thermo Scientific) and the release curve was plotted employing the program Excel (Fig. 26).

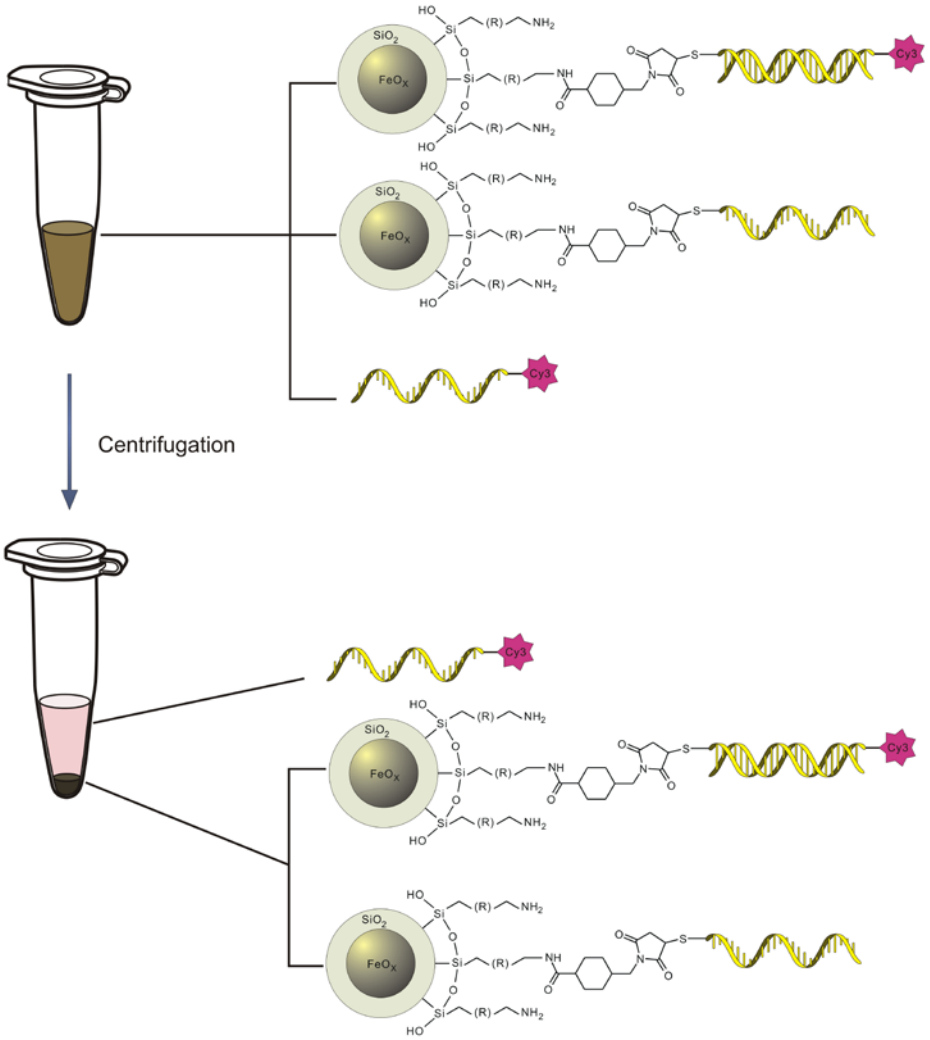

Figure 25: Release experiments of dsDNA-nanoparticle-conjugates. Aliquots taken at different temperatures contained a mixture of dsDNA-NP-conjugates, ssDNA-nanoparticle-conjugates and Cy3-labeled ssDNA. The amount of released Cy3-labeled ssDNA could be monitored by fluorescence measurements in the supernatant after centrifugation, since hybridized dsDNA-nanoparticle-conjugates and ssDNA-nanoparticle-conjugates remained in the pellet.

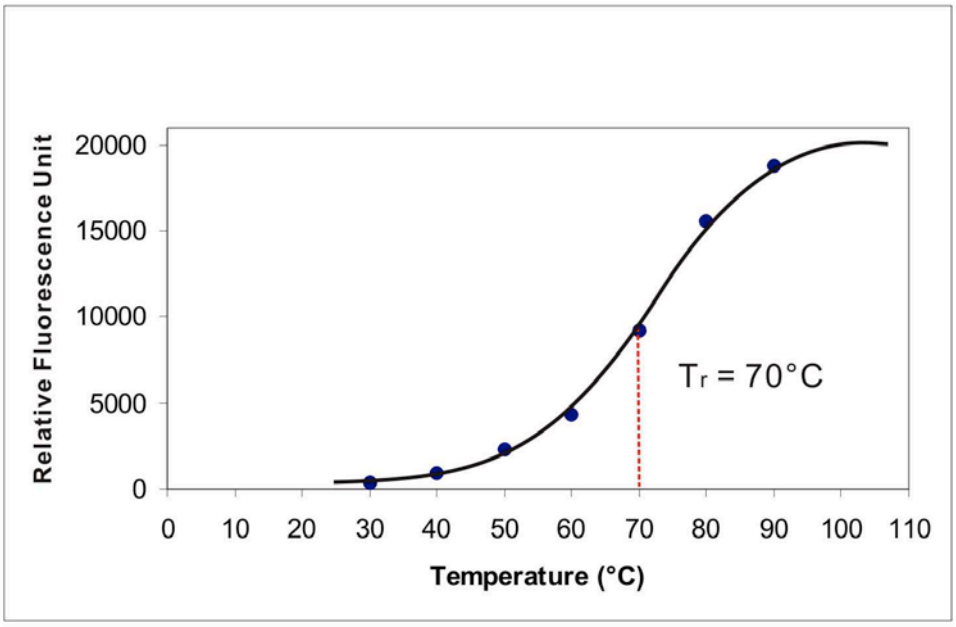

Figure 26: Release curve of Si-SH/si-Cy3-nanoparticle conjugates. The release experiment of Si-SH/Si-Cy3-nanoparticle conjugates was performed in PBS buffer at pH 7.2. The release of 50% of mobilizable strands (T_r) occurred at 70 °C.

The overall appearance of this release curve is similar to a melting curve of a duplex DNA. In analogy to such a melting curve, a release temperature (T_r) was defined as the point where 50% of the hybrid is completely dissociated. The release of 50% mobilizable strand occurred at 70°C for the applied Si-SH/Si-Cy3-nanoparticle conjugates.

To evaluate the reliability of this approach, the release curve of the duplex bound to nanoparticles was compared with the melting curve of the free duplex with the same sequence in solution. Double-stranded DNA Si-SH/Si-Cy3 (2 µM) was dehybridized and rehybridized in PBS buffer (pH 7.2). The melting curve of dsDNAs was monitored with a Spectrophotometer HP 8452A Diode-Array. A temperature profile with increments of 1°C and hold times of 1 min was chosen within a range from 20°C to 90°C (Fig. 27).

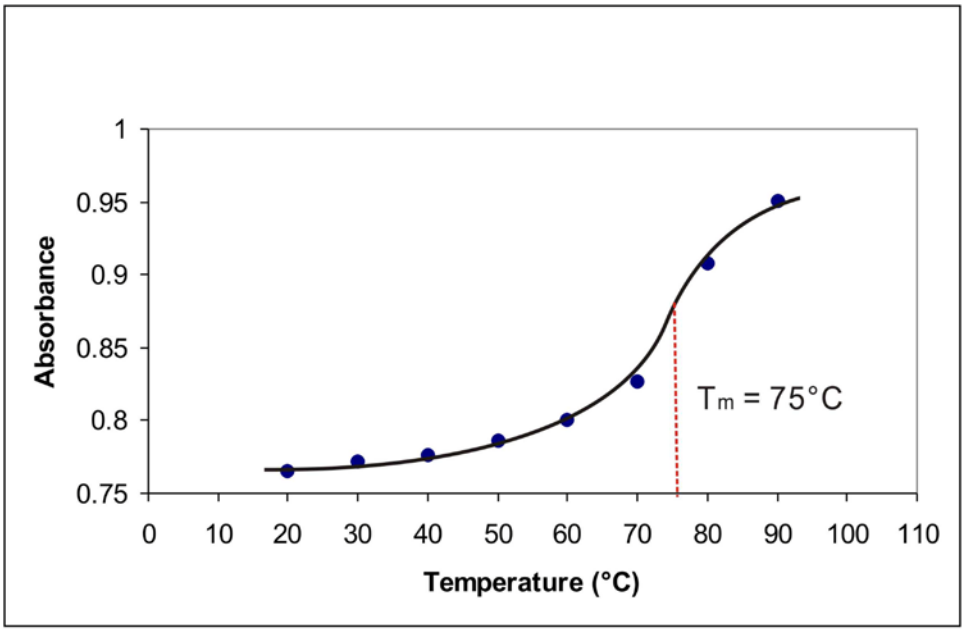

Figure 27: Melting curve of DNA Si-SH and Si-Cy3. After denaturing and renaturing, the melting curve of dsDNA Si-SH/Si-Cy3 was taken in PBS buffer (pH 7.2) at a concentration of 2 µM. The melting temperature (T_m) of the dsDNA under these conditions is 75°C.

The melting temperature was determined as 75°C and is located 5°C above the release temperature. This difference is likely due to surface effects of nanoparticles that destabilize the duplex in the conjugate and the corresponding dehybridization (cooperative melting) of DNA in solution (Mirkin *et al.*, 1996; Storhoff *et al.*, 2000; Jin *et al.*, 2003; Kiang, 2003).

The melting curve (Fig. 27) of the duplex records partial and complete dehybridization events, while the measurement of a release curve (Fig. 26) can monitor complete dehybridization events only. Therefore, the comparison of the melting curve reveals a broader range of absorbance increase as compared to the release curve of dsDNA Si-SH/Si-Cy3-nanoparticle conjugates.

4.1.3 Choice of the Sequence of the dsDNA Linker

DNA duplexes of different sequence were screened to optimize the release of mobilizable strands within the narrow thermal interval, which is defined by 37°C as

the body temperature of a patient and by 50°C as the medium temperature of MFH for drug release in the tumor.

The choice of the sequences tested was based on the concept that the melting curves of duplexes composed of complementary homopolymers are sharper than those of duplexes with heterogeneous sequences. These melting properties are due to their uniform structure and stability along the whole length of the molecule (Cantor & Schimmel, 1980). The evaluation of GC-rich sequences was avoided, since homopolymeric stretches of guanosines tend to form stable self-structured conformations. This would severely complicate the melting properties of the conjugates. Therefore, the selection of sequences was focused on AT-rich oligodeoxynucleotides.

The sequences listed in Table 14 were synthesized by IBA (Göttingen) and coupled via sulfo-SMCC to SR-E2 nanoparticles. The table summarizes the melting and release temperatures of these conjugates.

Table 14: The melting temperature (T_m) is defined as the temperature, where half of the helical structure is lost. The release temperature (T_r) is defined as the temperature, where half of the mobilizable strands are fully separated from the conjugate.

DNA-duplex	**Sequence (5´-3´)**	**T_m**	**T_r**
Si-SH	SH-ATG CTT CCA CGA GCC TTT CGA ATA GAC TAC CGC CTC GCA G	75°C	70°C
Si-Cy3	Cy3- CTG CGA GGC GGT AGT CTA TT		
San-SH	SH-TTT TTA GGT GTA GTG CGT GTC	63°C	57°C
San-Cy3	Cy3-GAC ACG CAC TAC ACC TAA		
Er-SH	SH- TTT TTT TTT TTT TTT TTT TTT GCC	57°C	54°C
Er-Cy3	Cy3-GGC AAA AAA AAA AAA AAA AAA		
Yi-SH	SH-TTT TTT TTT GGG TTT TTT TTT CGC	59°C	54°C
Yi-Cy3	Cy3-GCG AAA AAA AAA CCC AAA AAA		

Due to the higher stability of GC-base pairs as compared to AT-base pairs, the melting and release temperatures depend on the GC content of the sequences. The 20-mer duplex formed by Si-SH and Si-Cy3 is significantly more stable than the other three duplexes. Even the 18-mer hybrid of San-SH and San-Cy3 has higher T_m and T_r values as the other two 21-mer duplexes, which are AT-rich.

The data reveal for all different duplexes that the melting temperatures are higher than the release temperatures of the conjugates.

The sharpest release curve was obtained with the DNA duplex Yi-SH/Yi-Cy3, which is a homopolymeric AT sequence with a central and a terminal GC triplet (Fig. 28). It provided a T_r of 54°C. This release curve meets the initial criteria of a stable duplex at body temperature. At 50°C, however, the release of mobilizable strand was an insufficient 33% and was thus falling short of initial expectations.

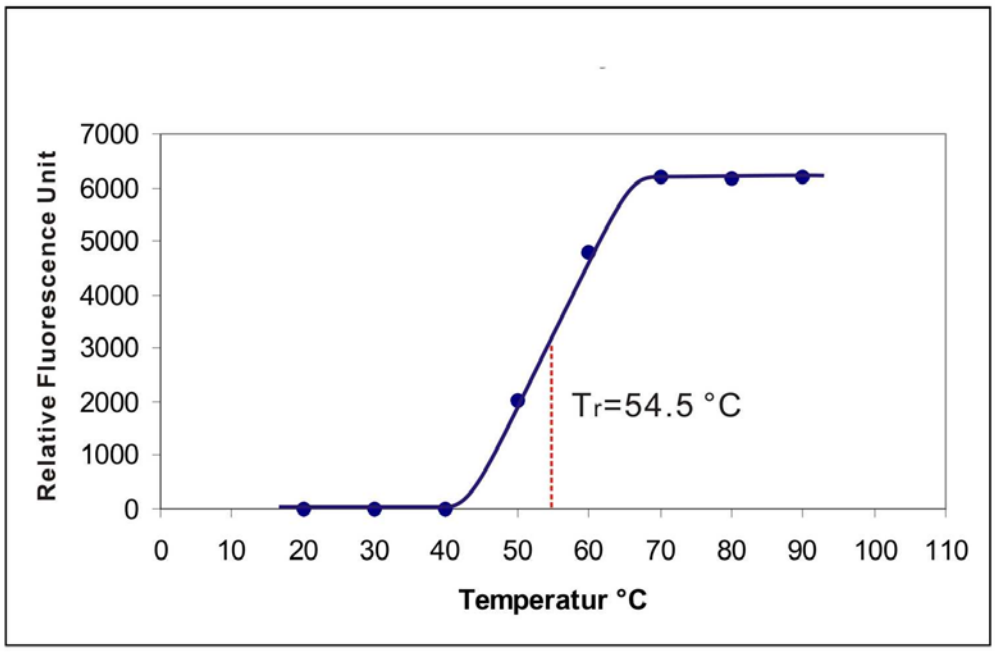

Figure 28: Release curves of dsDNA-NP-Conjugates. The release curve of Yi-SH/Yi-Cy3-NP-conjugates. The T_r is 54.5 °C and the release interval is 30°C (from 40°C to 70°C)

4.1.4 Release Experiment in the Magnetic Field Applicator MFH®-12-TS A

To mimic the conditions of a drug delivery system *in vivo*, a release curve was measured employing the applicator MFH®-12-TS A, which was designed at MagForce (Berlin) for experiments in the laboratory scale and with small animals (Fig. 29). Here, the temperature increase is achieved by inherent properties of the superparamagnetic nanoparticles. Due to their superparamagnetic behavior, the

particles are heated by a Brownian and Néel-process by an alternating magnetic field with frequency of 100 kHz and field strength of 0–15 kA/m.

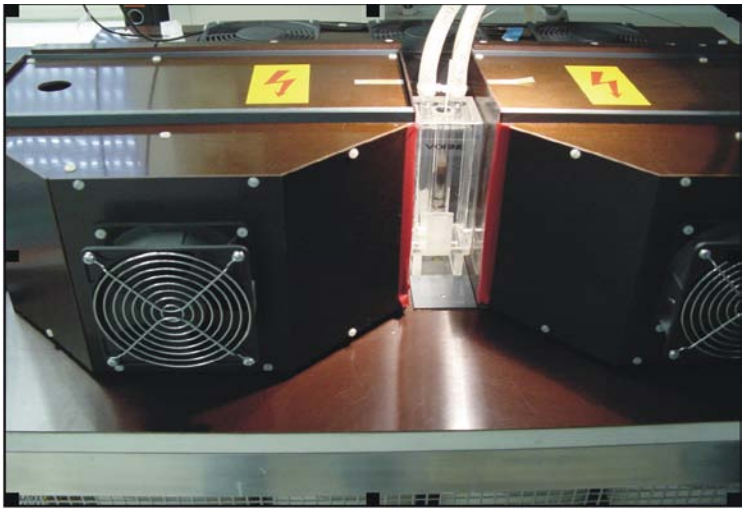

Figure 29: Magnetic field applicator MFH®-12-TS A. The mixture of dsDNA Yi-SH/Yi-Cy3-NP-conjugates and iron oxide NP without shell were placed in the isothermal chamber in the middle of the applicator. (Reprinted with permission from Magforce Nanotechnologies AG, Berlin, Germany)

The measurement of the release curve was performed with dsDNA Yi-SH/Yi-Cy3-NP-conjugates. During the experiment, the temperature profile was monitored by a fiberoptic probe (Fig. 30A). While the profile shows an overall temperature increase from 35°C to 60°C, the sharp temperature decreases visible in the diagram mark the sampling points as the magnetic field has to be turned off for safe handling. Samples were taken after keeping a constant temperature for 10 min in the suspension. The sample was centrifuged and the supernatant was utilized for fluorescence spectroscopy. The resulting graph is shown in Fig. 30B, representing a significant increase in the release of Cy3-labeled single strand with field strength and thus sample temperature.

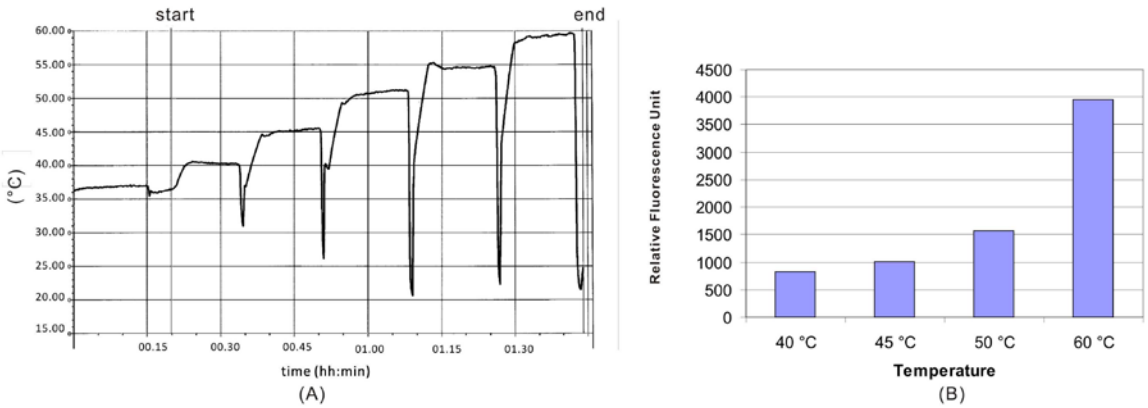

Figure 30: (A) Temperature profile of the DNA modified nanoparticle suspension in an AC magnetic field with increasing field strength (2–12 kA/m). (B) Release profile of the fluorescent dye after treatment of the nanoparticles in an AC magnetic field.

4.1.5 dsDNA-Nanoparticle-Doxorubicin Release Experiment

It was tested whether the cytostatic drug doxorubicin could be implemented into the concept of temperature-controlled release from nanoparticles. Doxorubicin (DOX) is an anthracycline anti-tumor drug and is clinically employed in chemotherapy. The inherent fluorescence of doxorubicin makes it an ideal candidate for all *in vitro* studies due to easy localization and quantification. Doxorubicin can bind to DNA by intercalation into the duplex and inhibits the macromolecular biosynthesis. Systematic application of doxorubicin, however, is known to be cardiotoxic to some individuals (Singal and Iliskovic, 1998; Yeh *et al.*, 2004). This side-effect could be avoided by a local administration of the drug.

The duplex TG-SH/AC (TG-SH: 5´-SH-TTT TTT TTT TTG GGT TTT T; AC: 5´-CGA AAA ACC CAA AAA AAA-3´) was immobilized via sulfo-SMCC to SR-E2 nanoparticles. The melting curve revealed a T_m of 55°C and the release curve a T_r of 49°C. The conjugates (200 µl, 1 pmol/µl) were incubated with 200 µl doxorubicin solution (1000 mg/L) at 20°C for 18 h under constant rotation. The sample was centrifuged at 13000 g for 5 min to remove unbound doxorubicin. The pellet was washed with 400 µl cell culture medium (RPMI 1640) and then resuspended in 300 µl of this medium. As a negative control, 200 µl iron oxide nanoparticles SR-E2 (1 pmol/µl) were treated with doxorubicin in an identical manner. The dsDNA-NP-doxorubicin-conjugates and the negative control were incubated in a thermomixer at 37°C for 5 min. Aliquots were taken from the well-mixed conjugates and immediately centrifuged at 13000 g for 5 min. The supernatants were carefully removed and transferred into a fresh microfuge tube. Upon increasing temperatures in the thermomixer, this step was repeated at 50°C, 65°C and 80°C, respectively (Fig. 31).

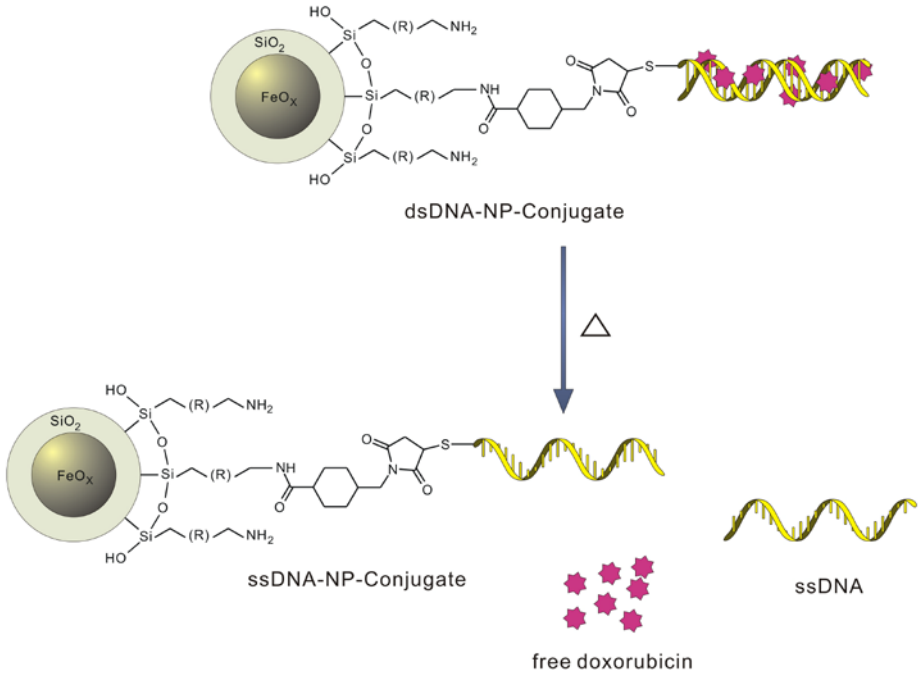

Figure 31: Release experiment of dsDNA-nanoparticle-doxorubicin conjugates. Doxorubicin can intercalate into double-stranded DNA. With increasing temperature the dsDNA is dehybridized slowly and the doxorubicin is released from the conjugates.

The fluorescence intensity of doxorubicin in the supernatant (excitation at 470 nm, emission at 566 nm) was read by a multifunctional microplate reader (TECAN). The temperature-dependent release of doxorubicin could be calculated with the help of a standard calibration curve (Fig. 32).

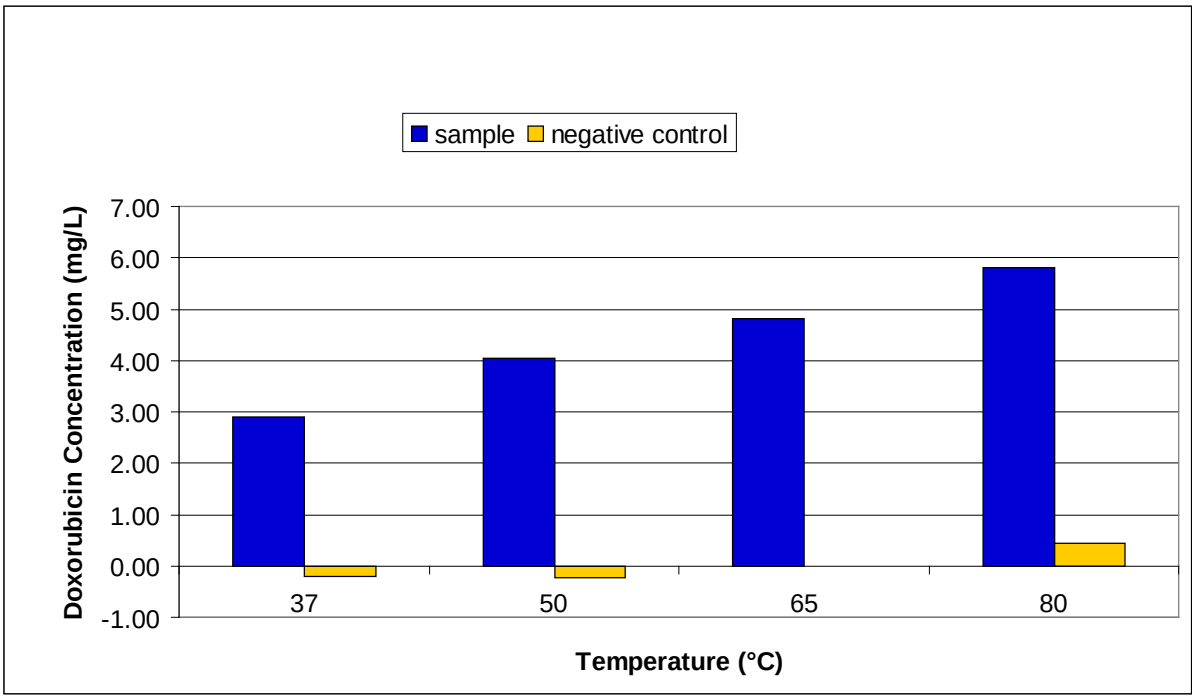

Figure 32: Doxorubicin release from dsDNA-nanoparticle-DOX-conjugates. Blue columns represent the doxorubicin concentration in the supernatant of dsDNA-nanoparticle-DOX-conjugates at different temperature. The yellow columns show the doxorubicin concentration in the negative control.

The data demonstrate that the release of doxorubicin from the dsDNA-NP-drug delivery system is clearly temperature-dependent, as higher doxorubicin concentrations can be observed with increasing temperatures. These results, however, also reveal that there is already a significant release of doxorubicin at body temperature of 37°C, which can be explained by helix destabilization upon intercalation of doxorubicin.

4.2. Ribozyme-based Nanoparticle-Drug Delivery System

The concept of a temperature-controlled drug release from nanoparticles requires the absence of any drug release at body temperature to prevent unspecific and adverse reactions in the patient. In addition, the concept proposes a significant release of drugs at about 50 °C. The dehybridization experiments described in the last chapter demonstrated an insufficient delivery at this temperature. A low percentage of released nucleic acid, however, could become meaningful, if these rare events were amplified by a catalytic reaction.

This reasoning led towards the conception of a ribozyme-nanoparticle-drug-delivery system, which is outlined in Figure 33. It is composed of two components. The first component consists of a complex of a catalytically active nucleic acid strand (ribozyme) and a complementary strand, which acts in an inhibitory fashion and is thus termed inhibitor strand. The inhibitor strand is covalently bound to the surface of an iron oxide nanoparticle. Depending on the base pair interactions and the molar ratio between the ribozyme and inhibitor strands, these hybridized double strands are stable below and at 37°C, while the ribozyme strand would be released gradually above this temperature. At body temperature, the helical interaction with the inhibitory strand can completely prevent any activity of the ribozyme strand. Upon heating of the particles in an alternating magnetic field, the complex will melt and the ribozyme strand is released. The free ribozyme can now attack the second component, which is a cytostatic drug that is bound via a substrate strand to a second nanoparticle. Once the substrate strand is specifically cleaved by the ribozyme, the drug is released and delivered to the surrounding tissue.

This concept relies on the stability of all components involved. If the substrate strand is cleaved by any cellular activity besides the released ribozymes, unspecific reactions can be expected. Moreover, if the released ribozyme strands are degraded by abundant nucleases, the specific release of the cytostatic drug would be abolished. The concept of a temperature-controlled drug release from nanoparticles was thus extended towards mirror-image nucleic acids, which are known to possess an extraordinary stability in a cellular environment (Klussmann *et al*., 1996; Nolte *et al*., 1996).

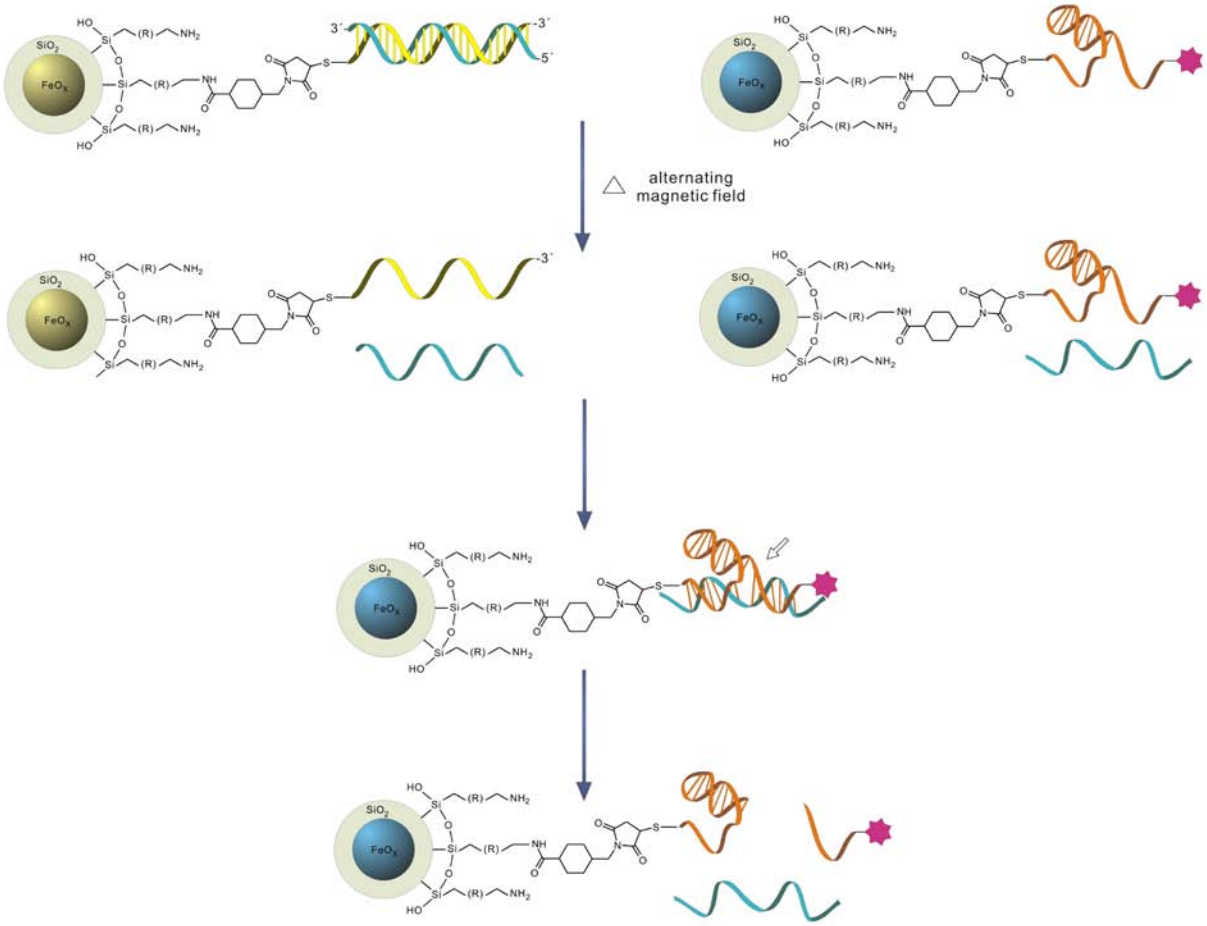

Figure 33: Ribozyme-based nanoparticle-drug delivery system. The system consists of two components. In the first component (upper left part of the Figure), the inhibitorstrand is covalently bound to the surface of an iron oxide nanoparticle. The ribozyme (blue strand) is hybridized to the inhibitor (yellow strand) at T ≤ 37°C. Once the particles are heated in an alternating magnetic field, the local temperature will be raised. Consequentially, the complex will melt and the ribozyme will be released. The free ribozyme now attacks the second component (upper right part of the Figure), where a substrate strand connects the drug to a nanoparticle. One end of the substrate strand is covalently bound to the nanoparticle, while on the other end it carries an active ingredient (red star). Free ribozyme will specifically cleave the substrate strand and the active ingredient is released into the surrounding tissue.

4.2.1. Choice of the Ribozyme, Substrate and Inhibitor

The ribozyme concept requires that the hybrid of ribozyme and inhibitor strand is stable at 37 °C, while a significant amount of ribozymes needs to be released at elevated temperature. For the proof of concept, a target temperature of 49°C was chosen. Moreover, the substrate strand should be cleaved efficiently at this temperature. Two different hammerhead ribozymes (Ruffner, 1990, Hertel et al. 1992)

were tested for their ability to fulfill these criteria. Their sequences are displayed in Table 15.

Table 15: Sequences of ribozymes, their corresponding substrates and inhibitors. The arrows denote the sites of cleavage.

Group I		
Ribozyme 1	RNA	5´-GGC UCG ACU GAU GAG GCG C-3´
Substrate 1	RNA	5´-GCG CCG AAA CAC CGU GUC ↓ UCG AGC-3´
Inhibitor 1	DNA	5´-GCG CCT CAT CAG TCG AGC C-3´
Inhibitor 1-2bp	DNA	5´-G CCT CAT CAG TCG AGC C-3´
Group II		
Ribozyme 2	RNA	5´-GGC GAC CCU GAU GAG GCC GAA AGG CCG AAA CCG U-3´
Substrate 2	RNA	5´-ACG GUC ↓ GGU CGC C-3´
Inhibitor 2A	DNA	5´- ACG GTT TCG GCC TTT CGG CCT CAT CAG GGT CGC C-3´
Inhibitor 2A-2bp	DNA	5´- CG GTT TCG GCC TTT CGG CCT CAT CAG GGT CGC -3´
Inhibitor 2B	DNA	5´- ACG GTC GGT CGC C -3'

Ribozyme and inhibitor strands were hybridized in 50 mM Tris-HCl (pH 7.5) and 10 mM $MgCl_2$ in different molar ratios. Substrate strands, which were ^{32}P-labeled at their 5´-ends, were added to these hybridized strands. The mixture was divided into aliquots and simultaneously incubated at 37 °C or 49 °C for 50 min. The reactions were analyzed by 20% polyacrylamide gel electrophoresis and quantified through phosphorimaging. Since the full length duplex of ribozyme and inhibitor strand allowed insufficient release of ribozymes at 49 °C, shorter variants of the inhibitor strands were tested (Tab. 15). The best results were obtained with ribozyme 1 and the inhibitor 1-2bp at a hybridization ratio of 1:0.95 (Fig. 34, lanes 7 and 8). This sample showed full-length substrate at 37 °C and a significant cleavage band at 49 °C.

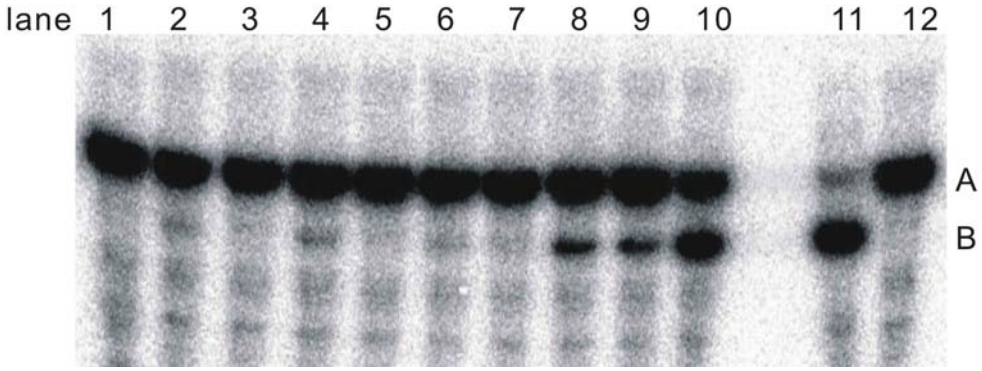

Figure 34: Optimization of the ribozyme cleavage reaction. Phosphorimage of a 20% denaturing polyacrylamide gel to analyze the effect of five different hybridization ratios of ribozyme 1 and inhibitor 1-2bp on the cleavage of substrate 1. A indicates the position of the full length substrate 1 with a size of 24 nucleotides. B marks the position of the 5´- fragment of cleaved substrate1 with a size of 12 nucleotides. The ratio of ribozyme 1 and inhibitor 1-2bp in lanes 1 and 2 was 1:1.01, in 3 and 4 was 1:1, in 5 and 6 was 1:0.99, in 7 and 8 was 1:0.95 and in 9 and 10 was 1:0.9. Samples 1, 3, 5, 7 and 9 were incubated at 37 °C for 50 min, while samples 2, 4, 6, 8, 10, 11 and 12 were incubated at 49 °C for 50 min. Lane 11 shows a reaction in the absence of inhibitor. Lane 18 shows the untreated substrate strand.

4.2.2. Activity of Mirror-Image Ribozymes

Mirror-image oligoribonucleotides (L-form nucleic acids) have proven to possess reciprocal chiral specifities (Klussmann *et al*., 1996; Nolte *et al*., 1996). Since it has been recently shown for the first time that mirror image hammer head ribozymes are able to cleave sequence specific mirror image target sequences (Erdmann, V.A., personal communication; Wyszko & Erdmann, 2010), I tried successfully to introduce the mirror image nucleic acid technology in this project.

The L-form nucleic acids were purchased from IBA (Göttingen, Germany). The substrate strand carried a thiolgroup at its 5'-terminus to allow the immobilization to nanoparticles in later experiments (see below). The 3'-end of this oligoribonucleotide was labeled with the fluorescent dye Alexa 647 for its sensitive detection (Tab. 16).

Table 16: Mirror-image nucleic acids. The arrow denotes the site of cleavage.

Name	Type	Sequence
L-Rib1	L-RNA	5´-GGC UCG ACU GAU GAG GCG C-3´
L-Sub1	L-RNA	5´-SH-GCG CCG AAA CAC CGU GUC ↓ UCG AGC-Alexa 647-3´

Due to the functionalization of the L-form substrate (L-sub1) with a 5'-thiol group, these oligoribonucleotides were prone to dimerize upon formation of disulfide bonds (Fig. 35, lane 1). This dimerization, however, could be avoided in the presence of 1 mM TCEP (Fig 35, lane 2). To test for the activity of the L-form ribozyme, the monomerized substrate L-Sub1 was reacted with the ribozyme L-Rib1 (Fig 35, lane 3). The appearance of a product band with a size of 6 nucleotides was indicative for the reciprocal activity of the mirror image ribozyme.

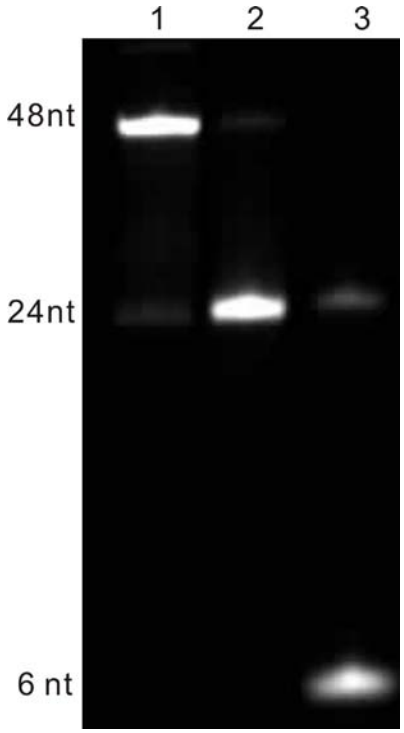

Figure 35: Cleavage assay with L-form ribozyme. A 20% denaturing polyacrylamide gel analysis was performed to analyze the cleavage reaction. The gel was scanned for Alexa 647-fluorescence in a QUANTUM-Fluorescence Imagingsystem (PeqLab, Germany). Lane 1 was L-Sub1 without TCEP-treatment displaying a strong band for L-Sub 1 dimer (48 nucleotides) and a weak band for L-Sub 1 monomer (24 nucleotides). Lane 2 was L-Sub1 after TCEP-treatment. Lane 3 was TCEP-treated L-Sub 1 after ribozyme cleavage, where a product band appeared with a size of 6 nucleotides.

4.2.3. Stability of Mirror-Image Nucleic acids

A comparative study of D- and L-form ribozymes was performed to assess their stability towards nuclease degradation. The naturally occurring ribonucleases should be unable to digest L-oligonucleotides due to their inherent mode of stereospecific catalysis.

Both, ribozyme 1 and mirror-image L-Rib1, were exposed to human serum for different time periods. The long-term incubations in the hour range were carried out in an incubator at 94.5 % humidity and 5 % carbon dioxide to stabilize the pH value of the serum. After different time intervals, aliquots were taken from the incubation solution and analyzed on a 15 % denaturing polyacrylamide gel (Fig. 36). The polyacrylamide gel were stained by soaking in EtBr solution and visualized under an ultraviolet transilluminator. As can be deduced from the gel analysis, the ribozyme in its natural D-configuration (ribozyme 1) was almost completely digested in human serum after 50 seconds, while the ribozyme in the mirror image L-form (L-Rib1) was staying intact even after 48 hours of incubation in serum.

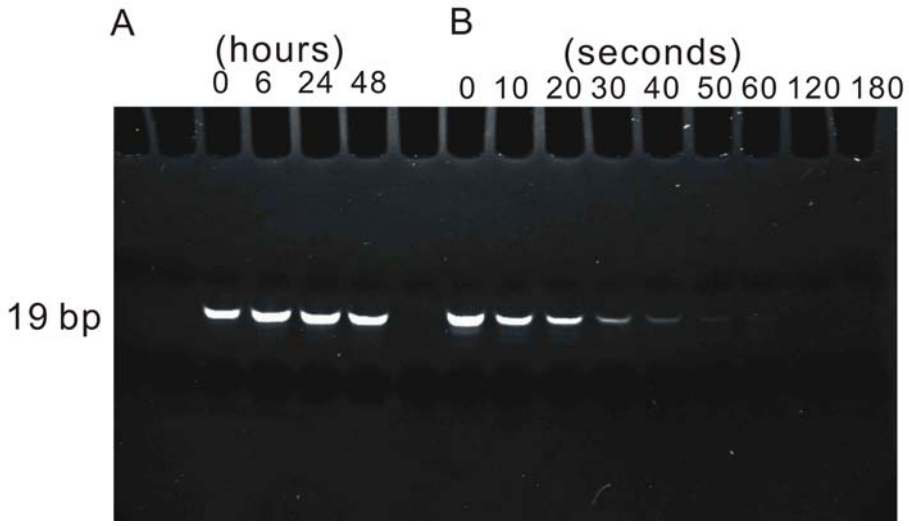

Figure 36: Stability of ribozyme 1 and L-Rib1 in human serum. Aliquots of RNA (30 pmol each) were taken from the incubation solution at the indicated times and analyzed on a 15% polyacrylamide gel after ethidium bromide staining. Part A shows the ribozyme strand (L-Rib1) in its mirror image configuration, while part B displays the ribozyme strand (ribozyme 1) in its natural configuration.

4.2.4. Release Experiments in Buffer

After completion of testing mirror image ribozyme assays in solution, the studies were extended towards the model system with nanoparticles. The scheme of this study is outlined in Figure 37. The ribozyme strand is hybridized to the inhibitor strand, which is immobilized on a first nanoparticle. Upon thermal release, the ribozyme can cleave

the substrate strand, which connects a fluorescent dye to a second nanoparticle. The fluorescent dye serves here as the substitute for a drug. The dye will be released through cleavage of the substrate strand.

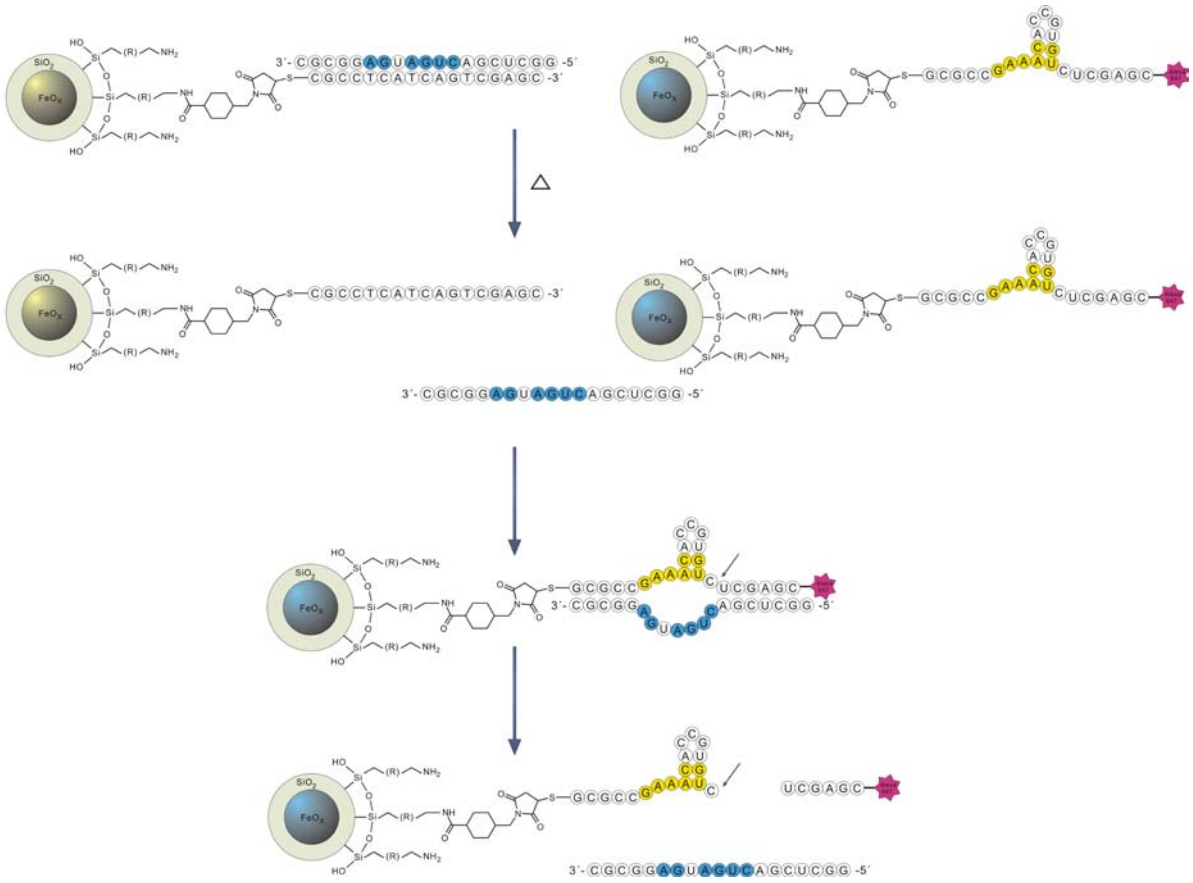

Figure 37: Ribozyme-based nanoparticle-drug delivery system. Nanoparticle/L-Inh 1-2pb/Rib 1 conjugates (yellow particles) und Nanoparticle/L-Sub1 conjugates (blue particles) were mixed in a 1:1 molar ratio in 50 mM Tris-HCl buffer (pH 7.5), 10 mM $MgCl_2$ and divided into two aliquots. One sample was incubated at 37 °C, the other at 49 °C. Through heating in a thermomixer at 49 °C the L-Inh 1-2bp/Rib 1 complex was separated and the L-Rib 1 was released. The free L-Rib 1 specifically cleaved the L-Sub1 strand and hence the fluorescent dye Alexa fluor 647 was released into the supernatant.

Table 17: Nucleic acid sequences for the release experiment of the ribozyme-based delivery system. The arrow denotes the position of cleavage.

Name	Type	Sequence
L-Rib1	L-RNA	5´-GGC UCG ACU GAU GAG GCG C-3´
L-Sub1	L-RNA	5´-SH-GCG CCG AAA CAC CGU GUC ↓ UCG AGC-Alexa 647-3´
L-Inh1-2bp	L-DNA	5´-SH-G CCT CAT CAG TCG AGC C-3´

Prior to release experiments, the linear range of Alexa Fluor® 647 was evaluated for measurements in a NanoDrop 3300 (Thermo Scientific, USA). The standard calibration curve confirmed a linear relationship for labeled L-Sub1 within a range of 2 µM to 100 nM (Fig 38).

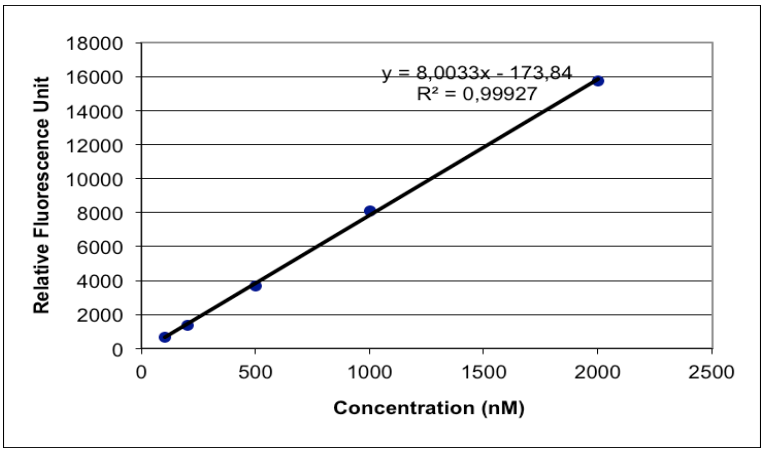

Fig. 38: Standard calibration curve for L-Sub 1. The relative fluorescent units (RFU) were plotted against the concentrations (nM) of Alexa Fluor® 647–labeled L-Sub 1.

All reactions were performed with mirror-image oligoribonucleotides. According to the initial experiments described in chapter 4.2.1, the ribozyme L-Rib 1 was used in combination with inhibitor L-Inh1-2bp and substrate L-Sub1 (Tab. 17). Ribozyme and inhibitor strands were hybridized in PBS buffer at pH 6.7. Experimental results revealed an optimal ratio with a 1.1 molar excess of inhibitor strand (data not shown). The hybrids were coupled via sulfo-SMCC to the amino functions of iron oxide nanoparticles SR-E2. In addition, the Alexa 647-labeled substrate strands were separately immobilized to SR-E2 nanoparticles. The conjugates were resuspended in reaction buffer (50 mM Tris-HCl, pH 7.5; 10 mM $MgCl_2$) and mixed in a 1:1 ratio (each 170 pmol in 45 µl). The mixture was subsequently divided into two aliquots and incubated simultaneously at 37°C or 49°C. Aliquots were taken from each sample after 1, 2, 3, and 4 h, respectively. After immediate centrifugation at 13000 g, the RFU values of the supernatants were measured in a NanoDrop 3300 (Fig. 39).

As a positive control, free ribozyme strand L-Rib1 (0.625 µM) was added to the L-Sub1 conjugates in reaction buffer. Accordingly, as a negative control the L-Sub1 conjugates were incubated merely in reaction buffer. Both of the controls were incubated at either 37°C or 49°C. The RFU values of the supernatants after

incubation at 49°C are displayed in Figure 39. As expected, the different temperatures had no significant effect on the values obtained (data not shown).

Increasing fluorescent signals over time were observed for 49°C samples and the positive controls, while the signals of 37°C samples were insignificant as compared to negative controls (Fig. 39). The positive control reached saturation within an incubation time of 4 h (data not shown), indicating a maximal release of the fluorescent label bound to nanoparticles at 1.2 µM. It is noteworthy that already 1.1 µM or 92 % of this maximal release could be obtained after a 4 h incubation at 49°C in the model system. This result demonstrated that a temperature controlled and efficient release of a fluorescent label from nanoparticles could be achieved through the employment of mirror image ribozymes.

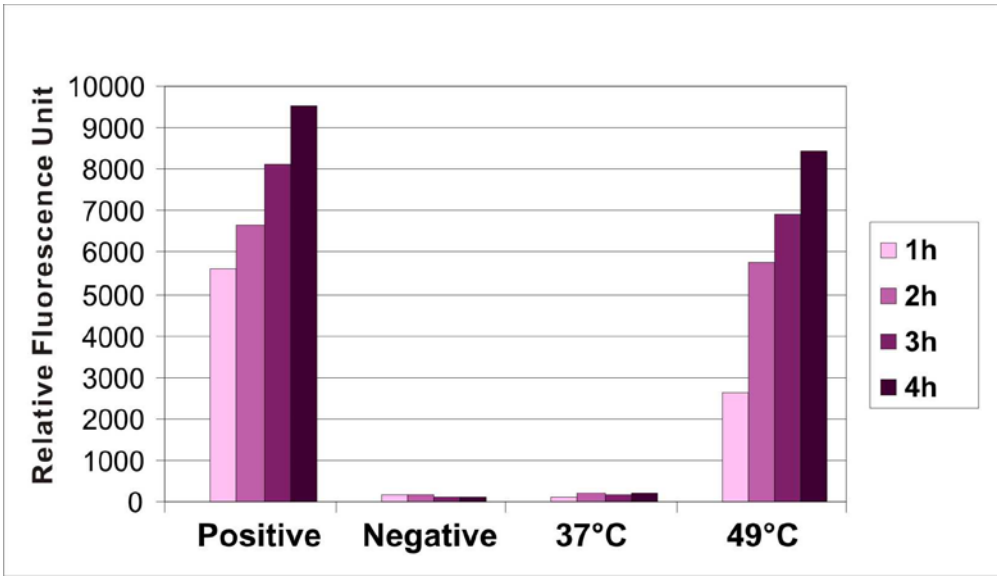

Figure 39: Fluorescent release assay for the ribozyme-based nanoparticle drug-delivery system in buffer. The RFU values in supernatants were recorded in a NanoDrop 3300 and plotted at the indicated times. Positive refers to the control, in which free ribozyme strand L-Rib1 (0.625 µM) was added to the L-Sub1 conjugates in reaction buffer. Negative refers to the control, in which the L-Sub1 conjugates were incubated merely in reaction buffer.

4.2.5. Release Experiments in Human Serum

To mimic the intended use of the conjugates under *in vivo* conditions, the release experiments, as described in chapter 4.2.4, were performed in human serum. The serum samples were kept in an incubator at either 37°C or 49°C with an atmosphere

of 94.5% humidity and 5% carbon dioxide to maintain stable pH conditions throughout the 4 h period of the experiment.

In human serum, an initial release of fluorescent label could already be observed at 37°C (Fig. 40). This release, however, did not increase over the time investigated. Moreover, the negative control showed identical behavior within the error of detection limit. The release can thus be attributed to substrate strands, which were non-covalently bound to the nanoparticles and were being released through unspecific interactions with serum components.

A significant release of fluorescent label with increasing values over time was detectable at 49°C (Fig. 40). The values of release were not as high as those obtained in the positive control and thus in the presence of free ribozyme strand L-Rib1. These results indicated that the established model system allows a temperature controlled release of fluorescent label from nanoparticles in the presence of human serum components.

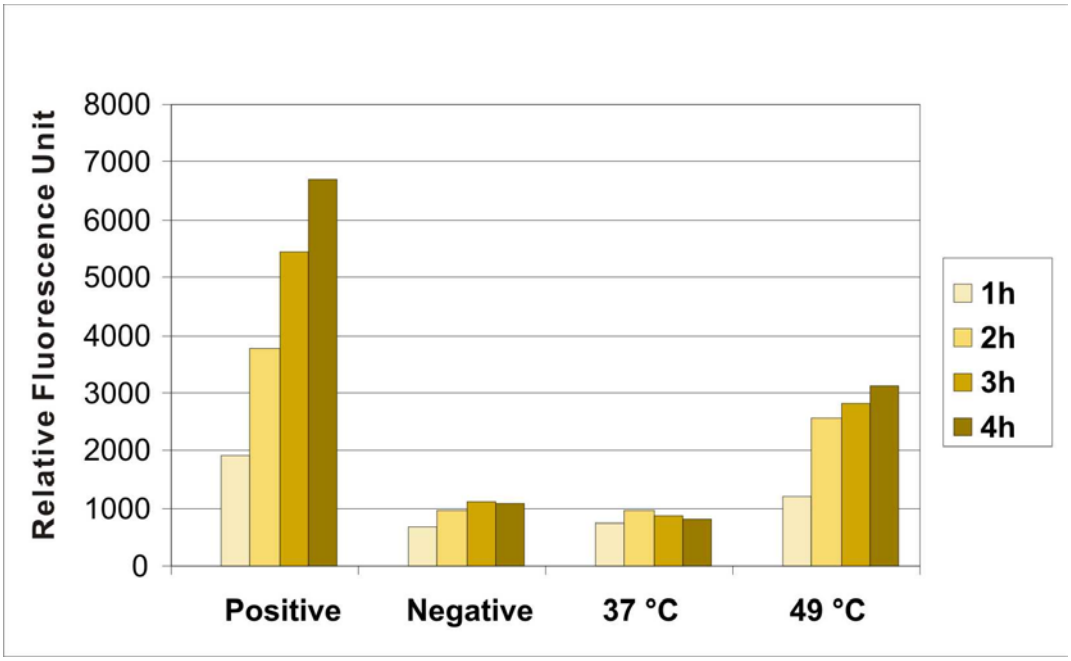

Figure 40: Release assay in human serum for the ribozyme-based nanoparticle-drug delivery system. The fluorescent signal of positive control and 49°C sample increased over time, while the values of negative control and 37°C sample remained at a basic level. Positive refers to the control, in which free ribozyme strand L-Rib1 (0.625 µM) was added to the L-Sub1 conjugates in serum. Negative refers to the control, in which the L-Sub1 conjugates were incubated merely in serum.

4.2.6. Stability of Nanoparticle-Nucleic Acid-Conjugates

To assess the stability of the conjugates during storage, L-Sub1-nanoparticle conjugates were kept at a concentration of 1 µM in PBS buffer (pH 7.2) at 4 °C for 50 days. After this time period, ribozyme strand L-Rib1 (0.5 nmol in 5 µl) was added to a 45 µl sample, while the reference sample obtained H_2O only. After incubation at 30°C for 1 h, both samples were centrifuged at 13000 g and the fluorescent signals of supernatants were measured in a NanoDrop 3300. As shown in Figure 41, the conjugates proved a substantial stability over the time period investigated.

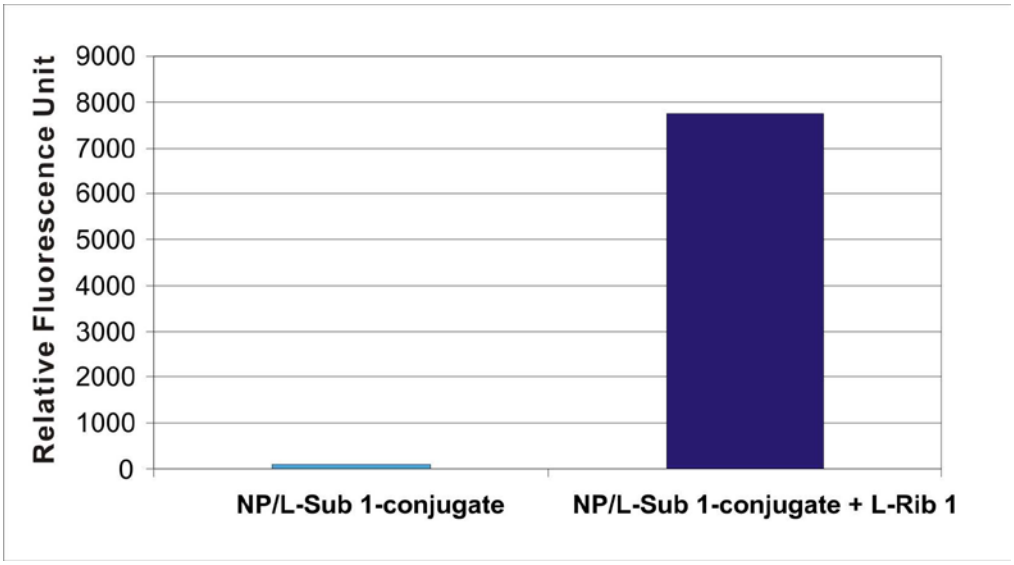

Figure 41: Stability assay of nanoparticle / L-Sub 1 Conjugates. The left column depicts the fluorescent signals in the supernatant of nanoparticle / L-Sub 1 conjugates. The right column shows the fluorescent signals in the supernatant of nanoparticle / L-Sub 1 conjugates after treatment with L-Rib 1.

4.2.7. Cellular Uptake of Nanoparticle-Nucleic acid-Conjugates

A key point for the application of the concept for a controlled and local chemotherapy is the ability of the conjugated nanoparticles to be internalized by cells. An efficient cellular uptake could significantly contribute to the overall therapeutic effect. The uptake of the conjugated nanoparticles was quantified by measuring the iron concentration through Atomic Absorption Spectroscopy (AAS), since each nanoparticle consist of about. 70,000 iron atoms (see Chapter 4.1.1.).

The uptake studies were performed with C3H RS1 cells, which were derived from a spontaneous murine mamma carcinoma by MagForce Nanotechnologies AG (Berlin). C3H RS1 cells were seeded in a 24-well cell culture plate at a density of $5x10^4$ cells/well and grown at 37 °C for 24 h. Afterwards, the medium was completely replaced with 500 µl/well fresh medium containing L-Sub1-NP-conjugates or L-Inh1-2bp/Rib1-NP-conjugates at an iron concentration of 50 µg/ml. After incubation of the cells at 37 °C for 1.5, 6 and 24 h, respectively, the C3H RS1 cells were washed two times with 500 µl fresh medium and detached by a trypsin-EDTA treatment. The cells were then centrifuged at 100 g for 5 min. The cell pellets were resuspended in 200 µl of 37 % HCl and treated in an ultrasonic bath for 10 min. The iron concentrations of the samples were then determined by atomic absorption spectroscopy.

As shown in Fig. 42, about 12.5 pg Fe ($1.92x10^6$ iron oxide nanoparticles) of L-Sub1-nanoparticle conjugates was uptaken per C3H RS1 cell after a 24 hours incubation at 37 °C. About 13.5 pg Fe ($2.07x10^6$ iron oxide nanoparticles) of L-Inh1-2bp/Rib1-nanoparticle conjugates was uptaken per cell under identical conditions. These data demonstrate that both conjugates possess a favorable uptake behavior.

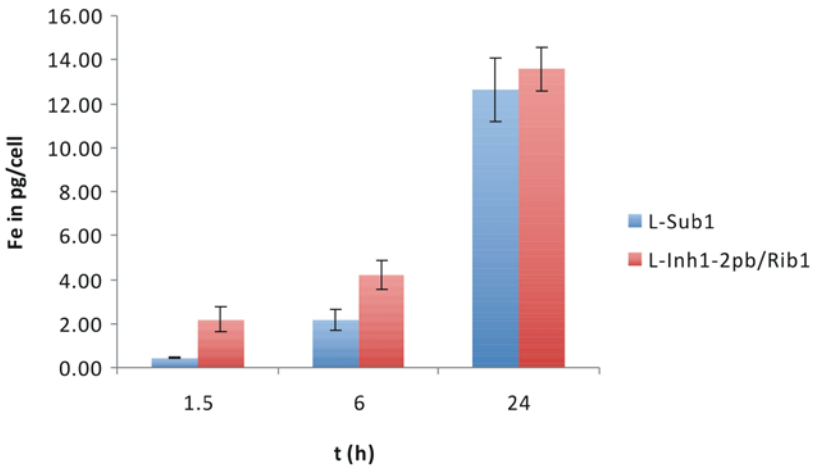

Figure 42: ASS-results for cellular uptake of nucleic acids conjugated iron oxide nanoparticles. The uptake of L-Sub1-NP-conjugates is displayed with blue bars for samples incubated at 37 °C. Red bars show the uptake of L-Inh1-2bp/Rib1-NP-conjugates for samples incubated at 37 °C.

4.2.8. Intracellular distribution of nanoparticle-nucleic acid-conjugates

TEM (transmission electron microscopy) analysis was performed to evaluate the distribution of the nucleic acids - FeO_xNP - conjugates inside cells. C3H RS1 cells were incubated with L-Sub1-NP-conjugates or L-Inh1-2bp/Rib1-NP-conjugates (Fe concentration of 50 µg/ml) at 37 °C for 4h and 24 h, respectively. The TEM images of the C3H RS1 cells were taken by an EM 906 transmission electron microscope.

The conjugates appear in the TEM images as dark spots (Figs. 43 and 44). As can be derived from images of C3H RS1 cells after 4 h incubation with nanoparticles, the L-Sub1-NP-conjugates (Fig. 43) or L-Inh1-2bp/Rib1-NP-conjugates (Fig. 44) were already spread into the cytoplasmic compartment. After 24 h incubation, significantly more nucleic acids-NP-conjugates were observed in the cytosol. Occasionally, the particles were associated with the nuclear membrane, but were never observed inside the nucleus.

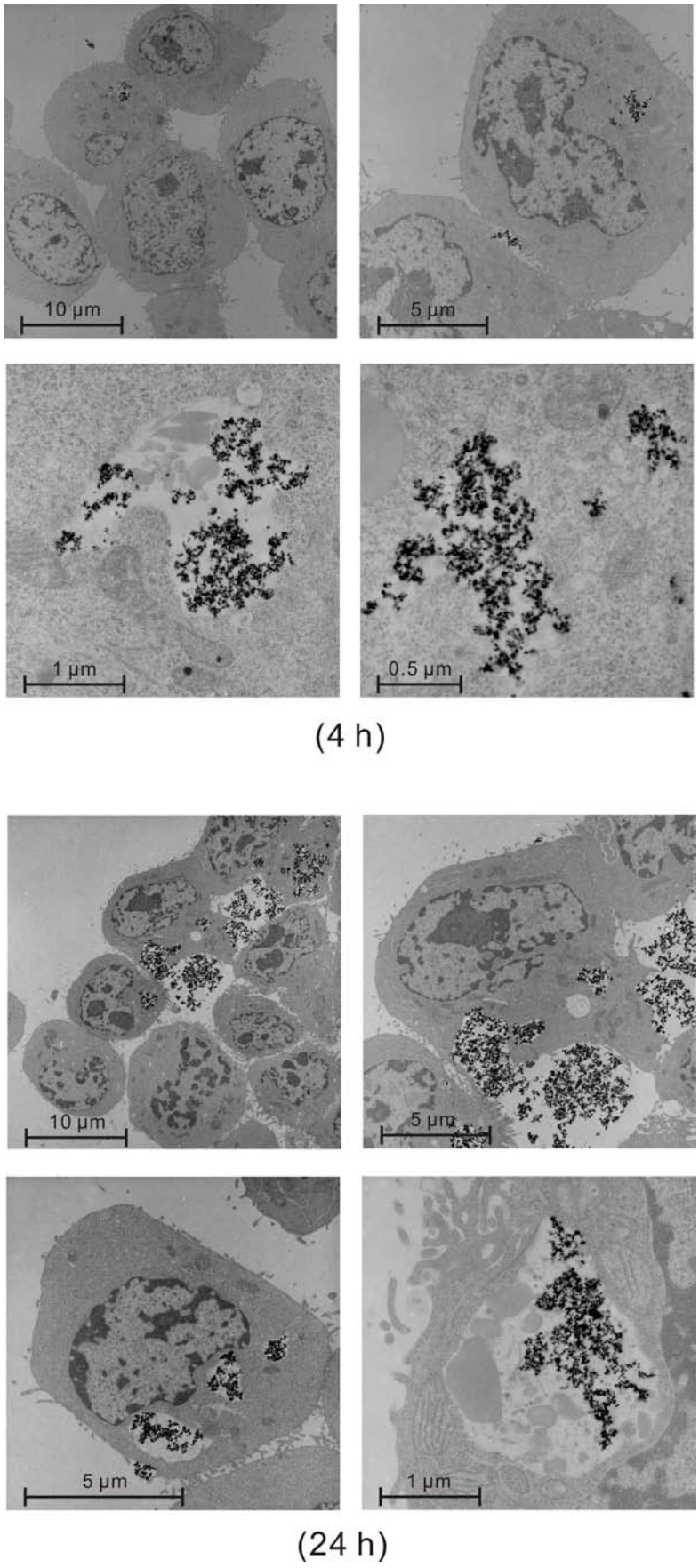

Figure 43: TEM images.(a): C3H RS1 cells were incubated with L-Inh1-2bp/Rib1-NP-conjugates for 4 h and 24 h. These images were kindly taken by N. Bohmer (MagForce Nanotechnologies AG, Berlin) in a transmission electron microscope (EM 906).

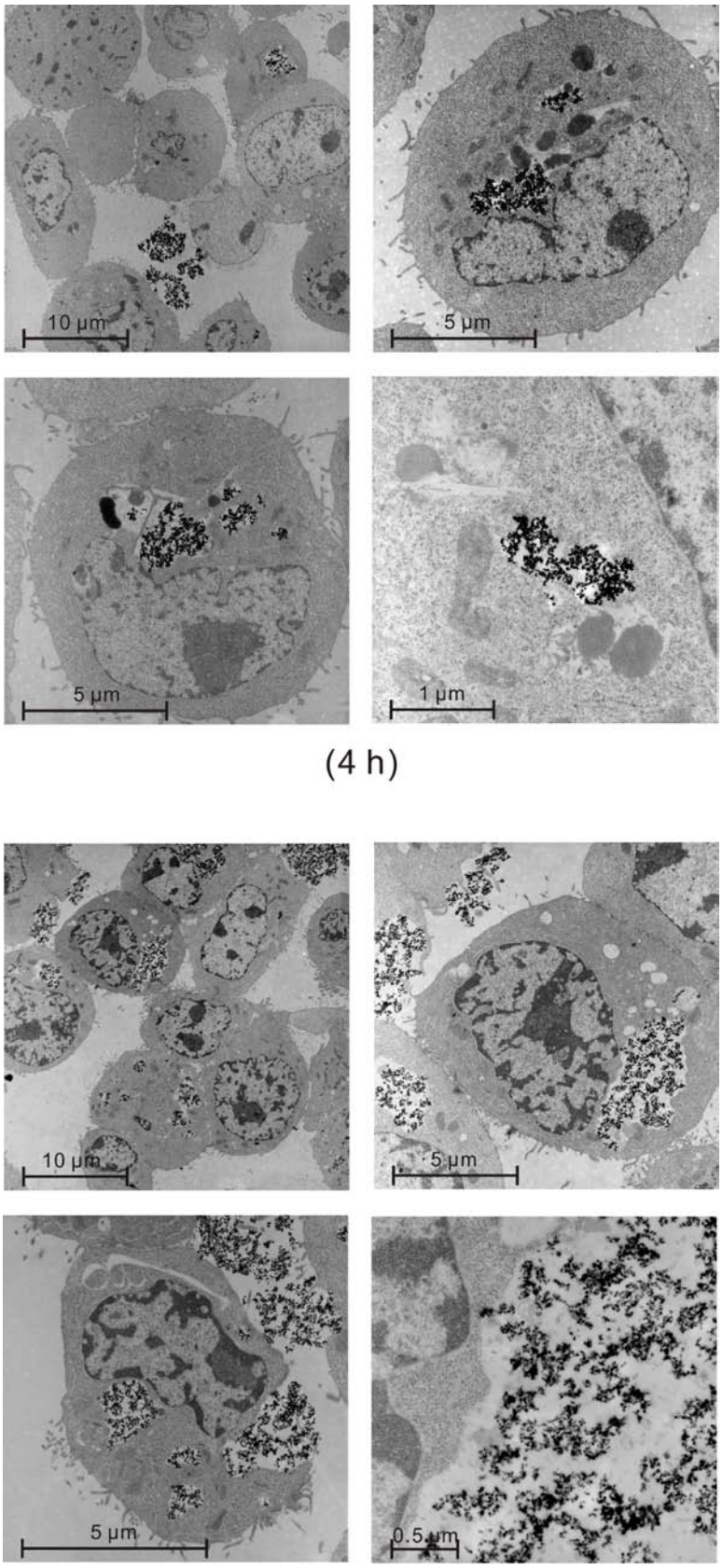

Figure 44 : TEM images:C3H RS1 cells were incubated with L-Sub1-NP-conjugates for 4 h and 24 h. These images were kindly taken by N. Bohmer (MagForce Nanotechnologies AG, Berlin) in a transmission electron microscope (EM 906).

4.3. Cytostatic Drug Coupling with Nucleic Acids

Studies were performed to explore the covalent coupling of a cytostatic drug to a functionalized oligonucleotide. Up to the present, there is no published report about such a covalent coupling to an oligonucleotide. Two different cytostatic drugs were chosen for these initial studies - chlorambucil (Chapter 4.3.1) and methotrexate (Chapter 4.3.3) - mainly due to their common property to carry a reactive carboxyl group that can be employed for a coupling reaction, while still maintaining their cytostatic effects (Reuben *et al.,* 1980; Majoros *et al.,* 2009).

4.3.1 Coupling of Chlorambucil

Chorambucil is a chemotherapeutic drug, which is marketed as Leukeran by GlaxoSmithKline (USA). It is a nitrogen mustard that is used clinically against chronic lymphatic leukemia, lymphomas, and advanced ovarian and breast carcinomas (Armitage, 1993). The clinical application of this anticancer drug, which exhibits its cytotoxicity due to its alkylating properties, is limited by its toxic side effects such as nausea, myelotoxicity, and neurotoxicity (Dorr & Fritz, 1982). These adverse reactions should be significantly reduced in the context of a local and controlled chemotherapy as pursued within the concept of this work. As other alkylating agents, Chlorambucil has shown an increased efficacy, when administrated in combination with thermotherapy (Dahl, 1988). Moreover, it has already been coupled covalently to antibodies through its carboxyl group, while maintaining its toxicity in the conjugate (Beyer *et al*. 1998; Kratz *et al.* 1998).

1-Ethyl-3-[3-dimethylaminopropyl]carbodiimide hydrochloride (EDC) was chosen as a first compound to connect chlorambucil to the oligodeoxynucleotide Yi-NH_2 (5´-NH_2-GCG AAA AAA AAA CCC AAA AAA-3´, Mw: 6628 g/mol). It is a zero-length crosslinking agent used to couple carboxyl groups to primary amines. The hydrochloride of EDC has a molecular weight of 191.7 g/mol (Fig.45 a) and as free base the molecular weight of EDC is 155.2 g/mol (Fig. 45 b).

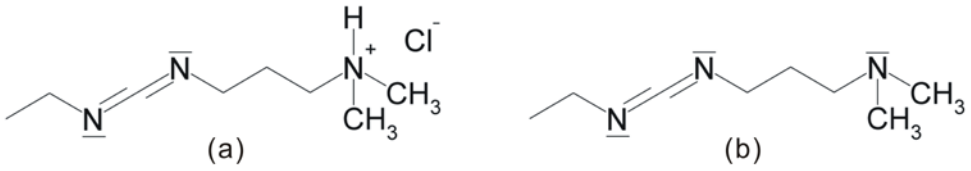

Figure 45: EDC. (a) Hydrochloride EDC. (b) Free base EDC.

Experiments with EDC were carried out in different buffer systems following the protocols of the supplier (Pierce, USA). The products of reactions (500 pmol each) were analyzed and compared to unreacted DNA Yi-NH_2 (100 pmol) by 20 % denaturing polyacrylamide gels. The gel was stained with SYBR Gold and visualized on an ultraviolet transilluminator at 302 nm.

The gel analysis of the reaction mixture in PBS buffer at pH 6.7 did not reveal any new product, as compared to the unreacted oligonucleotide, indicating the absence of a specific coupling event (Fig. 46, lanes 1 and 3). The mixture in 0.1 MES buffer at pH 4.8 displayed several new bands with an apparent length of 20 to 40 nucleotides, which would indicate the formation of different new products (Fig. 46, lane 4).

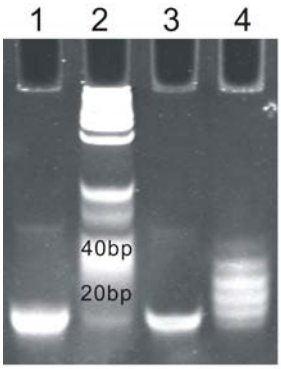

Figure 46: DNA Yi-NH_2 coupling with Chlorambucil using EDC. PAA gel (20 %) stained with SYBR Gold. Lane 1, PBS pH 6.7 as reaction buffer, lane 2, DNA marker, lane 3, unreacted Yi-NH_2; lane 4, 0.1 M MES pH 4.8 as reaction buffer.

These results were confirmed by MALDI-TOF MS analysis (Fig. 47). The mixture in PBS buffer at pH 6.7 showed a major peak at 6631 g/mol with additional sodium adducts like the unreacted DNA Yi-NH_2, confirming the absence of any specific reaction. For the mixture in 0.1 M MES buffer pH 4.8, multiple products could be observed with a mass increase of about 156 amu and multiples thereof.

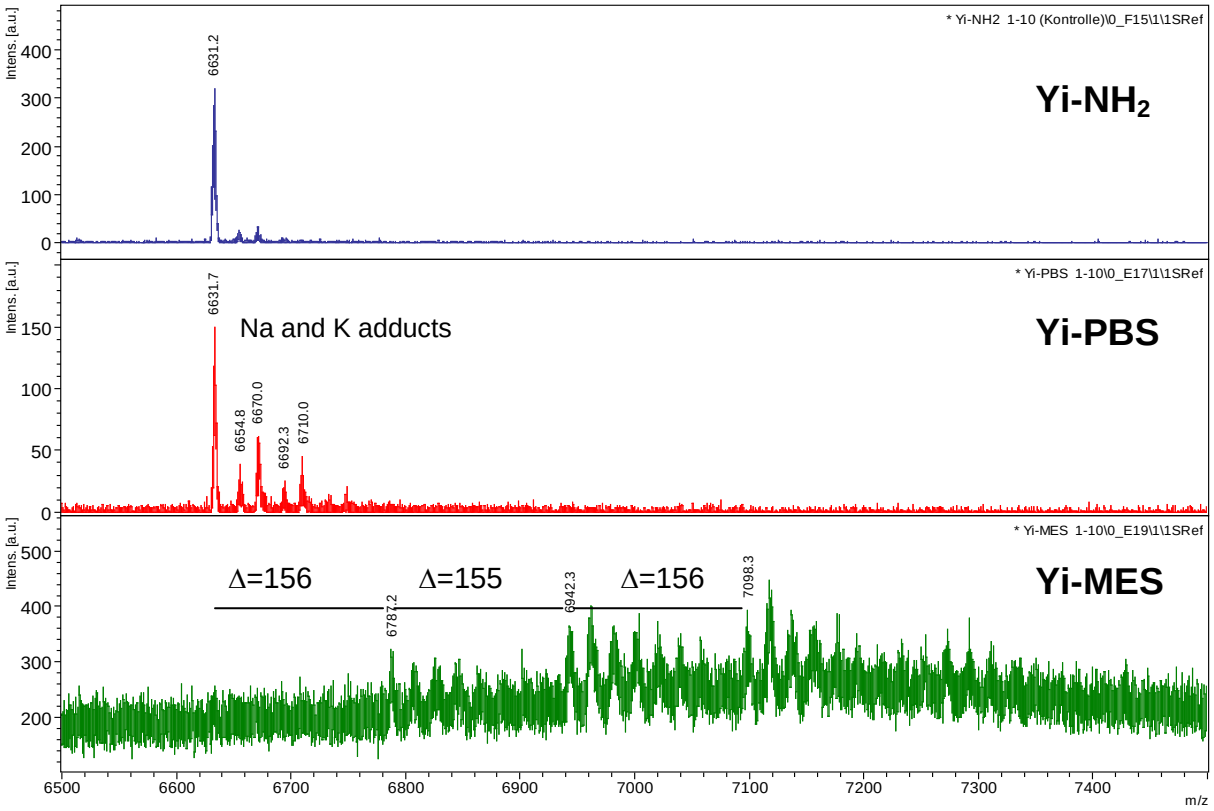

Figure 47. MALDI-TOF MS analysis of DNA Yi-NH_2 coupling with chlorambucil using EDC. Top: spectrum of original DNA Yi-NH_2. Middle: spectrum of products in PBS buffer at pH 6.7. Bottom: spectrum of products in MES buffer at pH 4.8.

The anticipated coupling delivering a theoretically would have delivered a chlorambucil-DNA-conjugate with a gain in molecular mass of 286 amu. It is conceivable that the the multiple adducts observed at pH 4.8 are simply due to ion pair formation between the acidic form of EDC (Fig. 45a) and the negatively charged phosphate groups of the oligodeoxynucleotide, which would lead to a successive gain in molecular mass of 156 amu. The anticipated product, however, was not detected irrespective of reactions under different pH conditions.

The coupling strategy was thus switched to carbonyldiimidazole (CDI) as the cross-linking agent. This compound (MW: 162) is a highly active carbonylating agent, which can activate carboxylic acids for conjugation with other nucleophiles. The anticipated reaction scheme is outlined in Figure 48. The carboxyl group of chlorambucil reacts with CDI in DMSO to form an active intermediate, which can be further reacted with the 5´-amino group of DNA Poly T-NH_2 (5´-NH_2-TTT TTT TTT TTT TTT TTT TTT-3´, MW: 6503 g/mol) to form amide bonds (Fig. 48) in aqueous environment. The

experiments were essentially carried out as described by the supplier of CDI (Pierce, USA), while different buffer conditions were employed to optimize the reactions.

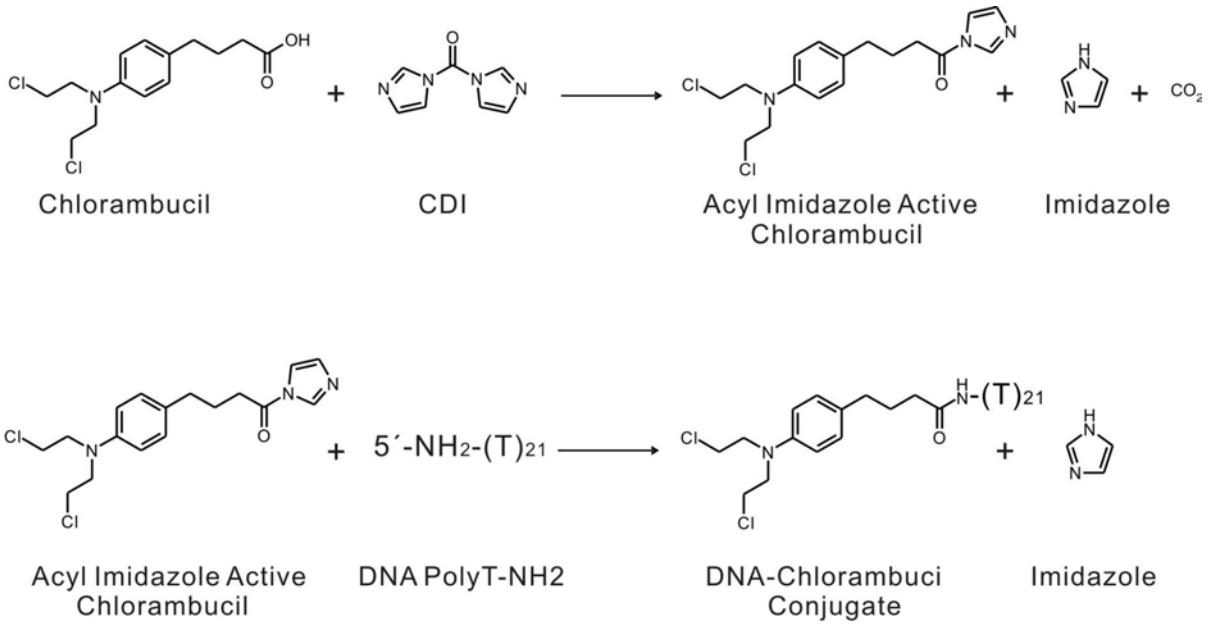

Figure 48: Coupling of chlorambucil with CDI. The carboxyl group of chlorambucil reacts with CDI to form an active acylimidate in DMSO (top). The intermediate reacts with the amino group of the oligonucleotide to form an amide bond in aqueous buffer under release of imidazole (bottom).

The reaction of chlorambucil with CDI was monitored by thin layer chromatography (TLC) on HPTLC Silica Gel 60 F_{254} plates. The plates were developed in 70 % methanol in water (Fig. 49). Chlorambucil gave a single ultraviolet-absorbing spot at R_f of 1, while the reaction product showed a major ultraviolet-absorbing spot at R_f of 0.9. This result indicated that a significant amount of chlorambucil had reacted towards a new intermediate product.

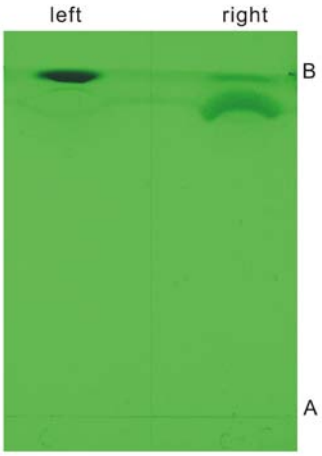

Figure 49. HPTLC Silica gel 60F_{254} image visualized at UV light of 254nm. Left lane: Chlorambucil. Right lane: Chlorambucil-CDI-intermediate. A denotes the start line; B marks the solvent end line.

The intermediate product was reacted further with the 5´-amino group of DNA Poly T-NH_2 in different solvents (DMSO; 0.1 M MES, pH 4.8; 0.1 M sodium borate pH 9.3; and PBS, pH7.4). Products were analyzed by 20 % denaturing polyacrylamide gel and MALDI-TOF MS.

The products of reactions (500 pmol each) were analyzed and compared to unreacted DNA poly T-NH_2 (100 pmol) by 20 % denaturing polyacrylamide gels. The gel was stained with SYBR Gold and visualized on an ultraviolet transilluminator at 302 nm.

The gel analysis of the reaction mixture in DMSO, 0.1 M MES at pH 4.8 and PBS buffer at pH 7.4 did not reveal any significant change (Fig. 50, lanes 2, 3 and 6) as compared to the unreacted oligonucleotide (Fig. 50, lane 4) indicating the absence of coupling reactions. The product in 0.1 M sodium borate pH 9.3 delivered a different pattern by gel analysis: While a new band could not be detected, the band of the unreacted oligonucleotide disappeared (Fig. 50, lane 5). This indicates that under these conditions a reaction must have occurred.

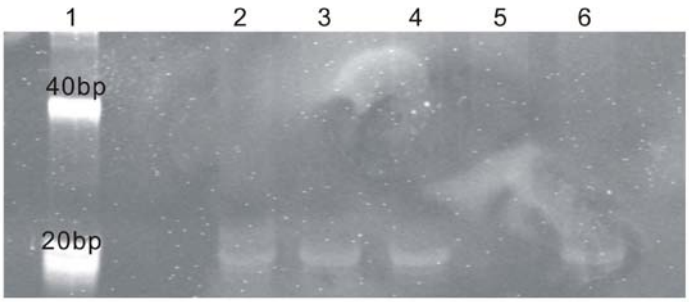

Figure 50. PAA gel (20 %) stained with SYBR Gold. Lane 1: DNA marker, lane 2: Reaction in DMSO. Lane 3: 0.1 M MES pH 4.6 as reaction buffer. Lane 4: Unreacted DNA Poly T-NH_2. Lane 5: 0.1 M sodium borate pH 9.3 as reaction buffer. Lane 6: PBS pH7.4 as reaction buffer.

MALDI-TOF MS analysis confirmed these findings. The reaction products of chlorambucil and DNA poly T-NH_2 in DMSO, 0.1 M MES at pH 4.8, PBS at pH7.4 and PBS at pH 6.7 showed a peak corresponding to a molecular mass of 6506 g/mol like the unreacted DNA poly T-NH_2. The peak series with higher masses can be attributed to sodium adducts of these oligodeoxynucleotides. The product of reaction in 0.1 M sodium borate buffer pH 9.3 causes a new peak with a mass increment of about 232 amu (Fig. 51). The expected product, however, should have delivered a

peak with an increased molecular mass of 286 amu. This finding indicates that the reaction followed a different scheme than anticipated.

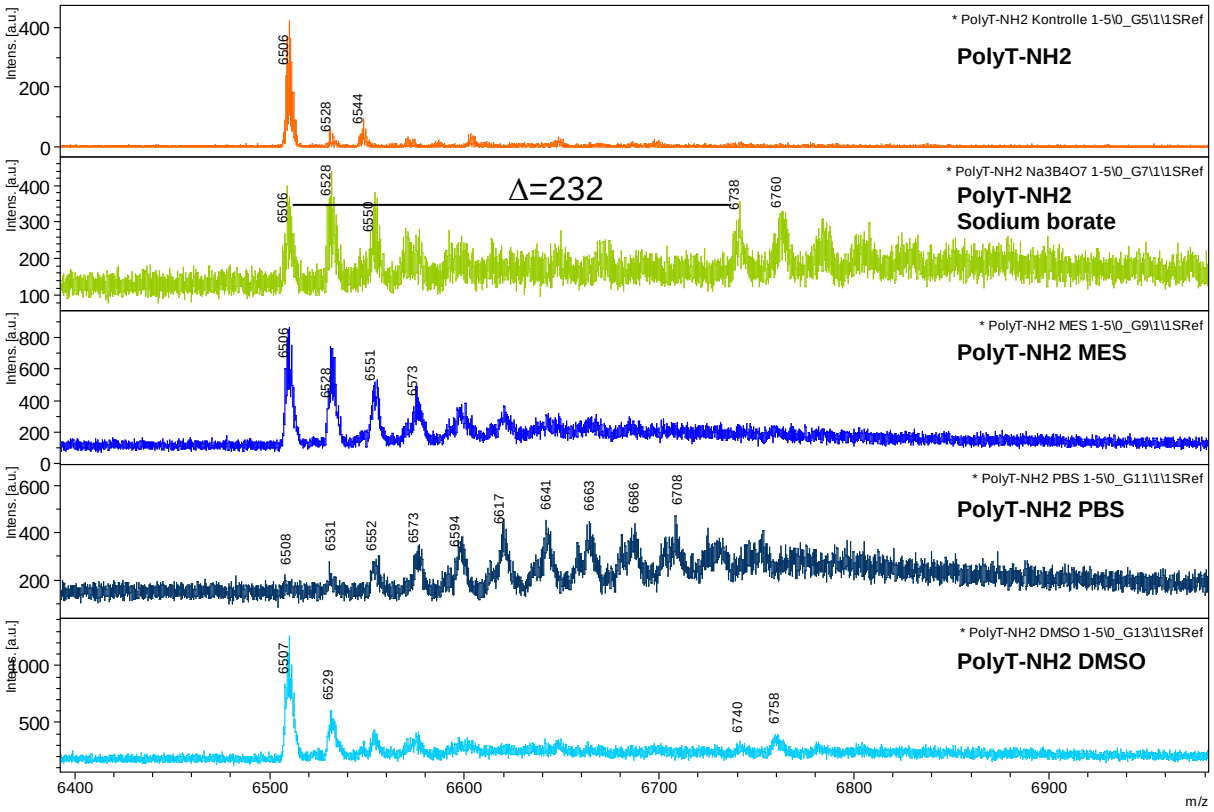

Figure 51. MALDI-TOF analysis DNA poly T-NH_2 coupling with Chlorambucil using CDI. Top: spectrum of original DNA poly T-NH_2. Middle up: spectrum of products in 0.1 M sodium borate buffer. Middle: spectrum of product in 0.1 M MES buffer. Middle down: spectrum of products in PBS buffer. Bottom: spectrum of product in DMSO.

Dicyclohexyl carbodiimide (DCC) was used to optimize the conjugation between chlorambucil and DNA. DCC is one of the most frequently employed coupling agents for the formation of peptide bonds. NHS is used together with DCC to prepare active esters of carboxylate-containing compounds. The carboxyl group of chlorambucil could thus react with DCC/NHS in organic solution (DMF) to form an active NHS ester intermediate, which could further react in aqueous environment with the amino group of DNA Poly T-NH_2 (5´-NH_2-TTT TTT TTT TTT TTT TTT TTT-3´, MW: 6503 g/mol) to form an amide bond (Fig. 52). The experiments were essentially performed as proposed by the supplier of DCC (Pierce, USA).

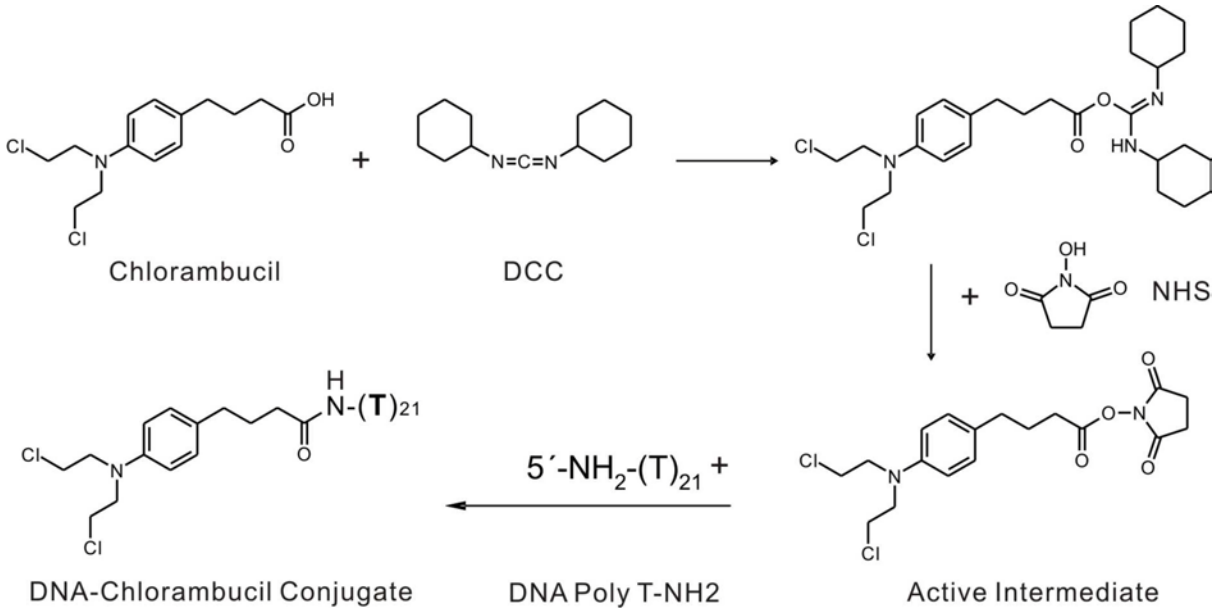

Figure 52: Coupling with DCC/NHS. DCC and NHS react with the carboxyl group of chlorambucil to form an active NHS ester intermediate in DMF (top). The intermediate reacts with the amino group of DNA to form an amide bond in 0.1 M sodium borate buffer at pH 9.3 (bottom).

Chlorambucil and its NHS ester intermediate were plotted on HPTLC Silica Gel 60 F_{254} plates, which were developed in 70 % methanol in water (Fig. 53). Chlorambucil gave a single ultraviolet-absorbing spot at R_f of 1, while the product of reaction showed a major ultraviolet-absorbing spot at R_f of 0.9. This result indicated that chlorambucil reacted with DCC and NHS near to completion.

Figure 53. Left lane: Chlorambucil. Right lane: Chlorambucil-NHS ester-intermediate. A denotes the start line; B marks the solvent end line

The activated chlorambucil was reacted further with the 5´-amino group of DNA Poly T-NH_2 in 0.1 M sodium borate buffer at pH 9.3. The gel analysis revealed a significant change (Fig. 54, lanes 2 and 3). The band of the unreacted

oligonucleotide close to the marker position of 20 nucleotides disappeared almost completely in the reaction mixture, while a diffuse band pattern was observable around and above the reference position of 40 nucleotides. This indicated a complete reaction of activated chlorambucil with the oligonucleotide DNA Poly T-NH_2.

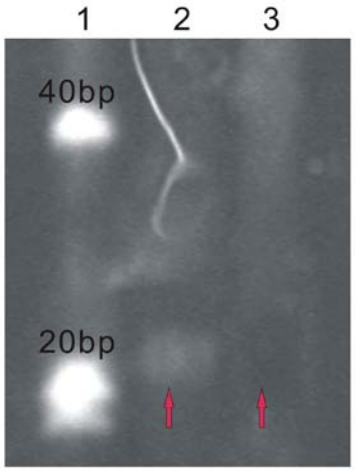

Figure 54. Polyacrylamide gel (20 %) stained with SYBR Gold. Lane 1: DNA marker. Lane 2: DNA Poly T-NH_2. Lane 3: Chlorambucil - DNA poly T-NH_2 – Conjugate.

These results were confirmed by MALDI-TOF MS analysis (Fig. 55). The mass peak of the unreacted DNA at 6506 g/mol disappeared in the spectrum of product(s), demonstrating a complete turnover of DNA Poly T-NH_2 during the reaction, while a new peak appeared at 6720 g/mol (Fig. 55). This new peak is followed by several mass peaks with a distance of 22 amu indicating adducts of sodium cations. The expected conjugate, however, would have delivered a main mass peak of 6791 g/mol. This difference between anticipated and obtained result can be attributed to the loss of the two chlorine atoms of chlorambucil during the reaction.

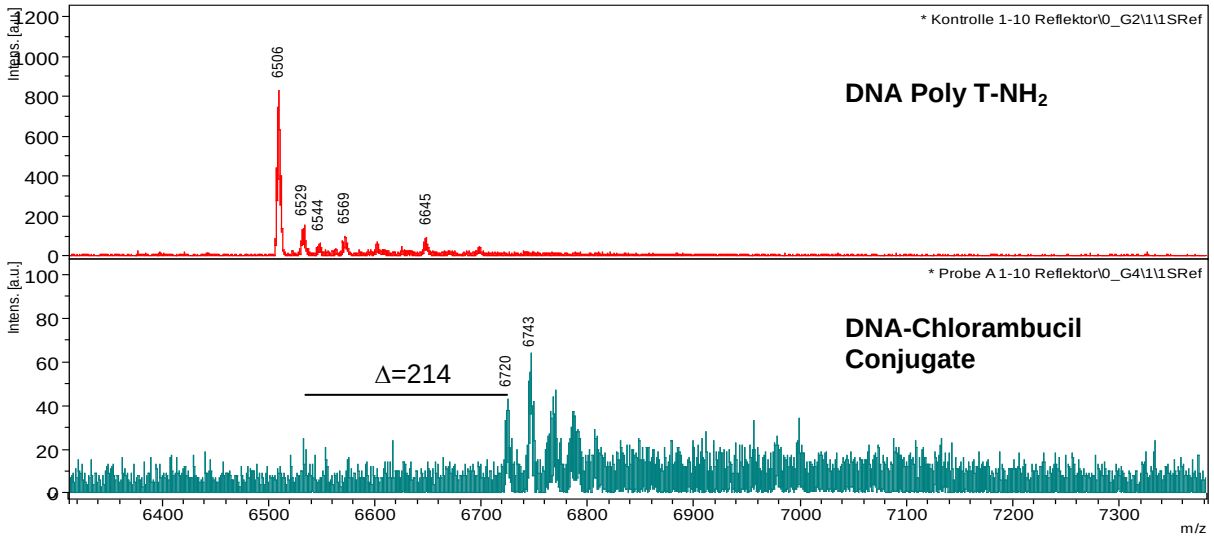

Figure 55. MALDI-TOF analysis DNA poly T-NH_2 coupling with Chlorambucil using DCC/NHS. Top: Spectrum of original DNA Poly T-NH_2. Bottom: Spectrum of products in 0.1 M sodium borate buffer pH 9.3.

4.3.2. Cytotoxicity of Chlorambucil Conjugates

The DNA Poly T-NH_2-chlorambucil conjugates were evaluated for their cytotoxicity in the MTT assay, which is a test system for cell viability. This assay employs RuSi-RS1 cells that are derived from human glioblastoma cells (Jordan *et al*., 1999). Viable cells are measured indirectly through their ability to reduce MTT ((3-(4,5-Dimethylthiazol-2-yl)-2,5-diphenyltetrazolium bromide) to formazan dyes (Mosmann, 1983).

Cells were plated at a density of 2500 cells/well in 96-well cell culture plates at 37 °C. After 24 h, the cells were treated with 600 µl of DNA-chlorambucil conjugates (0.1 mM), DNA Poly T-NH_2 (0.1 mM) or chlorambucil (9.5 mg/L, 19 mg/L, 38 mg/L and 76 mg/L) in medium. The control cells were incubated with 600 µl medium without additives. The cells were further incubated at 37°C for 24 h and the survival rates were determined by absorbance readouts using a Tecan-plate reader.

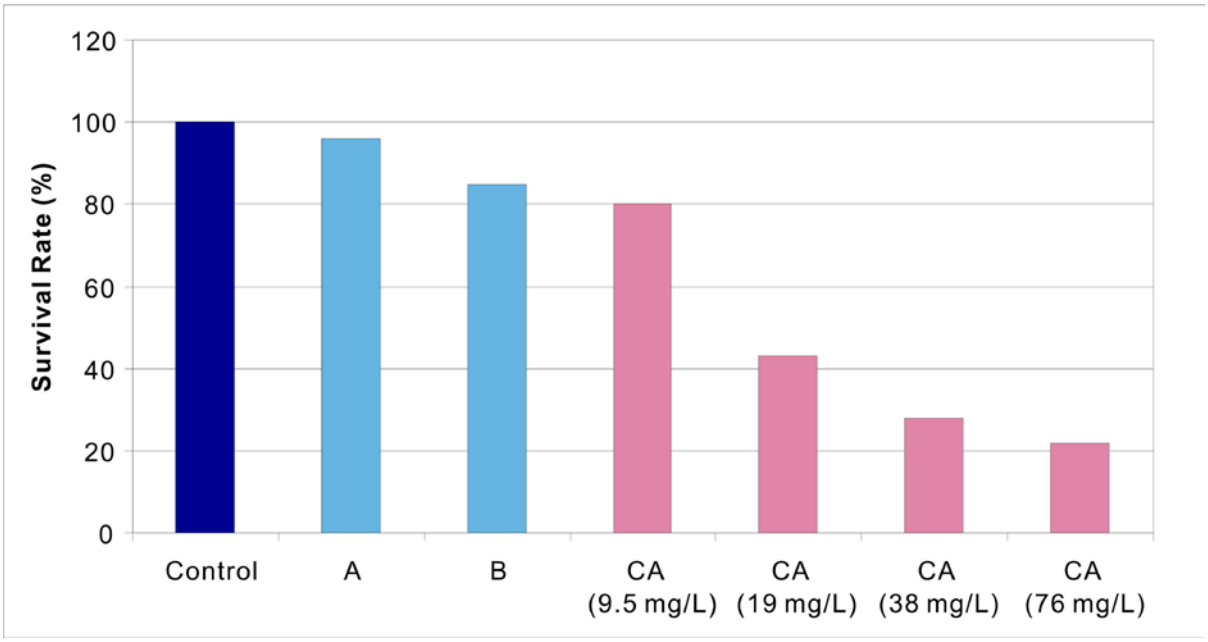

Figure 56: Survival Rate of RuSi-cells. The column A demonstrated the survival rate of RuSi-cells with the treatment of DNA-chlorambucil conjugates. The column B presented the survival rate with the treatment with DNA Poly T-NH_2. The red columns showed the survival rate of Rusi-cells after incubation with chlorambucil at the indicated concentrations. The control refers to the control cells, which were incubated with 600 µl medium without additives.

The control reactions with increasing amounts of chlorambucil could significantly inhibit cell growth. There is no significant difference of survival rates between the treatment of cells with DNA-chlorambucil conjugates and with either unreacted DNA or the negative control (Fig. 56). These results indicate that the cytotoxic activity of chlorambucil was lost during the coupling reaction.

4.3.3. Coupling of Methotrexate

Methotrexate (MTX) is an active compound used as a cytostatic drug in chemotherapy (Majoros *et al.* 2009). MTX is an analogue of folic acid (vitamin B9) and can competitively inhibit dihydrofolate reductase (DHFR), an enzyme that catalyses the conversion of dihydrofolate to the active tetrahydrofolate. The binding constant of methotrexate to DHFR is in the nanomolar range (Rajagopalan *et al.,* 2002), which is about one thousand-fold higher than that of folate. Since folic acid is needed for the *de novo* synthesis of the nucleoside thymidine and folate is needed for purine base synthesis, all purine and thymidine synthesis will be inhibited by methotrexate and subsequently the synthesis of DNA, RNA, thymidylates, and

proteins will be inhibited (Deacon *et al.,* 1985)

It was reported that MTX can easily be conjugated to dendrimers, while still maintainig its cytotoxic activity (Majoros *et al.,* 2009). Similar to chlorambucil, methotrexate has a primary carboxyl group, which could allow a direct coupling with amino-functionalized oligonucleotides via crosslinking strategies. The coupling protocol using DCC/NHS, which was established for the conjugation between chlorambucil and oligonucleotides (see Chapter 4.3.1.), was thus further applied to couple methotrexate to DNA sub1 (5´- NH_2 - GCG CCG AAA CAC CGU GUC UCG AGC -3´). Carboxylic acid groups of methotrexate could react with DCC/NHS in organic solution (DMF) to form active NHS ester intermediate, which can further react in aqueous environment with the amino group of DNA sub1 to form amide bonds (Fig. 57).

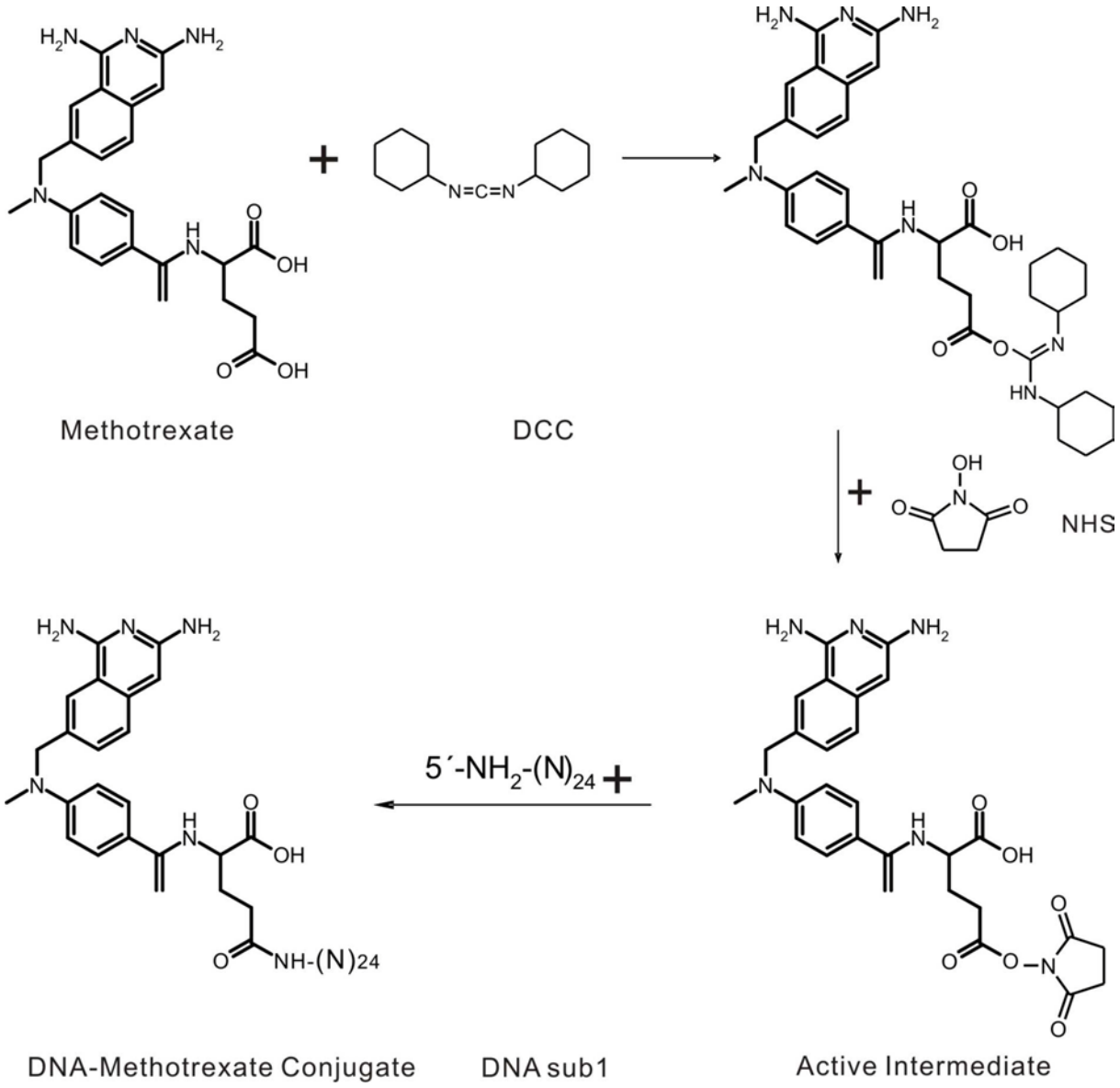

Figure 57: Coupling of Methotrexate with DCC/NHS. The carboxyl group of methotrexate reacts with DCC/NHS to form an active NHS ester intermediate in DMF. The intermediate reacts with the amino group of DNA to form an amide bond in 0.1 M sodium borate buffer at pH 9.3.

The reaction was monitored by MALDI-TOF MS analysis (Fig. 58). The mass peak of the unreacted DNA sub1 at 7538 g/mol was reduced in the spectrum of the reaction mixture, while a new peak appeared with the anticipated product mass of 7974 g/mol. This finding is consistent with the reaction scheme outlined in Figure 57.

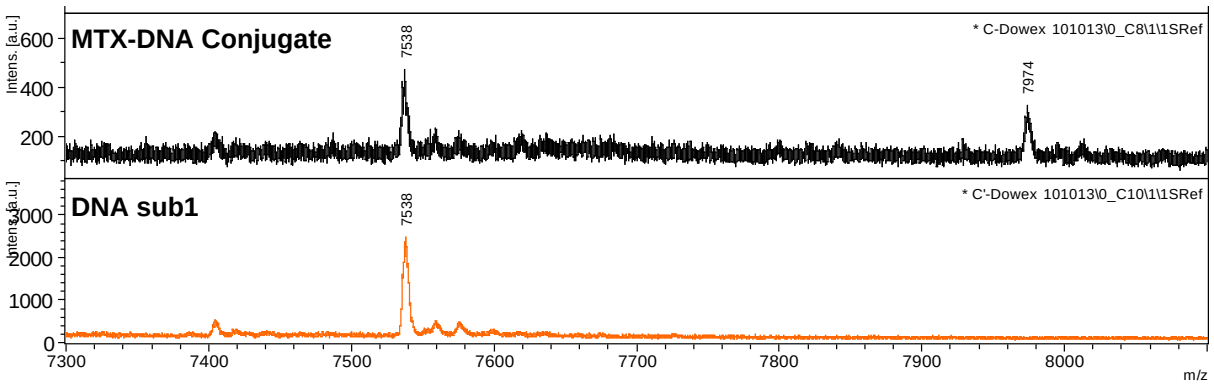

Figure 58: MALDI-TOF analysis DNA sub1 coupling with methotrexate using DCC/NHS. Top: Spectrum of mixture after reaction in 0.1 M sodium borate buffer at pH 9.3. Bottom: Spectrum of unreacted DNA sub1.

4.3.4. Cytotoxicity of Methotrexate Conjugates

The cytotoxicity of methotrexate-DNA conjugates was assessed by the MTT assay as described above (Chapter 4.3.3). The assay was performed with the colonic adenocarcinoma line WiDr (ATCC CCL 218, Jordan *et al.*, 1999), since this line is very sensitive to methotrexate. The WiDr cells were plated at a density of 2500 cells/well in 96-well cell culture plate at 37 °C. After 24 h the cells were treated with 600 µl of DNA-MTX conjugate (0.1 mM in medium, as referred to the initial concentration of DNA in the reaction mixture) or DNA sub1 (0.1 mM in medium). As a control, the cells were incubated with 600 µl medium without additives. As an additional control, a purified reaction mixture, which lacked the DNA, was added to the medium. As positive controls, the cells were treated with MTX at different concentrations (10 mg/L, 1 mg/L, and 0.1 mg/L in medium). After 24 h the medium was completely replaced. The cells were further incubated at 37 °C for 24 h and the survival rates of the cells were determined using the MTT assay

The DNA-MTX conjugate showed a significantly reduced survival rate as compared to the negative control or unreacted DNA (Fig. 59A). These results are, in the first instance, consistent with the successful conjugation of MTX and DNA, which left the cytotoxic properties of MTX unaffected. However, the survival rate is as much reduced by treatment of WiDr-cells with the control reaction, where DNA was omitted (Fig. 59C). This finding indicates an incomplete removal of unreacted MTX from DNA-MTX conjugates during the established purification procedure. Thus, while the

successful synthesis of DNA-MTX conjugates was clearly demonstrated through mass analysis, their cytotoxic properties remain to be proven after complete removal of unreacted MTX by an improved purification protocol.

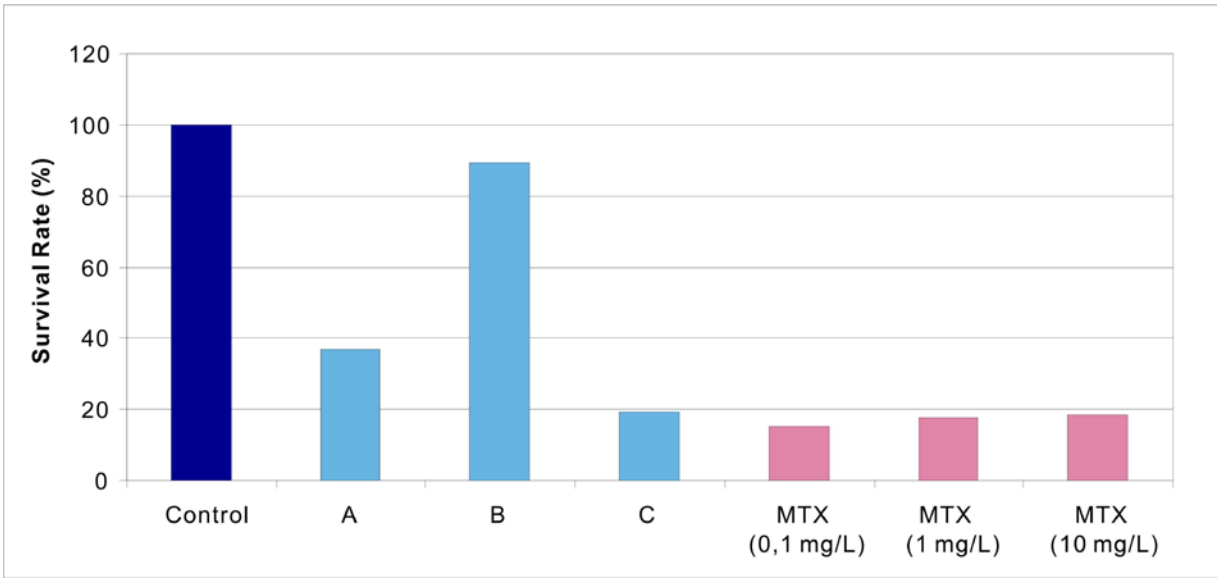

Figure 59: Survival rate of WiDr-cells. Column A indicates the survival rate of WiDr-cells in the presence of DNA-MTX-conjugates. Column B is the survival rate after the treatment with unreacted DNA sub1. Column C presents the MTX control sample, where MTX was treated with DCC/NHS und purified with the identical protocol used for DNA-MTX-conjugates. The red columns showed the survival rate of WiDr-cells after incubation with MTX at the indicated concentrations. The control refers to the control cells, which were incubated with 600 µl medium without additives.

5 Discussion

The task of this work was to explore the thermal release of cytotoxic drugs from nanoparticles through the use of nucleic acids. At first, a DNA duplex was employed as a thermolabile linker between nanoparticle and drug. One strand of the duplex, the immobile strand, was covalently linked to a nanoparticle, while the complementary strand, the mobilizable strand, was attached to a fluorescent dye. The dye served here as substitute for a cytostatic drug to monitor and quantify the release of the mobilizable strand (Chapter 5.1).

Since the results of this duplex approach lagged behind expectations, a new approach was conceptualized during the course of this work. Here, the mere stochiometric release of mobilizable strands were amplified through a catalytic event. In addition, mirror image oligonucleotides were employed to obtain stability against degradation by nucleases. Again, a fluorescent dye was used as a substitute for the drug to monitor the release reaction (Chapter 5.2).

Finally, conditions were explored to attach a cytotoxic drug to an oligonucleotide. This is an essential step towards the intended development of a controlled local chemotherapy of cancer (Chapter 5.3).

5.1 The Hybrid Approach

The concept of a DNA duplex as a thermolabile linker between nanoparticle and drug necessitates the attachment of oligonucleotides to the surface of nanoparticles. Superparamagnetic iron oxide nanoparticles with different active groups on the surface were provided by the cooperation partner MagForce Nanotechnologies AG (Berlin, Germany). Oligonucleotides with different active groups at their 5’-termini were tested under different crosslinking protocols to maximize the surface coverage of the particles.

The main problem during the attempts to graft the surface of the nanoparticles with oligonucleotides was the strong aggregation of the particles during and after the

coupling process. The iron nanoparticles applied in magnetic fluid hyperthermia to treat solid tumors are designed in a manner to be colloidally dispersed in water before they are injected into tumors. Once the nanoparticles are exposed upon injection to physiological ion conditions, they immediately tend to aggregate (Thiesen & Jordan, 2008). This property benefits the desired hyperthermic effect, but posed a serious problem for the coupling protocols.

To reduce this aggregation and to enhance the stability under physiological conditions, nanoparticles with an iron oxide core and a silica shell were prepared by MagForce Nanotechnologies AG (Berlin). While this coating considerably improved the dispersibility of the particles, a certain aggregation could still be observed. To overcome this problem, different crosslinking reagents were tested for the coupling reactions. This issue could not be solved completely, no matter which crosslinker was used for the coupling reactions. However, it could be shown that that an extensive wash step with water after each coupling reaction can profoundly enhance the dispersion of the conjugates.

The surface coverage of nanoparticles with oligonucleotides was quantified by their ability to capture fluorescently labelled complementary strands. The amount of released complementary strands upon thermal treatment of the conjugates was taken as the apparent number of bound oligonucleotides. Among all of the tested crosslinkers, EDC and sulfo-SMCC showed the best results. Control experiments, however, revealed for the coupling protocols with EDC a high amount of complementary strands that bind in a nonspecific manner. In contrast, the protocol with sulfo-SMCC achieved a surface coverage of 15 bound oligonucleotides per nanoparticle, while the nonspecific binding was negligible.

A covalent immobilization of 15 oligonucleotides per nanoparticle appears low in comparison with the number of reactive groups that were available on the surface of the iron oxide nanoparticles. The colorimetric NBA assay revealed 550 primary amino groups per particle. Thus, only 2.72% of the available aminogroups were used for covalently binding oligonucleotides.

This low coupling efficiency is unlikely due to an inefficient crosslinking event. Only

30 accessible amino groups remained after sulfo-SMCC activation as revealed by the NBA assay. This would suggest a surface coverage of still 520 reactive intermediates per particle. Another potential reason for a low coupling efficiency could be the dimerization of the functionalized oligonucleotides, which carried a sulfhydryl group at their 5'-termini. Therefore, the coupling of the oligonucleotides to the reactive intermediates was performed in the presence of TCEP (tris-(2-carboxyethyl)phosphine hydrochloride) to reduce disulfide bonds. Initially, this compound was not removed from the reaction mixture, because early reports suggested that TCEP was unreactive with electrophilic maleimides. However, it has been also reported that TCEP is able to react with maleimide groups (Getz *et al*., 1999). It was therefore tested, whether this suspicion would be valid. Immobilized TCEP (Pierce, Rockford, USA) was used to reduce the dimerized oligonucleotides and was then removed before the final coupling reaction. A significant difference in surface coverage of immobilized oligonucleotides could not be assessed, though.

The achieved surface coverage, however, is well in accord with published data. Bruce and Sen (2005) coupled 5´-NH_2-modified oligonucleotides via glutaraldehyde to aminopropyltriethoxysilane-coated iron oxide nanoparticles. The resulting amount of covalently immobilized oligonucleotides was 37 times smaller than the density of free amino groups detected by colorimetric analysis. This result would correspond to a coupling efficiency of 2.67% and is hence almost identical to the value obtained in this work.

Bruce and Sen (2005) reason that the low surface coverage of oligonucleotides as compared to reactive groups is likely due to steric hindrance. An oligonucleotide is a large molecule compared to the nitrobenzaldehyde used in the colorimetric assay. In addition, repulsive forces through electrostatic interactions might take part in reducing the number of bound DNA molecules.

Frutos *et al*. (1998) achieved a better surface coverage than reported here, even though they employed a rather similar protocol to immobilize DNA strands on biochips. They coupled 5´-thiol-modified DNA to reactive amino groups on gold thin films via sulfo-SMCC. The DNA density on the chips achieved a value of 5×10^{12} molecules/cm^2 (reviewed in Pirrung, 2002). The iron oxide nanoparticles employed

here have a diameter of 15 nm on average, which would correspond to a surface area of about 700 nm^2 assuming a spherical shape of the particles. Therefore, the DNA density in this work reached a mere 2 x 10^{12} molecules/cm^2. This lower surface coverage in comparison with the immobilization on biochips is likely due to the problem mentioned above. The accessible surface for the coupling of oligonucleotides might be reduced through the aggregation of the iron oxide nanoparticles.

The employment of longer spacers or even dendrimers might enhance the surface coverage of the nanoparticles in future approaches. This strategy could reduce steric hindrances and electrostatic repulsions. In addition, spacers or dendrimers may contribute to further improve the dispersion of the nanoparticles and hence could lead to a larger accessible surface.

After establishing the covalent attachment of oligonucleotides to nanoparticles, the study focused on DNA hybrids that could fulfill the requirements for a conditional drug delivery. Hybrids of different length and sequence were investigated, whether a significant release of a mobilizable strand could be measured under hyperthermic conditions of 50°C and whether no release could be observed at body temperature of 37°C.

The characterization of the DNA-nanoparticle conjugates was performed through release curves, where the complete dissociation of mobilizable strand from conjugates was measured at different temperatures. These release curves are correlated to the melting curves of the respective helices, but they differ. The direct recording of melting curves with conjugates was prevented by the strong absorption of the nanoparticles in the UV range. Therefore, the melting curves were obtained through measuring the respective helices in solution.

The comparison revealed a sharper profile of release curves as compared to melting curves for all helices investigated. The melting curve of nucleic acids is monitored by measuring the absorption at a wavelength of 260 nm during a steady temperature increase. The formation of base pairs leads to a decrease in UV absorption (hypochromism), since the transition probability of the π-electrons of the purine and

pyrimidine bases is decreased in the excited state during the stacking of the bases within the double helix. As a result, the molar extinction coefficient is being reduced accordingly (Devoe & Tinoco, 1962). Due to this effect, any separation of a base pair will lead to an increase in UV absorption, irrespective on any full separation of strands. In contrast, the corresponding release curve will monitor a full separation event only. This readily explains the sharper profiles that were obtained by measuring the release of mobilizable strands. This finding is in accord with earlier reports that the DNA melting profile in DNA-linked nanostructure systems is usually sharper than that for the corresponding dehybridization of DNA in solution (Mirkin *et al.*, 1996; Storhoff *et al.*, 2000; Jin *et al.*, 2003; Kiang, 2003). In addition, Park *et al.*, (2007) have reported that cooperativity plays a crucial role in producing a sharp melting profile.

The dehybridization of a DNA helix depends on a variety of factors, such as pH value, ionic strength, ion type or presence of organic solvents. These parameters, however, are invariant for a strategy that aims at physiological conditions. Thus, only length and sequence of the hybrids were varied to meet the temperature requirements of a hyperthermic drug release. Theoretically, the melting behavior of duplexes formed from a mixture of complementary homopolymers should be sharper than that of duplexes with heterogeneous sequences, because their structure and stability are uniform along the whole length of the molecule. Sequences with long stretches of guanosines, however, were avoided due to their ability to form very stable tetraloop structures.

Four different hybrids were investigated. One hybrid contained a heterogeneous sequence, while the other three contained stretches of homogeneous AT sequences. The release curves basically confirmed the predictions. The sharpest profile was obtained with the DNA duplex Yi-SH/Yi-Cy3, which is an AT-rich 21-mer. This hybrid, which was stable at body temperature, revealed a mere 33% release of mobilizable strand at 50 °C, though. This result indicated that improved strategies are needed for the development of a conditional drug release.

To improve the hybrid approach, it was attempted to combine the initial strategy with a cytotoxic drug that can intercalate into a double stranded DNA. The cytostatic drug

doxorubicin, which is widely used in tumor chemotherapy, was applied for this approach. It can intercalate between double stranded DNA to inhibit the biosynthesis of macromolecules. Due to its convenient fluorescent properties, it could be easily monitored during the experiments performed. As expected, the data of dehybridazation experiments in the presence of doxorubicin revealed a temperature dependant release of this intercalator. About half of this drug, however, was already released at body temperature when compared to the value obtained at 80 °C. This early release is likely due to helix destabilization upon intercalation of doxorubicin. This could probably be prevented by employing longer and hence more stable helices. However, the slow increase of doxorubicin release upon temperature enhancement renders a significant release of doxorubicin under hyperthermic conditions to be rather unlikely.

In summary, the concept of conditional drug release through a hybrid approach necessitates a stable DNA helix at body temperature, while a significant amount of helices needs to be dissociated under hyperthermic conditions. The present data implicate that the inherent properties of DNA prevent such a scenario under physiological conditions irrespective of length and sequence variations. Thus, at present, a therapeutic development based on a mere hybrid approach seems inapplicable.

5.2 The Ribozyme Approach

Due to the incomplete release of mobilizable strands in the hybrid approach, a new concept was developed to amplify this limited event by a catalytic step. The mobilizable strand was conceptualized as a ribozyme, which is able to specifically cleave a substrate strand. In this approach, the substrate strand serves as linker between nanoparticle and drug. Upon thermal release of the mobilizable strand and hence the ribozyme from its complementary strand, the substrate strand will be cleaved and the cytotoxic drug will be released into the adjacent sphere. The complementary strand to the ribozyme exerts here an inhibitor function to the cleavage reaction and was therefore termed inhibitor strand.

The hammerhead ribozyme was chosen for this system, since this catalytic RNA can hydrolyze the phosphodiester bonds of RNA in a sequence-specific manner. Furthermore, it can be truncated to a minimal active motif, which is the smallest ribozyme known so far. A small size of the ribozyme employed will help to reduce costs of production in view of potential pharmaceutical applications.

Furthermore, while the natural function of the hammerhead ribozyme is an intramolecular (in *cis*) reaction, it has been artificially enabled to cleave in an intermolecular (in *trans*) fashion (Uhlenbeck, 1987). This intermolecular mode of catalysis is an essential requirement to function in the aimed concept of a two step reaction. First, the ribozyme strand needs to be dehybridized from its complementary strand through heating. Then, the free ribozyme travels via diffusion to the substrate strand and releases upon cleavage the cytotoxic drug in a second step.

A key point in this strategy is the choice of length and sequence of the participating oligonucleotide strands. The following properties should be optimized.

(i) The ribozyme strand should stay annealed to its complementary strand at body temperature of 37°C.

(ii), A maximal amount of ribozyme strands need to be dehybridized under conditions of hyperthermia of about 50 °C.

(iii) The catalytic turnover of reaction should be efficient under these hyperthermic conditions.

The minimal hammerhead motif is composed of a catalytic core region surrounded by three helical stems. As long as the these helices contain five to six base-pairs each, the catalytic turnover is at its maximal rate and the reaction follows a standard Michaelis-Menten kinetics (Thomson *et al*., 1996). The overall reaction of a hammerhead ribozyme can be divided into three steps: the association of ribozyme and substrate strands, the cleavage reaction upon formation of an active transition state and finally the dissociation of ribozyme and product strands. The rate limiting step is the cleavage reaction for the minimal hammerhead motif. Once a length of about six base-pairs in the stems is exceeded, the product dissociation becomes the rate limiting step and the catalytic turnover is decreased.

A cleavage reaction under conditions of hyperthermia of about 50 °C is no major obstacle for a minimal hammerhead ribozyme. The overall rate of reaction will be significantly decreased below 25 °C or above 50 °C only (Takagi and Taira, 1995). At lower temperatures than 25 °C, the cleaved fragments adhere to the ribozyme more tightly and product dissociation becomes the rate limiting step, while at higher temperatures than 50 °C, the formation of the ribozyme-substrate complex is hampered by thermal melting. In the range of 25 to 50 °C, the chemical cleavage step is the rate-determining step and the catalytic rate increases slightly with rising temperature.

Two different minimal hammerhead ribozymes were tested for their ability to fulfill the above mentioned criteria. A hammerhead strand, taken from Ruffner (1990), showed the most promising results with a length of 17 nucleotides (Ribozyme 1). The complementary strand, however, had to be shortened by two nucleotides to obtain a significant release of ribozyme in the system. The inhibitor strand had thus a length of 15 nucleotides only (Inhibitor 1-2bp). It could be demonstrated that the substrate strand with 21 nucleotides could be significantly cleaved at 49 °C, while the substrate remained uncleaved at 37 °C.

A major disadvantage in the therapeutic application of RNA is the abundance of ribonucleases that are prone to rapidly degrade all oligonucleotide strands employed. This could interfere with the intended concept in a twofold manner. First, the ribozyme would have a very short half-life time inside a patient. This could prevent any significant cleavage event and would consequentially prevent the conditional release of the cytotoxic drug. Second, the substrate strand could be cleaved by a ribonuclease. This would lead to an unconditional release of the drug and would thus obliterate the idea of a controlled local chemotherapy.

The ribozyme approach was therefore pursued with the initial plan to implement mirror image RNA. Enantiomeric compounds display reciprocal chiral specificities due to the basic principles of stereochemistry (Pasteur, 1861; Fischer, 1894). The reciprocal specificity of a protein enzyme was demonstrated by a mirror image protease, which could cleave a mirror image peptide (Milton *et al.*, 1992). This basic principle was also applied in the development of spiegelmers, which are the mirror

image of selected nucleic acids (Nolte *et al*. 1996; Klußmann *et al*. 1996). Most notably, these mirror image RNAs showed an extraordinary stability against nuclease degradation. The principle of reciprocal specificities for a ribozyme was shown by Jäschke and colleagues through the selection of an enantioselective catalyst (Seelig *et al*. 2000).

It was therefore predictable that the mirror image form of Ribozyme 1 (L-Rib 1) is able to cleave the mirror image substrate strand. In addition, a stability assay revealed that this oligonucleotide stayed intact even after 48 hours of incubation in human serum, while the natural ribozyme (D-Rib 1) was almost completely digested within 50 seconds.

To establish a proof of concept for the ribozyme approach, the mirror image form of the oligonucleotides were immobilized to nanoparticles. Even though the duplex of ribozyme and inhibitor strand could be bound to the same nanoparticle as the substrate strand, the present work focused for two reasons on a strategy of separate immobilizations. First, this separate binding eases the quantification and optimization of all reactions involved. Second and more important, it is conceivable that nanoparticles could eventually circulate into the non-pathogenic tissue of a patient. If substrate strands are immobilized on the same nanoparticle as ribozyme strands, an undesired release of a ribozyme is rather likely to result in a cleavage event due to close molecular proximity, while an immobilization on different nanoparticles renders this event more unlikely.

The release experiments performed with the immobilized oligonucleotides displayed the expected results. A fluorescent dye Alexa Flour 647 was used as a substitute for the cytotoxic drug to monitor the cleavage. A significant release of dye could be observed at a concentration of conjugates of about 1 µM at the elevated temperate of 49°C, while the release was insignificant at body temperature as compared to the controls.

Although the experiments performed in human serum were demonstrating a significant release of fluorescent dye upon hyperthermic conditions as well, the overall reaction after 4 hours of incubation was strongly reduced as compared to the

release in buffer. Control experiments reveal two reasons for this decrease.

First, when the reaction was performed in the presence of free ribozyme strands instead of ribozyme strands released from inhibitor strands, the amount of cleavage product in serum was almost as high as in buffer. This result indicates that the hybrid of ribozyme and inhibitor strand is more stable in serum than in buffer. This might simply be due to different ionic conditions, which would favor a duplex over a structured ribozme-substrate complex. In addition, it is conceivable that there are achiral compounds in human serum, such as polyamins, which could stabilize a double helix in a more specific manner. A future systematic optimization of ribozyme inhibitor duplexes with lower stability might improve release conditions for the intended *in vivo* application of the ribozyme approach.

The second observation from the control reactions was the reduced release of fluorescent dye in human serum at earlier time points, such as after one or two hours of incubation, even in the presence of free ribozyme strands. This indicated a significant decrease in reaction rates. The cleavage rate of the hammerhead ribozyme depends on many factors such as substrate concentration, environmental temperature, ionic strength and pH value. The reaction conditions for the cleavage in buffer were systematically optimized for the minimal hammerhead motif (Fedor & Uhlenbeck 1990, 1992; Hertel *et al*. 1994). The most frequently adopted reaction conditions and the ones used in this work were 50 mM Tris-HCl at pH 7.5 and 10 mM $MgCl_2$. This high concentration of divalent cations readily explains the higher reaction rate of cleavage in buffer as compared to human serum. Under physiological conditions the intracellular concentration of Mg^{2+} is between 0.1 and 1 mM depending on the type of tissue (London 1991; Romani *et al*. 1992; Uetani *et al.* 2003). Thus, the low concentration of magnesium in the cytoplasm may be a critical factor that generally limits the cleavage efficiency of a minimal hammerhead ribozyme *in vivo*.

5.3 Conjugation of Cytotoxic Drugs to Oligonucleotides

A fluorescence dye was covalently attached to the 3´-end of L-substrate strands during the release experiments as a substitute for the active pharmaceutical ingredient to monitor the release reactions. To complete the intended development of a temperature controlled release system, it was therefore attempted to explore the covalent attachment of cytotoxic drugs to oligonucleotides. The first candidate was chosen to be Chlorambucil (Leukeran®). This compound is a nitrogen mustard, which is applied against chronic lymphatic leukemia, lymphomas, advanced ovarian and breast carcinomas during clinical treatments (Armitage 1993; Beyer *et al*. 1998; Kratz *et al.* 1998). Chlorambucil is accessible for chemical modifications due to the presence of only one carboxyl group in the molecule. Already several decades ago, chlorambucil was used to prepare antibody conjugates (Ghose *et al.* 1972; Dullens *et al.* 1975; Smyth *et al*. 1986). Beyer and Kratz have developed chlorambucil derivatives to enhance the conjugation efficiency of chlorambucil and proteins (Beyer *et al*. 1998; Kratz *et al.* 1998). In addition, chlorambucil was also coupled to oligoprolyl-phenylalanyl-tRNA^{Phe} (Reuben *et al*. 1981).

Chlorambucil has molecular mass of 304.21 g/mol. If chlorambucil would be coupled to the primary amine of a funtionalized oligonucleotide upon forming an amide bond, the DNA molecule should gain an additional molecular mass of 286 g/mol. The results of conjugating Chlorambucil to DNA using EDC as a crosslinker showed an increase in molecular mass of a mere 156 g/mol through MALDI-TOF analysis, indicating a different reaction course than anticipated. The second zero-length crosslinker used in this work was CDI. Again, the desired gain in molecular mass was not achieved. The third attempt to conjugate chlorambucil to an oligonucleotide was carried out with the zero-length crosslinker DCC/NHS. TLC analysis revealead an almost complete turnover of the oligonucleotide. The product showed an additional molecular mass of 214 g/mol and thus again not the anticipated increase. The coupling protocol necessitated a reaction under alkaline conditions. This is noteworthy, since an earlier report revealed that chlorambucil can exist in different forms upon elevated pH values (Linford 1963). It might have coupled in a form lacking its two chloro atoms, which would be consistent with the data obtained through MALDI analysis. The conjugate revealed no significant toxic effect on human

glioblastoma cells.

Therefore, the studies were extended towards the coupling of methotrexate (MTX), which is an analogue of folic acid. It can competitively inhibit dihydrofolate reductase (DHFR) and can inhibit the synthesis of purine bases. Majoros *et al.* (2009) reported that MTX can be conjugated to dendrimers, while maintaining its cytotoxic activity. The established protocol, which was used for the conjugation of chlorambucil to an oligonucleotide using DCC/NHS, was employed again to covalently couple MTX. As expected, a conjugate with an additional molecular mass of 436 g/mol could be observed by MALDI-TOF analysis. This indicated a successful reaction between methotrexate and the oligonucleotide. In addition, the methotrexate-DNA conjugates displayed a significant toxic effect on colonic carcinoma cells. A control reaction, however, revealed that the conjugate still contained impurities of unreacted MTX. Thus, while the successful attachment of a cytotoxic drug could be established, the proof of its cytotoxity in the conjugated form remains to evaluated through improved purification schemes.

5.4 Prospects of the Novel Drug-Delivery System

The novel ribozyme-nanoparticle-drug delivery system displayed the expected properties. A temperature controlled release through specific cleavage of mirror image RNAs bound to nanoparticles was achieved as planned and desired. The study with the mamma carcinoma line revealed an efficient uptake of about 2×10^6 conjugated nanoparticles per cell after 24 hrs of incubation. A cytoplasmatic localization of these nanoparticles could be established through transmission electron microscopy.

Since each nanoparticle carries about 15 immobilized substrate strands, a complete release of drugs through cleavage would deliver 3×10^7 compounds per cell. The mamma carcinoma cells used in this study revealed an average diameter of about 14 µm as determined by transmission electron microscopy. Assuming that these cells have a spherical shape, the average cell volume would be about 1×10^{-12} liters. The cytoplasmatic concentration of released drug could hence reach an intracellular

concentration of 50 µM at complete release, corresponding for methotrexate to value of 22 mg/l. This concentration exceeds more than 200-fold the effective value of 0.01 mg/l in culture medium, which already revealed a maximal effect on survival rate of cells. Thus, even an incomplete release of drugs from nanoparticles could develop a significant impact on targeted cells.

The efficient uptake of oligonucleotide-nanoparticle conjugates offers the interesting option, to even consider the attachment of cytotoxic drugs, which are unable to pass cellular membranes by themselves. In this context, it is noteworthy to mention that the established scheme is not limited to cytotoxic drugs only. The established delivery system could also be employed to the treatment of diseases, which would profit from a local administration and which might encounter severe problems with cellular uptake.

The advantage of this novel drug delivery system focuses on the “local” and “controlled” treatment. The employment of mirror image RNA ensures a high specificity of drug release. This concept avoids the undesired cleavage of the nucleic acid bridge between nanoparticle and drug by the action of abundant nucleases. In addition, the concept of binding ribozyme and substrate strands on separate nanoparticles reduces the undesired proximity of these two compounds in locations far from the site of administration.

A current disadvantage of this drug delivery system can be seen in the reduced ribozyme activity in human serum as compared to the ideal *in vitro* conditions. This problem has already impeded a multitude of attempts to efficiently interfere with gene expression through hammerhead cleavage of mRNAs. This disadvantage, however, could be reduced in future developments through the employment of ribozymes with a lower requirement of divalent cations (Burke and Greyhouse, 2005; Persson *et al.* 2002; Fedoruk-Wyszomirska *et al.* 2009).

Furthermore, the approach could be extended to the use of mirror image deoxyribozymes (Erdmann, V. A., personal communication). This might be superior to the current strategy, since the solid phase synthesis of DNA is less complicated than of RNA due to the absence of 2’-hydroxyl groups. The ease in preparing the

compounds could significantly reduce costs of production once the established delivery scheme is considered for future clinical developments.

6 Summary

Worldwide, more than 10 million people are afflicted with cancer every year. The classical cancer treatment are surgery, radiotherapy and chemotherapy. The side effects of these therapies, however, strongly restrict the quality of the patients´ life. New and more effective cancer treatments devoid of strong side effects are urgently needed.

The Berlin company MagForce Nanotechnologies AG pursues a new therapeutic approach to fight a variety of solid tumors (NanoTherm® therapy). In this therapy, iron oxide nanoparticles are injected directly into the tumor. The particles are heated under an externally applied alternating magnetic field. The tumor cells can be directly damaged by high temperature or be sensitized to a combined radio- or chemotherapy.

The present study was attempted to combine this approach with nucleic acid technologies. The nucleic acids serve as a thermolabile linkage between nanoparticle and cytotoxic drug. A combined thermo- and chemotherapy was envisaged that would exert a local effect and would promise minimal side effects.

It was first tested whether a double stranded nucleic acids can function as a thermolabile linkage between nanoparticles and active ingredient. A coupling protocol for the covalent immobilization of oligonucleotides to iron oxide nanoparticles was established for this concept. The temperature dependent release of complementary strands was optimized by variation of the length and the sequence of hybrids. The release of immobilizable strands, however, was incomplete under thermal conditions, which can be reached during the NanoTherm® therapy (about 50°C).

Therefore, an expanded concept was pursued. The mere partial release of complementary strand was amplified through a catalytic step. The released single strand is a ribozyme that can efficiently cleave a substrate strand. This substrate strand is the bridge between nanoparticle and drug. Furthermore, the oligonucleotides used were replaced by their enantiomeric compounds, which render the system stable against enzymatic degradation. This temperature-dependent

controlled drug release system was successfully tested with a fluorescent dye as a model for the active ingredient in buffer and in human serum. The results shown are a first step towards a local, thermally-switchable therapeutic approach that could expand future prospects of the NanoTherm® therapy in the treatment of solid tumors.

7 Zusammenfassung

Weltweit erkranken jedes Jahr mehr als 10 Millionen Menschen an Krebs. Die drei Säulen der heutigen Tumortherapie sind Operation, Bestrahlung und Chemotherapie. Die dabei entstehenden Nebenwirkungen schränken allerdings die Lebensqualität der Patienten stark ein. Neue und effektivere Verfahren ohne die starken Nebenwirkungen einer systemischen Chemotherapie werden dringend benötigt.

Die Berliner Firma MagForce Nanotechnologies AG verfolgt einen neuen Therapieansatz zur Bekämpfung verschiedener solider Tumoren (NanoTherm® Therapie). Dabei werden Eisenoxid-Nanopartikel direkt in den Tumor eingebracht. Durch ein von außen angelegtes Magnetwechselfeld werden die Partikel erwärmt. Im Tumor entstehen Temperaturen, die die Krebszellen irreparabel schädigen und für eine kombinierte Chemotherapie sensibilisieren.

Mit der vorliegenden Arbeit wurde versucht, diesen Therapieansatz mit Nukleinsäure-Technologien zu kombinieren. In der Zielsetzung soll eine Nukleinsäure als thermolabile Brücke zwischen einem Nanopartikel und einem zytotoxischen Wirkstoff dienen. Damit könnte eine kombinierte Thermo- und auch Chemotherapie erreicht werden, die lokal begrenzt bleibt und damit geringere Nebenwirkungen verspricht.

Zunächst wurde getestet, ob eine doppelsträngige Nukleinsäure als thermolabile Brücke zwischen Nanopartikel und Wirkstoff dienen kann. Für das Konzept wurde ein Kopplungsprotokoll zur kovalenten Immobilisierung von Oligonukleotiden an Eisenoxid-Nanopartikel etabliert. Dann wurde die thermische Freisetzung von komplementären Gegensträngen optimiert, wobei Länge und Sequenz der Hybride variiert wurde. Unter den thermischen Bedingungen, die in der NanoTherm® Therapie erreicht werden (ca. 50°C), konnten allerdings die Gegenstränge nur unvollständig freigesetzt werden.

Daher wurde ein erweitertes Konzept verfolgt. Die nur partielle Freisetzung des Gegenstrangs wird durch einen katalytischen Schritt verstärkt. Der freigesetzte Einzelstrang ist ein Ribozym, das einen Substratstrang effizient spalten kann. Dieser Substratstrang bildet hier die Brücke zwischen Nanopartikel und Wirkstoff. Weiterhin

wurden die verwendeten Oligonukleotide durch ihre enatiomeren Verbindungen ersetzt, so dass eine hohe Stabilität des Systems gegenüber enzymatischem Abbau erreicht werden konnte. Dieses temperaturabhängig kontrollierte Wirkstofffreisetzungssystem wurde in Puffer und in humanem Serum mit einer Fluoreszenz-Sonde als Modell für den Wirkstoff erfolgreich geprüft. Die gezeigten Ergebnisse sind ein erster Schritt in Richtung eines lokalen, thermisch-schaltbaren Therapieverfahrens, das als Weiterentwicklung der NanoTherm®-Therapie in der Zukunft einen Beitrag zur Bekämpfung von soliden Tumoren haben könnte.

8. References

Ackland, S. P. & Schilsky, R. L. 1987. High-dose methotrexate: a critical reappraisal. *J Clin Oncol.* **5:** 2017-2031.

Andrä, W. & Nowak, H. 1998. Magnetism in medicine. 1st Edition. Wiley-VCH Verlag Berlin GmbH. 66-68.

Anderson , G. W. 1958. *N*,*N´*-Carbonyldiimidazole, a new reagent for peptide synthesis . *J. Am. Chem.Soc.* **80**: 4423 .

Arbab, A. S., Bashaw, L. A., Miller, B. R., Jordan, E. K., Lewis, B. K., Kalish, H., Frank, J. A. 2003. Characterization of biophysical and metabolic properties of cells labeled with superparamagnetic iron oxide nanoparticles and transfection agent for cellular MR imaging. *Radiology*. **229**: 838–846.

Armitage, J.O. 1993. Leukaran® (Chlorambucil). in *Current Clinical Guide*, 2nd ed. Borroughs Wellcome Co. Oncology Products Wellcome On- cology NCM Publ.Inc. New York, pp 37–45.

Arruebo, M., Fernández-Pacheco, R., Ricardo Ibarra, M., Santamaría, J. 2007. Magnetic nanoparticles for drug delivery. *Nanotoday.* **2**: 22-32.

Barany, C., and Merrifi eld, R. B. 1980. *In The Peptides* (E. Gross and J. Meienhofer, eds.), Academic Press, New York. pp. 1–284.

Beaudry, A. A., & Joyce, G. F. 1992. Directed evolution of an RNA enzyme. *Science*. **257**: 635-641.

Beaudry, A. A., Joyce, G. F. 1992. Directed evolution of an RNA enzyme. *Science*. **257**: 635-641.

Bhattacharyyaa, S., Bhattacharyaa, R., Curleyb, S., McNivena, M. A., Mukherjeea, P. 2010, Nanoconjugation modulates the trafficking and mechanism of antibody induced receptor endocytosis. *PNAS*. **107**: 14541–14546.

Breaker, R. R. & Joyce, G. F. 1994. A DNA enzyme that cleaves RNA. *Chem Biol.* **1**:223-229.

Cantor, C. R. and Schimmel, P. R. 1980.Biophysical chemistry. Part III: the behavior of biological macromolecules. W. H. Freeman and Company. SanFrancisco. p1134-1135.

Chu, B. C. F. , Kramer , F. R. ,Orgel , L. E. 1986. Synthesis of an amplifi able reporter RNA for bioassays . *Nucleic Acids Res.* **14**: 5591 – 5603 .

Cook, P. D., Acevedo, O. L., Davis, P. W., Ecker, D. J., Hebert, N. 1995 Synthesis of acyclic oligonucleotides as antiviral and antiinflammatory agents and inhibitors of

phospholipase A2. PCT Int. Appl., 126 pp. WO 9518820 A1 19950713 CAN 124:30276 AN 1995:982328.

Crick, F. H. C. 1968. The Origin of the Genetic Code. *J. Mol. Biol*. **38**: 367-379.

Dahl, O. 1988. Interaction of hyperthermia and chemotherapy. In Issels, R. D. & Wilmanns, W. Editors. *Hyperthermia and radiation: biological and clinical studies.* Berlin-Heiderberg, Germany. Springer-Verlag. pp 157-169.

Deacon, R., Chanarin, I., Lumb, M., Perry, J. 1985. Role of folate dependent transformylases in synthesis of purine in bone marrow of man and in bone marrow and liver of rats. *J Clin Pathol*. **38**: 1349–1352.

Derfus, A. M., von Maltzahn, G., Harris, T. J., Duza, T., Vecchio, K. S., Ruoslahti, E. and Bhatia., S. N. 2007. Remotely Triggered Release from Magnetic Nanoparticles. *Adv. Mater*. **19**:3932-3936.

Derfus, A. M., von Maltzahn, G., Harris, T. J., Duza, T., Vecchio, K. S.,Ruoslahti, E., Bhatia, S. N. 2007. Remotely Triggered Release from Magnetic Nanoparticles. *Advanced Materials.* **19**:3932-3936.

Devoe, H. & Tinoco, I. Jr. 1962. The hypochromism of helical polynucleotides. *J Mol Biol.* **4**: 518-527.

Dewey , R. E. , Timothy , D. H. , Levings III. , C. S. 1987. A mitochondrial protein associated with cytoplasmic male sterility in the T cytoplasm of maize. *Proc. Natl. Acad. Sci. USA* **84**: 5374 – 5378.

Dorr, R. T. & Fritz, W. L. 1982. *Cancer Chemotherapy Handbook*. Elsevier Science: New York.

Egholm, M., Buchardt, O., Christensen, L., Behrens, C., Freier, S.M., Driver, D. A., Berg, R.H., Kim, S.K., Nordén, B. and Nielsen, P.E. 1993. PNA Hybridizes to Complementary Oligonucleotides Obeying the Watson-Crick Hydrogen Bonding Rules. *Nature*. **365**: 566-568.

Ellington, A. D. & Szostak, J. W. 1990. In vitro selection of RNA molecules that bind specific ligands. *Nature*. **346**: 818–822.

Ellis, R. J., Van der Vies, S. M. 1991. Molecular chaperones. *Annual Reviews in Biochemistry*. **60**: 321–347.

Erdmann, V. A., Wyszko, E. 2010. WO 2010088899(A). Pharmaceutical composition for treating adverse reactions by administering spiegelmers. Application number: WO2010DE0015920100208.

Fischer, E. 1894. Einfluss der Configuration auf die Wirkung der Enzyme. *Ber. Dtsch. Chem. Ges.* **27**: 2985-2993.

Forster, A. C & Symons, R. H. 1987.Self-cleavage of plus and minus RNAs of a virusoid and a structural model for the active sites**.** *Cell.* **49**: 211-220.

Fujiwara , K., Matsumoto , N., Yagisawa , S., Tanimori , H., Kitagawa , T. , Hirota , M., Hiratani , K. , Fukushima , K., Tomonaga , A., Hara , K., Yamamoto , K. 1988. Sandwich enzyme immunoassay of tumor-associated antigen sialosylated Lewisx using b-D-galactosidase coupled to a monoclonal antibody of IgM isotype . *J. Immunol. Meth.* **112:** 77– 83.

Ghosh , S. S. , Kao , P. M. , McCue , A. W. , Chappelle , H.L. 1990. Use of maleimide-thiol coupling chemistry for effi cient syntheses of oligonucleotide–enzyme conjugate hybridization probes . *BioconjugateChem.* **1**: 71 – 76.

Gilbert, W. 1986. The RNA world. *Nature*. **319**: 618.

Gilchrist, R. K., Shorey, W. D., Hanselman, R. C., Parrott, J. C., Taylor, C. B., Medal, R. 1957. Selective Inductive Heating of Lymph Nodes. *Annals of Surgery*. **146**: 596-606.

Gilles , M.A. , Hudson , A.Q. ,Borders , C.L. 1990. Stability of water-soluble carbodiimides in aqueous solution . *Anal. Biochem.* **184**: 244 – 248.

Gneveckow, U., Jordan, A., Scholz, R., Brüss, V., Waldöfner, N., Ricke, J., Feussner, A., Hildebrandt, B., Rau, B., Wust, P. 2004. Description and characterization of the novel hyperthermia- and thermoablation-system MFH 300F for clinical magnetic fluid hyperthermia. Med Phys. 31:1444-1451.

Gordon, R. T., Hines, J. R., Gordon, D. 1979. Intracellular hyperthermia. A biophysical approach to cancer treatment via intracellular temperature and biophysical alterations. *Med Hypotheses*. **5**:83-102.

Gref, R., Minamitake, Y., Peracchia, M. T., Trubetskoy, V., Torchilin, V., Langer, R. 1994. Biodegradable long-circulating polymeric nanospheres. *Science*. **263**:1600-1603.

Guerrier-Takada, C., Gardiner, K., Marsh, T., Pace, N., Altman, S. 1983. The RNA moiety of ribonuclease P is the catalytic subunit of the Enzyme. *Cell*. **35** (3 Pt 2): 849-857.

Gupta, A. K., Gupta, M. 2005. Synthesis and surface engineering of iron oxide nanoparticles for biomedical applications. *Biomaterials*. **26**: 3995-4021.

Haley, B., Frenkel, E. 2008. Nanoparticles for drug delivery in cancer treatment. *Urol Oncol.* **26**: 57-64.

Hartman , F. C. , and Wold , F. 1966. Bifunctional reagents . *Cross-linking of pancreatic ribonuclease with a diimido ester. J. Am. Chem. Soc.* **88**: 3890 – 3891.

Haseloff, J. & Gerlach W.L. 1988. Simple RNA enzymes with new and highly specific endoribonuclease activities. *Nature.* **334**: 585-591.

Hashida , S., and Ishikawa , E. 1985. Use of normal IgG and its fragments to lower the nonspecifi c binding of Fab ' -enzyme conjugates in sandwich enzyme immunoassay . *Anal. Lett.* **18** (B9): 1143 – 1155.

Hertel, K. J., Pardi, A., Uhlenbeck, O. C., Koizumi, M., Ohtsuka, E., Uesugi, S., Cedergren, R., Eckstein, F., Gerlach, W. L., Hodgson, R., Symons, R. H. 1992. Numbering system for the hammerhead. *Nucleic Acids Res.* **20**: 3252.

Hoare , D. G., Koshland , D.E. 1966. A procedure for the selective modifi cation of carboxyl groups in proteins. *J. Am. Chem. Soc.* **88**: 2057.

Jordan, A., Scholz, R., Maier-Hauff, K., van Landeghem, F. K. H., Waldoefner, N., Teichgraeber, U., Pinkernelle, J., Bruhn, H., Neumann, F., Thiesen, B., von Deimling, A., Felix, R. 2006. The effect of thermotherapy using magnetic nanoparticles on rat malignant glioma. *Journal of Neuro-Oncology*. **78**: 7–14.

Jordan, A., Scholz, R., Wust, P., Fahling, H., Krause, J., Wlodarczyk, W., Sander, B., Vogl, T., Felix, R. 1997. Effects of magnetic fluid hyperthermia (MFH) on C3H mammary carcinoma in vivo. *Int J Hyperthermia*. **13**:587-605.

Jordan, A., Scholz, R., Wust, P., Schirra, H., Schiestel, T., Schmidt, H., Felix, R. 1999. Endocytosis of dextran and silan-coated magnetite nanoparticles and the effect of intracellular hyperthermia on human mammary carcinoma cells in vitro. *Journal of Magnetism and Magnetic Materials*. **194**: 185-196.

Jordan, A., Wust, P., Fahling, H., Johns, W., Hinz, A. and Felix, R. 1993. Inductive heating of ferrimagnetic particles and magnetic fluids: physical evaluation of their potential for hyperthermia. *Int. J. Hyperthermia* **9:** 51–68.

Jung, H., Dikomey, E. 1988. Some basic effects in cellular thermobiology. In Issels, R. D. & Wilmanns, W. Editors. *Hyperthermia and radiation: biological and clinical studies.* Berlin-Heiderberg, Germany. Springer-Verlag. pp 104-112.

Kampinga, H. H., Turkel-Uygur, N., Roti Roti, J. L., Konings, A. W. T. 1978. The relationship of increased nuclear protein content induced by hyperthermia to killing of HeLa S3 cells. *Radiation Research*. **117**: 511–522.

Kampinga, H. H. 2006. Cell biological effects of hyperthermia alone or combined with radiation or drugs: a short introduction to newcomers in the field. *Int J Hyperthermia.* **22**: 191-196.

Kampinga, H. H., Dikomey, E.2001. Hyperthermic radiosensitization: mode of action and clinical relevance. *International Journal of Radiation Biology*. **77**: 399–408.

Keller , G. H. , and Manak , M. M. 1989. *DNA Probes* . Stockton , New York .

Klussmann, S., Nolte, A., Bald, R., Erdmann, V. A., Fürste, J. P.1996. Mirror-image RNA that binds D-adenosine. *Nat. biotechnol.* **14**: 1112-1115.

Kohler, N., Sun, C., Wang, J., Zhang, M. 2005. Methotrexate-modified superparamagnetic nanoparticles and their intracellular uptake into human cancer cells. *Langmuir* **21**: 8858-8864.

Koshkin, A. A., Singh, S. K., Nielsen, P., Rajwanshi, V. K., Kumar, R., Meldgaard, M., Olsen, C. E., Wengel, J. 1998. LNA (Locked Nucleic Acids): Synthesis of the adenine, cytosine, guanine, 5-methylcytosine, thymine and uracil bicyclonucleoside monomers, oligomerisation, and unprecedented nucleic acid recognition. *Tetrahedron* **54**: 3607–3630.

Kruger, K., Grabowski, P.J., Zaug, A.J., Sands, J., Gottschling, D.E., Cech, T. R. 1982. Selfsplicing RNA: autoexcision and autocyclization of the ribosomal RNA intervening sequence of *Tetrahymena*. *Cell*. **31**: 147-157.

Kukowska-Latallo, J. F., Candido, K., A., Cao, Z. Y., Nigavekar S. S., Majoros, I. J., Thomas, T. P., Balogh, L., P., Khan, M., K., Baker, J. R. Jr. 2005. Nanoparticle Targeting of Anticancer Drug Improves Therapeutic Response in Animal Model of Human Epithelial Cancer. *Cancer Res*. **65**: 5317-5324.

Kuma, C. S. S. R. 2006. Nanomaterials for Cancer Therapy. 1st Edition. Wiley-VCH Verlag GmbH & Co. kGaA. 282-283.

Lepock, J. R. 2004. Role of nuclear protein denaturation and aggregation in thermal radiosensitization. *International Journal of Hyperthermi.* **20**: 115–130.

Lepock, J. R., Frey, H. E., Ritchie, K. P. 1993. Protein denaturation in intact hepatocytes and isolated cellular organelles during heat shock. *Journal of Cell Biology*. **122**: 1267–1276.

Letsinger, R. L., Mahadevan, V. J., 1965. Oligonucleotide Synthesis on Polymer Supports, *J. Am. Chem. Soc*. **87**: 3526-3527.

Lu, A. H.**,** Salabas, E. L.**,** Schuth, F. 2007. Magnetic Nanoparticles: synthesis**,** protection**,** functionalization, and application. *Angew. Chem. Int. Ed. Engl*. **46**: 1222-1244**.**

Majoros, I. J., Williams, C. R., Becker, A., Baker, J. R. Jr. 2009. Methotrexate delivery via folate targeted dendrimer-based nanotherapeutic platform. *Wiley Interdiscip Rev Nanomed Nanobiotechnol.* **1**: 502-510.

Michels, A. A., Kanon, B., Konings, A. W. T., Ohtsuka, K., Bensaude, O., Kampinga, H. H. 1997. HSP70 and HSP40 chaperone activities in the cytoplasm and the nucleus of mammalian cells. *Journal of Biological Chemistry*. **272**: 33283–33289.

Michels, A. A., Nguyen, V. T., Konings, A. W., Kampinga, H. H.1995. Bensaude O. Thermostability of a nuclear-targeted luciferase expressed in mammalian cells - Destabilizing influence of the intranuclear microenvironment. *European Journal of Biochemistry*. **234**: 382–389.

Mohanraj, V. J.& Chen, Y. 2006. Nanoparticles – A Review. *Tropical Journal of Pharmaceutical Research*. **5**: 561-573.

Morimoto, R. I. 1998. Regulation of the heat shock transcriptional response: cross talk between a family of heat shock factors, molecular chaperones, and negative regulators. *Genes Development*. **12**: 3788–3796.

Mosmann, T. 1983. Rapid colorimetric assay for cellular growth and survival: application to proliferation and cytotoxicity assays. *J Immunol Methods.* **65**: 55-63.

Nair, B. G., Nagaoka, Y., Morimoto, H., Yoshida, Y., Maekawa, T., Sakthi Kumar, D. 2010. Aptamer conjugated magnetic nanoparticles as nanosurgeons. *Nanotechnology.* **21**: 455102.

Nakajima , N., and Ikada , Y. 1995. Mechanism of amid formation by carbodiimides for bioconjugation in aqueous media . *Bioconjugate Chem.* **6** :123 – 130.

Nolte, A., Klussmann, S., Bald, R., Erdmann, V. A., Fürste, J. P.1996. Mirror-design of L-oligonucleotide ligands binding to L-arginine. *Nat. biotechnol* **14**:1116-1119.

Obika, S., Nanbu, D., Hari, Y., Morio, K., In, Y., Ishida, T., Imanishi, T. 1997. Synthesis of 2′-*O*,4′-*C*-methyleneuridine and -cytidine. Novel bicyclic nucleosides having a fixed C3'-*endo* sugar puckering. *Tetrahedron Lett.* **38**: 8735–87358.

Orgel, L. 2000. A Simpler Nucleic Acid. *Science* **290**: 1306–1307.

Orgel, L. E. 1968. Evolution of the Genetic Apparatus, *J. Mol. Biol*. **38**: 38167-39379.
Pankhurst, Q. A., Connolly, J., Jones, S. K., Dobson, J. 2003. Applications of magnetic nanoparticles in biomedicine. *J. Phys. D: Appl. Phys.* **36**: 167–181.

Pankhurst, Q., A., Connolly, J., Jones, S., K., Dobson, J. 2003. Applications of magnetic nanoparticles in biomedicine. *Journal of Physics D Applied Physics*. **36**: 167-181.

Pasteur, L. 1861. Recherches sur la dissymetrie moleculaire des produits organiques naturels (Lecons de chimie professees en 1860, ed Societe Chimique de Paris, L. Hachette et Cie, Paris, 1861).

Prody, G. A.; Bakos,J. T., Buzayan, J. M., Schneider,I. R.; Bruening, G. 1986. Autolytic processing of dimeric plant virus satellite RNA. *Science*. **231**:1577-1580.

Reuben, M. A., Ainpour, P. R., Hester, H. L., Neveln, V. L., Wickstrom, E. 1981. Synthesis and intramolecular crosslinking of chlorambucilyl (prolyl)n [3H]phenylalanyl-tRNAPhe (yeast), n = 0, 5, 11 and 15. *Biochim Biophys Acta.* **654**: 11-25.

Rosensweig, R. E. 2002. Heating magnetic fluid with alternating magnetic field. *J. Magn. Magn. Mater.* **252:** 370–374.

Roti Roti, J. L., Laszlo, A. 1988. The effects of hyperthermia on cellular macromolecules. *Thermal effects on cells and tissues*. M Urano, E Douple. VSP, Utrecht. 13–98.

Sambrook, J., Fritsh, E. F. & Maniates, T. 1989. Molecular Cloning– A Laboratory Manuel. *Cold Spring Harbor Laboratory Press: Cold Spring Harbor*, NY.

Sampson, J. R., Sullivan, F. X., Behlen, L. S., Di Renzo, A. B., Uhlenbeck, O. C.1987. Characterization of two RNA-catalyzed RNA cleavage reactions. *Cold Spring Harb Symp Quant Biol.***52**: 267-275.

Schmid, G. 2010. Nanoparticles: From theory to application. Second edition. WILEY-VCH Verlag. S293.

Schoning, K., Scholz, P., Guntha, S., Wu, X., Krishnamurthy, R., Eschenmoser, A. 2000. Chemical etiology of nucleic acid structure: the alpha-threofuranosyl-(3'->2') oligonucleotide system. *Science.* **290**: 1347.

Seelig, B., Keiper, S., Stuhlmann, F., Jäschke, A. 2000. Enantioselective Ribozyme Catalysis of a Bimolecular Cycloaddition Reaction. *Angew Chem Int Ed Engl*. **39**: 4576-4579.

Sheehan , J. C. , and Hess , G. P. 1955. A new method of forming peptide bonds . *J. Am. Chem. Soc.* **77**: 1067 – 1068.

Singal, P. K., Iliskovic, N. 1998. Doxorubicin-induced cardiomyopathy. *N Engl J Med* **339**:900–905.

Sounderya, N & Zhang, Y. 2008. Use of Core/Shell Structured Nanoparticles for Biomedical Applications. *Recent Patents on Biomedical Engineering*. **1:** 34-42

Staros, J. V. 1982. *N*-hydroxysulfosuccinimide active esters: *Bis* (*N*-hydroxysulfosuccinimide) esters of two dicarboxylic acids are hydrophilic, membrane impermeant, protein cross-linkers . *Biochemistry* **21**: 3950 – 3955.

Stupp, R., Mason, W. P., van den Bent, M. J. , Weller, M., Fisher, B., Taphoorn, M. J., Belanger, K., Brandes, A. A., Marosi, C., Bogdahn, U., Curschmann, J., Janzer, R. C., Ludwin, S. K., Gorlia, T., Allgeier, A., Lacombe, D., Cairncross, J. G., Eisenhauer, E., Mirimanoff, R. O. 2005. Radiotherapy plus concomitant and adjuvant temozolomide for glioblastoma. *N Engl J Med*. **352**: 987–996.

Symons, R. H. 1989. Self-cleavage of RNA in the replication of small pathogens of plants and animals. *Trends Biochem Sci.* **14**: 445-450.

Tuerk, C. & Gold, L. 1990. Systematic evolution of ligands by exponential enrichment: RNA ligands to bacteriophage T4 DNA polymerase. *Science*. **249**: 505-510.

Uhlenbeck, O. C. 1987. A small catalytic oligoribonucleotide. *Nature*. **328**:596-600.

van Tol, H., Buzayan, J. M., Feldstein, P. A., Eckstein, F., Bruening, G. 1990. Two autolytic processing reactions of a satellite RNA proceed with inversion of configuration. *Nucleic Acids Res.* 18:1971-1975.

Watson, J.D. & Crick, F.C.H. 1953. Molecular structure of nucleic acids; a structure for deoxyribose nucleic acid. *Nature* **171:** 737-738.

Williams , A., and Ibrahim , I.A. 1981. A mechanism involving cyclic tautomers for the reaction with nucleophiles of the water-soluble peptide coupling reagent 1-ethyl-3-(3-dimethyla-minopropyl) carbodiimide (EDC) . *J. Am. Chem. Soc.* **103**: 7090 – 7095.

Wittung, P., Nielsen P.E., Buchardt, Ole., Egholm, M. and Nordén, B. 1994. DNA-like Double Helix formed by Peptide Nucleic Acid. *Nature*. **368**: 561-563.

Woese, C. 1967. The Evolution of the Genetic Code, in: *The Genetic Code*, Haper & Row, Eds., New York. 179-195.

Yeh, E. T., Tong, A. T., Lenihan, D. J. 2004. Cardiovascular complications of cancer therapy: diagnosis, pathogenesis, and management. *Circulation*. **109**:3122–3131.

Yuan, F. 1998. Transvascular drug delivery in solid tumors. *Semin Radiat Oncol*. **8**: 164 –175.

Zhang, L. L., Peritz A., Meggers E. 2005. A simple glycol nucleic acid. *J Am Chem Soc* **127**: 4174–4175.

9 Appendix

9.1 Materials

9.1.1 Chemicals

Acetic Acid	Rothe, Germany
Acrylamide	Rothe, Germany
Agarose	Biozyme, Oldendorf, Germany
Ammonium sulfate	Fluka, St Quentin Fallavier, France
APS	Rothe, Germany
Bromophenol Blue	Serva, Heidelberg, Germany
CDI	Thermo Fisher Scientific, Germany
Chlorambucil	Sigma Aldrich, Germany
DCC	Thermo Scientific Pierce, USA
DMF	Rothe, Germany
DMSO	Rothe, Germany
DNA Ladder (10 bp)	Biolabs, Beverly, USA
D-PBS, 10x	Invitrogen, USA
DTT	BD Biosciences, USA
EDC	Thermo Scientific Pierce, USA
EDTA	Merck, Germany
Ethanol	Merck, Germany
Ethidium Bromide	Fluka, St Quentin Fallavier, France
Glycerol	Merck, Germany
Hydrochloric Acid	Merck, Germany
Magnesium Chloride	Merck, Germany
MES	Sigma Aldrich, Germany
Methanol	Rothe, Germany
Magnesium Sulfate	Merck, Germany
NHS	Sigma-Adrich, Germany
PBS 1x, pH 7.2	Invitrogen, USA
PBS 1x, pH 7.4	Invitrogen, USA
PDITC	Sigma-Aldrich, Germany
Potassium Chloride	Merck, Germany
Potassium Phosphate	Merck, Germany
r–^{32}P–ATP	Amersham/GE Healthcare, UK
Sera human S7023	Sigma-Aldrich, Germany
Sodium acetat	Riedel de Häen
Sodium borate	Sigma-Aldrich, Germany

Sodium chloride	Merck, Germany
Sodium Hydroxide	Merck, Germany
Spemine	Sigma-Adrich, Germany
Sulfo-GMBS	Thermo Scientific Pierce, USA
Sulfo-SMCC	Sigma-Adrich, Germany
Sulfo-SMCC	Thermo Scientific Pierce, USA
Sulfo-NHS	Thermo Scientific Pierce, USA
TAE buffer	Rothe, Germany
TBE buffer	Rothe, Germany
TCEP	Sigma-Adrich, Germany
TEMED	Rothe, Germany
Tris–HCl	Rothe, Germany
Tween 20	Serva, Heidelberg, Germany
Urea	Rothe, Germany
Xylencyanol	Rothe, Germany

9.1.2 Enzyme

T4 Polynucleotide Kinase Promega, New England Biolabs, Beverly, USA

9.1.3 Nanoparticles

Iron oxide nanoparticles with different modifications were provided by MagForce Nanotechnologies AG, Germany

Nanoparticle Name	Core	Shell	Modification
SR-E2	Iron oxide	silica	$-NH_2$
AB025	Iron oxide	silica	$-NH_2$
AB030	Iron oxide	silica	PEG/Diamo
NWP3/039	Iron oxide	silica	$-NH_2$
AB060	Iron oxide	silica	PDITC-activated
AB068	Iron oxide	silica	epoxylated
N.P. 086	Iron oxide	silica	-SH
N.P. 087	Iron oxide	silica	-SH
N.P. 088	Iron oxide	silica	-SH

MM-E2-014	Iron oxide	silica	$-NH_2$
AB 107	Iron oxide	---	Gold-layer

9.1.4 Nucleic Acids

All nucleic acids used for this work were purchased from IBA Göttingen, Germany

9.1.5 Buffers

Dulbecco's Phosphate–Buffered Saline (1x D–PBS) pH 6.7
137.9 mM NaCl
8.06 mM $Na_2HPO_4–7H_2O$
2.67 mM KCl
1.47 mM KH_2PO_4

Phosphate–Buffered Saline (1x PBS), pH 7.2
155.17 mM NaCl
2.71 mM $Na_2HPO_4–7H_2O$
1.54 mM KH_2PO_4

Phosphate–Buffered Saline (1x PBS), pH 7.4
155.17 mM NaCl
2.97 mM $Na_2HPO_4–7H_2O$
1.06 mM KH_2PO_4

Loading Buffer for Agarose Gel (6x)
0.03% Bromphenolblue
0.03% Xylencyanol
15% Ficoll®400
10 mM Tris-HCl (pH 7.5)
50 mM EDTA (pH 8.0)

Urea PAGE Loading Buffer (2×)
2x TBE
16 M Harnstoff
0.04 % Bromphenolblue
0.04 % Xylencyanol

T4 Polynucleotide Kinase Reaction Buffer (10×)
500 mM imidayole–HCl (pH 6.6)
100 mM MgCl2
50 mM DTT

1 mM spermidine
1 mM EDTA

TAE Buffer (10×)
400 mM Tris– Acetat (pH 8.0)
10 mM EDTA

TBE Buffer (10×)
900 mM Tris–borate (pH 8.0)
20 mM EDTA

TE Buffer
10 mM Tris–HCl (pH 8.0)
1 mM EDTA

Reaction buffer (Release-experiment of Ribozyme-NP-drug delivery system)
50 mM Tris–HCl (pH 7.5)
10 mM $MgCl_2$

9.1.6 Devices and Consumption Materials

Agarose Gel Chamber	Bio-Rad, USA
Agilent 8452 Diode Array Spectrophotometer	Hewlett Packard, Palo Alto, CA, USA
Autoclave 500–D	Sterico, AG, Dietikon, Switzerland
Cell incubator Heraeus HERA cell	Thermo scientific, USA
Centrifuge 5415D	Eppendorf, Germany
Cool Centrifuge J2–21	Beckman, Fullerton, CA, USA
DOWEX™ 50WX8	Roth, Germany
Fluorescent image	Fuji, Japan
Freezer –20ºC	Bosch, Germany
Freezer –80ºC	Heraeus, Hanau, Germany
Freezer 4ºC	Bosch, Germany
GelDoc 2000	Bio Rad, Germany
Gel Electrophoresis System	Renner GmBH, Darmstadt, Germany
Gloves	Neolab
Glass Plate	Glaserei Graw & Meibert
HP 8452A Diode-Array, Spectrophotometer	Hewlett Packard (HP), Germany
Human serum	Sigma, Germany

Kimwipes	Kimberly-Clark, UK
Lyophilizer SC110AR	Savant, Instruments, Farmingdale, USA
MALDI-TOF/TOF-MS Ultraflex II	Bruker Daltonics, Germany
Magnetic Particle Seperator	Roche, Germany
Magnetic Stirrer	IKA–Combimag RCT, Germany
MFH®-12-TS A	MedTech Engineering GmbH, Germany
Microcentrifuge ProFuge 10K	Stratagene, USA
Microcon YM–3, 30Spin Filters	Millipore, USA
MicroSpin™ G-25 Column	GE Healthcare, Sweden
Microplate reader	TECAN, Schwitzland
Microwave	Toshiba, Japan
Mini–gel apparatus	Bio–Rad, USA
Nap 5, 10–Column	GE Healthcare, Uppsala, Sweden
NanoActivator™	Magforce AG, Germany
NanoDrop 3300	Thermo Scientific, USA
Oil Pump	Alcatel, Germany
PAA Gel champer	Renner GMBH, Dannstadt, Germany
Phosphorimager Exposure Cassette	Molecular Dynamics, USA
Phosphorimager Storm 840	Molecular Dynamics, USA
Phosphor Screen	Molecular Dynamics, USA
pH–Meter 766 Calimatic	Knick, Berlin, Germany
Pipette Tips with Filters	Eppendorf, Germany
Pipette Tips with Filters	Rothe, Germany
Pipettes P2, P20, P200, P1000	Abimed, Langenfeld, Germany
Pipettes P2, P20, P200, P1000	Eppendorf, Germany
Photometer UV–1202	Shimadzu, USA
Plexis Container	Nalgene, Germany
Plexis Shield	Jencons
Power Supply	ECPS 3000/150, Pharmacia
Purest Water Installation (Milli–Q)	Millipore, Bedford, MA
Refrigerated Vapor Trap	RVT400, Savant
Reaction Tubes, 1.5 ml, 2.0ml	Eppendorf, Germany
Reaction Tubes, 1.5 ml, 2.0ml	Rothe, Germany
Rotator	WVR, Germany
Respirator	Roth, Germany
Scintillation Counter LS 6000	Beckman, Fullerton, CA, USA
Shaker (Isotope Laboratory)	Yellow line, FHG–VERW
StrataClean™ resin	Stratagene, CA, USA
SYBR® Gold stain	Invitrogen, USA
Syringe Filter 0.22µm	Rothe, Germany
Table–top Centrifuge	Eppendorf, Germany
Thermomixer comfort	Eppendorf, Germany

TLC	Merck, Germany
Ultrasonic bath	VWR, Germany
UV–Visible Spectrophotometer (UV–1202)	Shimadzu, Duisburg, Germany
UV fluorescent (60 F_{254}) TLC plate	Merck, Germany
Vortex	Scientific Industries, Bohemia, USA
Water Bath	GFL, Germany

9.2 Abbreviations

3D	Three dimensional
A	adenosine
Å	angstrom, 10^{-10} meter
A260	absorption at λ=260 nm
A280	absorption at λ=280 nm
AC magnetic field	alternating magnetic field
amu	Atomic mass unit
APS	Ammonium persulfate
ATP	adenosine 5'–triphosphate
bidist. H_2O	bidistilled water
Bis	N, N'–methylene bisacrylamide
bp	base pair(s)
c	concentration
C	cytosine
°C	temperature in degrees Celsius
CDI	*N,N´*-Carbonyldiimidazole
Ci	curie, 1 Ci=37 MBq
Conc.	concentration
cpm	counts per minute
Da	Dalton
DCC	Dicyclohexyl carbodiimide
DHFR	dihydrofolate reductase
DIAMO	N-(2-aminoethyl)-3-aminopropyltrimethoxysilane
DMF	Dimethylformamide
DMSO	dimethylsulfoxide
DNA	deoxyribonucleic acid
DNase	desoxyribonuclease
dNTP	deoxyribonucleotide triphosphate
DOX	Doxorubicin
D-PBS	Dulbecco's Phosphate–Buffered Saline

ds	double–stranded
DTT	Dithiothreitol
ε	extinction coefficient
E. coli	Escherichia coli
EDC	1-ethyl-3-(3-dimethylaminopropyl)carbodiimide hydrochloride
EDTA	Ethylenediaminetetraacetic Acid
EtBr	3, 8–diamino–5–Ethyl–6–phenyl phenanthridinium Bromide
Fig.	figure
g	gram
G	guanosine
GBM	Glioblastoma multiforme
Gy	Gray
h	hour(s)
HIV	human immunodeficiency virus
HPLC	high performance liquid chromatography
HSF-1	heat shock transcription factor
HSP	heat shock protein
IC50s	50% inhibitory concentrations
Ig	Immunoglobulin
Kd	dissociation constant
Km	Michaelis-Menten constant
k*cat*	turnover number
l	liter
m	meter
M	mol/l, molar
MALDI TOF	matrix-assisted laser desorption/ionization time of flight
MES	2-(*N*-morpholino)ethanesulfonic acid
MF	Magnetic fluid
MFH	Magnetic fluid hyperthermia
min	minute(s)
mol	Mole(s)
mM	micromolar
mRNA	messenger ribonucleic acid
MS	microvascular density
MTT	3-(4,5-Dimethylthiazol-2-yl)-2,5-diphenyltetrazolium bromide
MTX	Methotrexate
NHS	*N*-Hydroxysuccinimid
nm	nanometer
nM	nanomolar
nmol	nanomol
NBA	nitrobenzaldehyde

NMR	nuclear magnetic resonance
nt	Nucleotide(s)
NP	nanoparticle
NTP	nucleotide triphosphate
OD	optical density
PAA	polyacrylamide
PAGE	polyacrylamide gel electrophoresis
PBS	phosphate buffered saline
PCR	polymerase chain reaction
PEG	polyethylene glycol
PDITC	1,4-phenylene diisothiocyanate
rcf	relative centrifugal force
RFU	Relative Fluorescence Unit
RNA	ribonucleic acid
rpm	rotations per minute
RT	room temperature
s	second(s)
SAR	specific absorption rate
SMCC	Succinimidyl 4-[*N*-maleimidomethyl]cyclohexane-1-carboxylate
SPM	superparamagnetic
SPR	surface plasmon resonance
ss	single–stranded
Sulfo-GMBS	N-[γ-Maleimidobutyryloxy]sulfosuccinimide ester
Sulfo-NHS	*N*-hydroxysulfosuccinimide
Sulfo-SMCC	sulfosuccinimidyl-4-(N-maleimidomethyl)cyclohexane-1-carboxylate
T	thymine
T	temperature
T_m	melting temperature
T_r	release temperature
t	time
Tab.	table
TAE	Tris–Acetic Acid–EDTA
TBE	tris-borate-EDTA
TCEP	tris(2-carboxyethyl)phosphine
TEM	Transmission electron microscopy
TEMED	N,N,N’,N’–Tetramethylethylenediamine
TER	thermal enhancement ratio
THF	Tetrahydrofuran
TLC	Thin layer chromatograph
Tris	Tris–(Hydroxymethyl)–Aminomethane
tRNA	transfer ribonucleic acid

U	unit(s)
UV	ultraviolet
V	volt(s)
V	volume
v/v	volume per volume
VEGF	vesicular endothelial growth factor
VSG	variant surface glycoprotein
W	watt (s)
w/v	weight per volume
v/v	volume to volume
X–gal	5'–Bromo–4'–Chloro–3'–Indolyl–β–D–galactoside
λ	lambda
µl	micro liter
µM	micro molar

Prefixes of units:

p (pico)	10^{-12}
n (nano)	10^{-9}
µ (micro)	10^{-6}
m (milli)	10^{-3}
k (kilo)	10^{3}
M (mega)	10^{6}

9.3 Acknowledgements

First and foremost, I would like to express my highest gratitude to my supervisor Prof. Dr. Volker. A. Erdmann for giving me the opportunity to perform the research for my doctoral thesis in his laboratory, for his support and continuous encouragement during my graduate experience, and for reviewing this thesis.

I am indebted to Prof. Roland Tauber for being my second supervisor and for reviewing this thesis.

I would like to express my sincere gratitude to Dr. Andreas Jordan for funding this research project and for critical reading of the thesis.

Great thanks go to Dr. Monika Fischler for all her supervision, discussion and supports on my Ph.D. program, and for her correction of this dissertation.

I also would like to express my great gratitude to Dr. Jens P. Fürste for many scientific discussions, suggestions, his help during my work, and for his critical reading of the thesis.

I appreciate Dr. Christoph Weise very much for his experimental supports by MALDI-TOF and for his critical reading of the thesis.

I would like to thank Arne Basler for his experimental supports by NBA-, AAS- and MTT-Assays. I would also like to thank Nils Bohmer for the implementation of the TEM investigations.

I am also very much indebted to the members of the Erdmann laboratory for their stimulating discussions and valuable suggestions as well as their friendships. Special thanks go to Claudia Gallin for her support at my most difficult time.

Thanks also to the students Grischa Fuge, Robert Quast, Johannes G. Schaefer, Erik Walinda and Anna-Helene Weiß for their contribution to the research project under my supervision.

I would not have been able to achieve all this without the support of my family and my friend. To them I owe more than to anyone else. They have guided me, encouraged

me, and sustained me. Most of all, they have always believed in me and loved me. All of this means more to me than I am able to express here in words.

Curriculum Vitae

For reason of data protection, the curriculum vitae is not included in the online version.

For reason of data protection, the curriculum vitae is not included in the online version

9.5 Publication

9.5.1 Patent

Temperature dependent activation of catalytic nucleic acids for controlled release. Jiang Gao, Monika Fischler, Volker A. Erdmann. (DE 10 2009 058769.1 ; US 61/282,471; International application No: PCT/EP2010/007702; Publication date 16.06.2011).

9.5.2 Presentation

Krebs-Therapie durch lokale und kontrollierte Freisetzung von Wirkstoffen. Jiang Gao. VIII. Bionnale der Biotechnologie. Speed Lecture Awards 2010. 21. April, 2010. Berlin.

9.5.3 Manuscript

A novel Concept for Hyperthermia induced local chemotherapy. Jiang Gao, Monika Fischler, Nills Bohmer, Volker A. Erdmann & Andreas Jordan. Manuscript in preparation.

9.5.4 Poster

Nanoparticle-drug-conjugates for magnetic fluid hyperthermia and controlled release. Jiang Gao, Monika Fischler, Andreas Jordan and Volker A. Erdmann. NanoMed 2009. 04-06 March, 2009, Berlin.

Nanoparticle-drug-conjugates for controlled release induced by magnetic fluid hyperthermia. Jiang Gao, Monika Fischler, Andreas Jordan and Volker A. Erdmann. NanoMed 2010. 02-04 December, 2010, Berlin.